NASA CR-166097
BBN Report No. 5114

Limits on the Prediction of Helicopter Rotor Noise Using Thickness and Loading Sources:

Validation of Helicopter Noise Prediction Techniques

by
George P. Succi

April 1983

Prepared Under Contract No. NAS1-16886
by
Bolt Beranek and Newman Inc.
Cambridge, MA 02238

for

NASA

National Aeronautics and
Space Administration
Langley Research Center
Hampton, VA 23665

Technical Report Documentation Page

1. Report No.	2. Government Accession No.	3. Recipient's Catalog No.
NASA CR-166097		

4. Title and Subtitle
Limits on the Prediction of Helicopter Rotor Noise Using Thickness and Loading Sources: Validation of Helicopter Noise Prediction Techniques

5. Report Date
April 1983

6. Performing Organization Code

7. Author(s)
George P. Succi

8. Performing Organization Report No.
5114

9. Performing Organization Name and Address
Bolt Beranek and Newman Inc.
10 Moulton Street
Cambridge, MA 02238

10. Work Unit No. (TRAIS)

11. Contract or Grant No.
NAS1-16886

12. Sponsoring Agency Name and Address
National Aeronautics and Space Administration
Washington, DC 20546

13. Type of Report and Period Covered
Contractor Report
1981-82

14. Sponsoring Agency Code

15. Supplementary Notes
Project Manager, Dr. F. Farassat
NASA Langley Research Center
Hampton, VA 23665

16. Abstract

The current techniques of helicopter rotor noise prediction attempt to describe precisely the details of the noise field and remove the empiricisms and restrictions inherent in previous methods. These techniques require detailed inputs of the rotor geometry, operating conditions, and blade surface pressure distribution. A previous study at BBN demonstrated that these methods worked well, but not perfectly. The purpose of this study was to explore further the Farassat noise prediction technique, and to determine whether high speed helicopter noise can be predicted using more detailed representations of the thickness and loading noise sources. These predictions were based on the measured blade surface pressures on a Bell AH-1G rotor and compared to the measured sound field. Although refinements in the representation of the thickness and loading noise sources improve the calculation, there are still discrepancies between the measured and predicted sound field. Analysis of the blade surface pressure data indicates shocks on the blades, which are probably responsible for these discrepancies.

17. Key Words	18. Distribution Statement
Acoustics, Noise, Aircraft Noise Helicopter Noise, Rotor Noise, Noise Prediction.	Unclassified - unlimited

19. Security Classif. (of this report)	20. Security Classif. (of this page)	21. No. of Pages	22. Price
Unclassified	Unclassified	90	

NASA CR-166097
BBN Report No. 5114

LIMITS ON THE PREDICTION OF HELICOPTER ROTOR NOISE USING THICKNESS AND LOADING SOURCES

George P. Succi

NASA Contract No. NAS1-16886

April 1983

Submitted to:
NASA Langley Research Center
Hampton, VA 23665
F. Farassat, Contract Monitor

TABLE OF CONTENTS

LIST OF FIGURES

page

LIST OF TABLES

SECTION 1

INTRODUCTION AND SUMMARY

In this report, analytical predictions of rotor noise are compared to the measured values of the helicopter noise field. The measured data is from the Operations Loads Survey of a Bell AH-1G two-bladed helicopter [1,2]. During this survey, simultaneous measurements of the noise and blade loads on a helicopter in forward flight were made. Six level flyovers ranging in speed from 20 to 67 m/s at an altitude of 91 m (300 ft) were chosen for study. The helicopter main rotor has two blades with radius of 6.71 m (22.0 ft) and a chord of 0.73 m (2.4 ft). The blade loads were digitized and the information was used as an input to a computer program based on the acoustic formulation of Farassat.

The influences of both thickness and loading terms were included. The results have been published previously by Succi and the main results are summarized in Figs. 1 and 2. These figures compare the measured and predicted sound field for a helicopter in level forward flight. The acoustic data are presented for a microphone located at the standing ear level on the ground directly under the helicopter flight path. The observation angle corresponds to the position of the helicopter when the sound is detected and the emission angle corresponds to the retarded position of the helicopter. At angles less than 90°, the helicopter is approaching the observer, at 90° it is overhead and at angles greater than 90° it is receding. At low forward speeds (V = 20 m/s), the predictions agree with measurements. At high forward speeds (V = 67 m/s), systematic discrepancies appear in the prediction.

A serious problem is that the noise is underpredicted for observation locations less than 40°, i.e., for observers near the disk plane in front of the helicopter. To explore this effect, a single observation point in this range has been chosen for detailed analysis.

The Fourier spectra for this point are presented in Fig. 3 together with the results of our original (solid dots) and new (open triangles) calculations, to be described below. Although the new calculations improve the prediction, the predicted sound level is still less than the measured sound level.

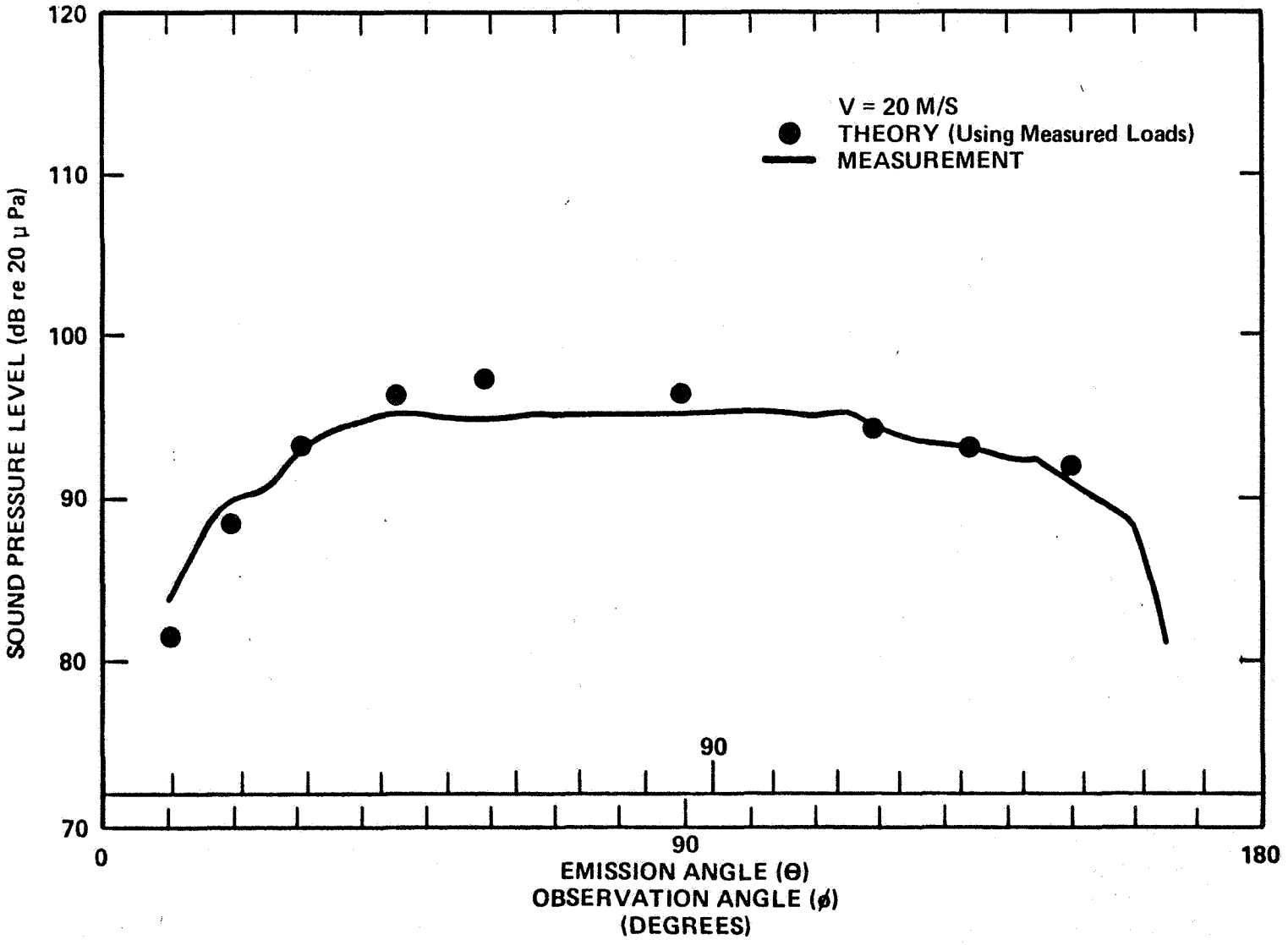

FIG. 1. COMPARISON OF MEASURED AND CALCULATED OVERALL SOUND PRESSURE LEVELS FROM A HELICOPTER DURING LOW SPEED LEVEL FLIGHT FOR A STATIONARY OBSERVER ON THE GROUND.

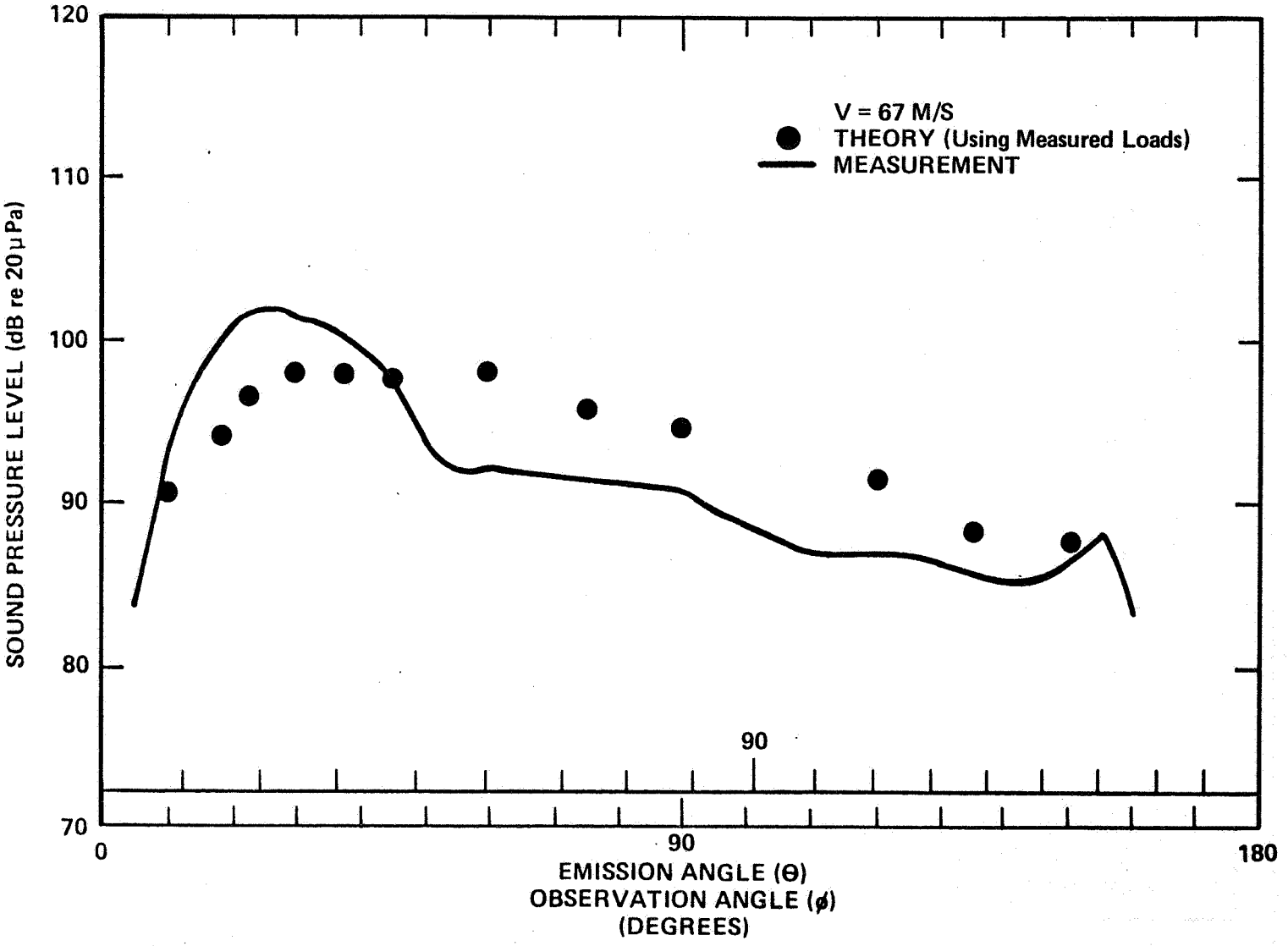

FIG. 2. COMPARISON OF MEASURED AND CALCULATED OVERALL SOUND PRESSURE LEVELS FROM A HELICOPTER DURING HIGH SPEED LEVEL FLIGHT FOR A STATIONARY OBSERVER ON THE GROUND.

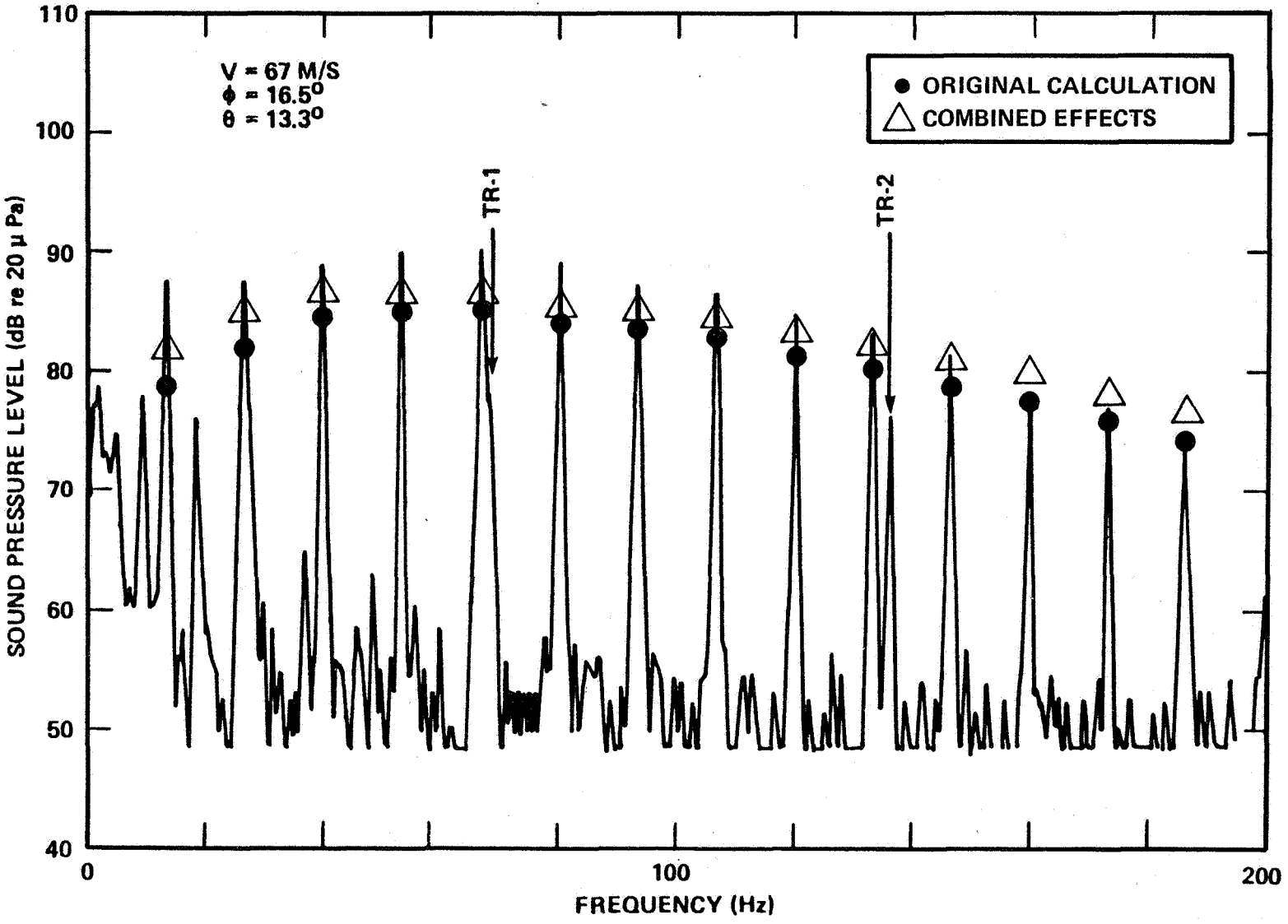

FIG. 3. INFLUENCE OF THE COMBINED EFFECTS ILLUSTRATED IN FIGS. 4 TO 7 ON THE PREDICTION OF THE ACOUSTIC SPECTRA AT THE POINT OF LEAST ACCURACY.

SECTION 2

DISCUSSION OF REFINED CALCULATION OF ROTOR SOUND FIELD

To discuss the new calculation we must first review the original calculation. This calculation used the known shape and motion of the rotor together with the measured blade surface pressures. Several assumptions were made. To represent the motion, the average velocity of the helicopter during its level flyover was used. To represent the pressure, only the component of pressure giving a force normal to the chord was used. Because the outermost measurement station was at the 95.5 percent radius, no load distribution information was available near the blade tips. Thus, for the original calculations, the loads were assumed to vanish linearly toward the tip. Moreover, the influence of pressure forces at the very tip of the blade, i.e., on the blunt surface perpendicular to the span at the rotor extremity, was not included.

Each of these effects was studied computationally and may be summarized as

1) Velocity perturbations

2) Chordwise pressures

3) Load distribution near the tip

4) Side edge tip pressures.

The influence of each of these effects is presented in detail in Table 1. Each effect will be discussed briefly. The new calculations in Fig. 3 correspond to the combined influence of all four of the above effects. Because of the discrepancy between the measurement and prediction, we will discuss three other potential noise sources. These sources are:

5) Shock noise

6) Quadrupole noise

7) Skin friction noise.

2.1 Velocity Perturbations

To represent the motion of the helicopter, the mean forward velocity was used. Fluctuations in forward velocity are relatively unimportant for low forward speeds because the tip

TABLE 1. MEASURED AND CALCULATED ACOUSTIC PRESSURE SPECTRA CORRESPONDING TO CONDITIONS OF FIGS. 3 TO 7.

Harmonic Number	A	B	C	D	E	F	G
1	88	79.2	81.9	79.5	79.2	79.2	82.3
2	88	82.8	85.1	83.5	82.8	82.8	85.6
3	89	84.4	86.0	85.2	84.4	84.4	86.7
4	90	85.3	86.1	86.3	85.3	85.3	86.9
5	91	85.3	85.7	86.3	85.3	85.3	86.6
6	89	84.6	85.2	85.8	84.6	84.6	86.3
7	88	83.9	84.5	85.3	83.9	83.9	85.8
8	87	83.0	83.4	84.5	83.0	83.1	84.9
9	85	81.8	82.5	83.5	81.8	81.9	84.0
10	83	80.5	81.4	82.4	80.5	80.5	82.9
11	81	79.2	79.7	81.3	79.2	79.2	81.3
12	79	77.9	78.2	80.0	77.9	77.9	80.0
13	77	76.3	76.5	78.5	76.3	76.3	78.6
14	75	74.5	74.4	76.8	74.5	74.5	76.8
OASPL	99	94.0	94.9	95.3	94.0	94.0	96.0

A - Measured

B - Original calculation

C - Measured upper and lower surface pressure at mean aircraft speed used in noise calculation

D - Instantaneous aircraft speed at emission time used

E - Estimated side edge pressure used

F - Tip region surface pressure assumed the same beyond 95 percent radius

G - Combined effect of C to F (new calculation)

Mach number is low. The greatest tip Mach number, which is achieved on the advancing blade, is .73 at a forward speed of 20 m/s and .87 at a forward speed of 67 m/s. At high forward speeds, (i.e., at high tip Mach number), the acoustic calculation is very sensitive to small changes in forward velocity. This effect occurs because the sound pressure is proportional to $(1-M_r)^{-3}$. The closer M_r is to one, the greater the sensitivity of the calculated signal to small changes in velocity. To improve the calculations, we matched the velocity (70.7 m/s) of the helicopter when the signal was emitted (Fig. 4). Inspection of Table 1 shows the overall level was increased by about 1.3 dB.

2.2 Chordwise Pressures

A second point of improvement was the model of the blade forces. Originally we chose the simplest form of the load distribution, i.e., to only use forces perpendicular to the chord. This procedure is reasonable because this normal to the chord is approximately in the direction of the lift, and the lift exceeds the drag by one to two orders of magnitude. This procedure is least accurate in the disk plane because the loading noise depends on the projection of the forces onto the direction from the blade to the observer. The normal to the chord is approximately perpendicular to the rotor disk plane, hence it is the forces parallel to the chord which have the greatest effect in the disk plane. Including the effect of the chordwise component pressure distribution increased the predicted noise by .9 dB (Fig. 5).

2.3 Tip Load Distribution

Measured blade loads were made out to the 95.5 percent station. Between measurement stations, the loads were assumed to vary linearly. Near the tip they were originally assumed to vanish linearly to zero. However, some experimental results for the flow field in the vicinity of a blade tip indicate that the classical spanwise loading, which vanishes smoothly to zero, is not valid near the tip. Chigier and Corsiglia [4] have reported detailed surface pressure measurements by Spivey [5] near the tip of a square tipped rectangular wing in a wind tunnel. The measurements show that the suction force on the upper surface of the blades is strong enough to cause a peak in the spanwise loading near the tip to a nearly rectangular distribution.

To see if this influenced the predicted sound field, we changed our original assumption about the load distribution. In place of tapering to zero, we now assume that the loads are constant from the 95.5 percent station to the tip. However, at

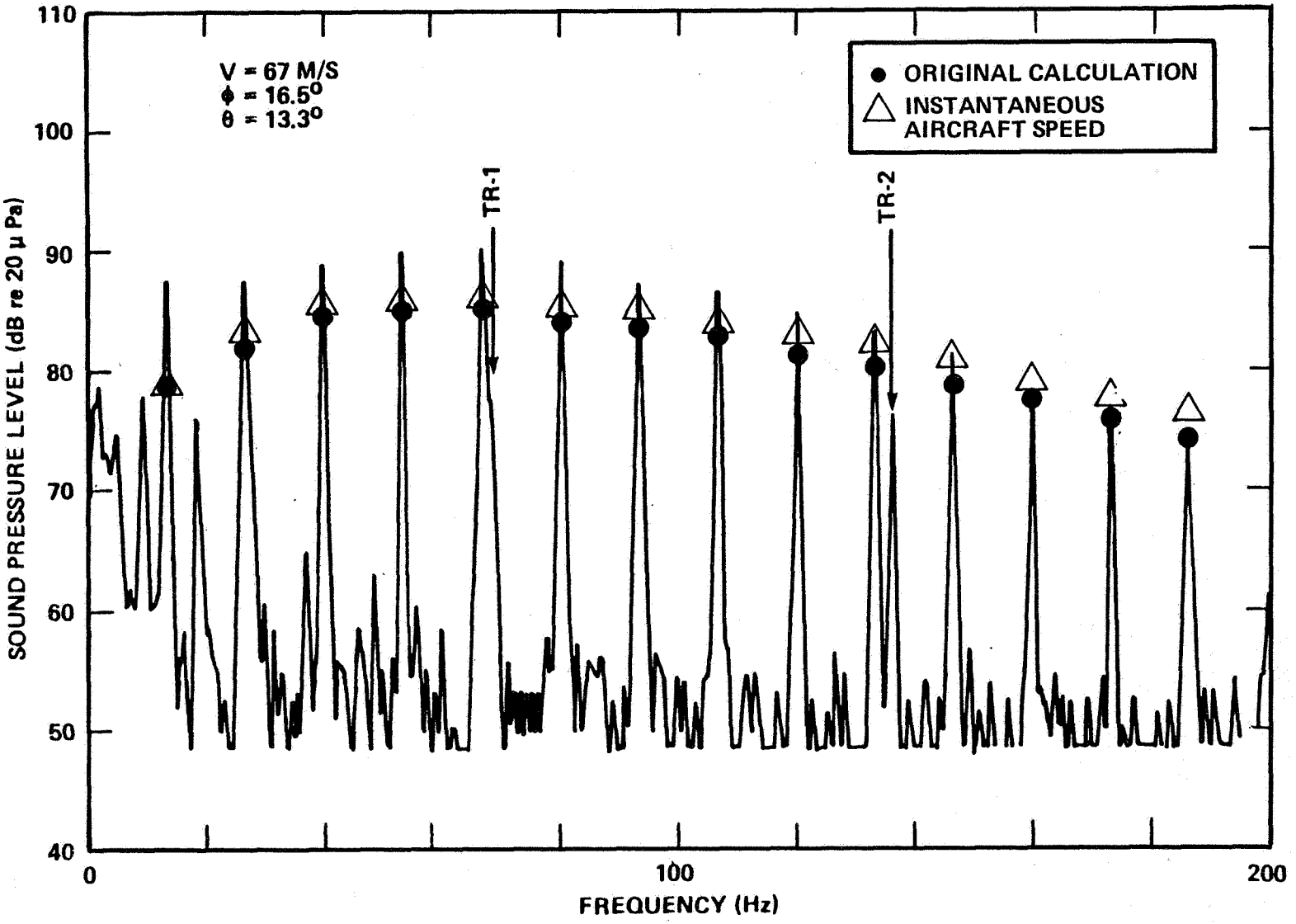

FIG. 4. INFLUENCE OF USE OF THE INSTANTANEOUS FLIGHT VELOCITY ON THE PREDICTION OF THE ACOUSTIC SPECTRA AT THE POINT OF LEAST ACCURACY.

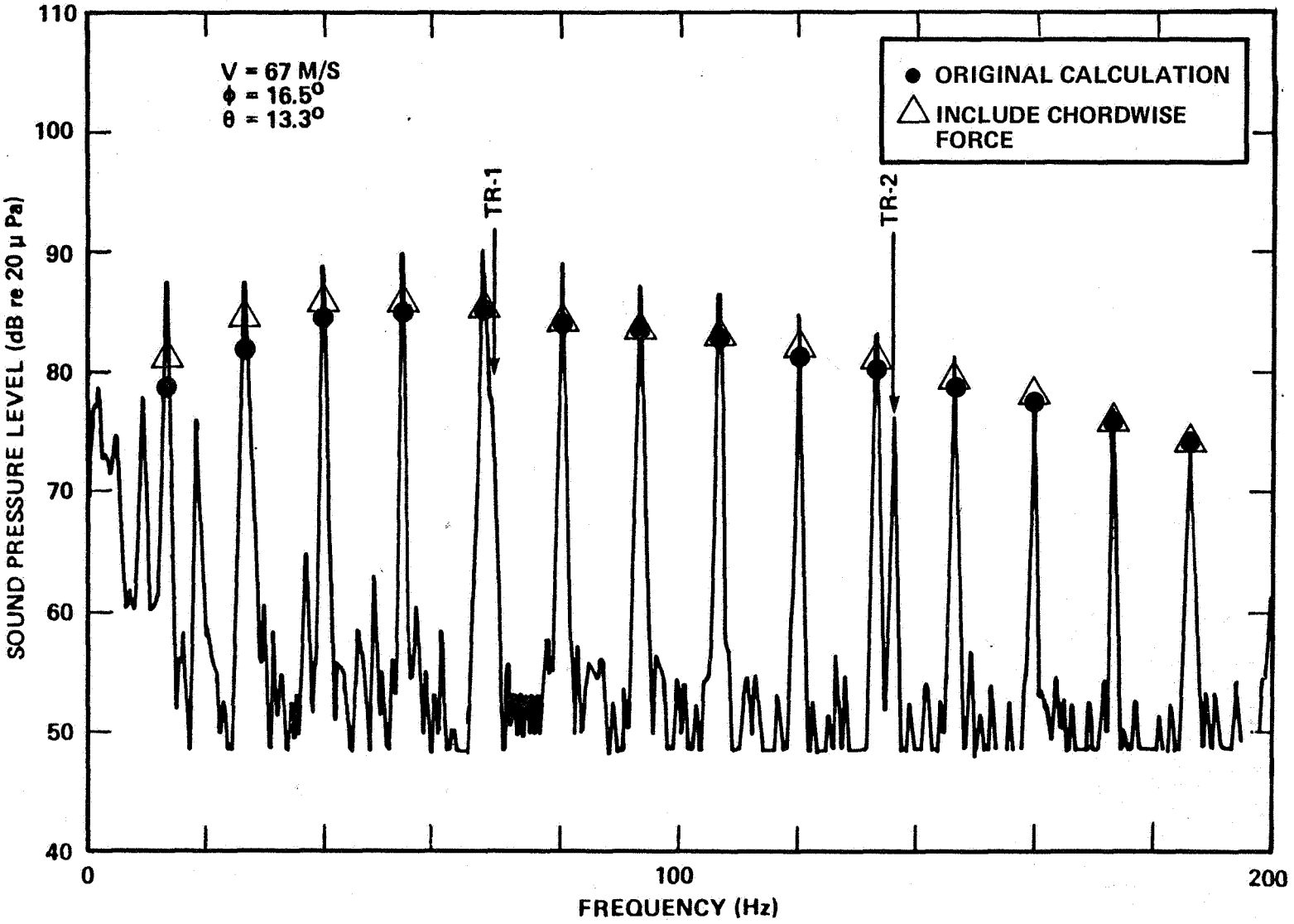

FIG. 5. INFLUENCE OF CHORDWISE PRESSURE DISTRIBUTION ON THE PREDICTION OF THE ACOUSTIC SPECTRA AT THE POINT OF LEAST ACCURACY.

this observation point, this change has no influence on the overall sound pressure level (Fig. 6).

NASA is presently reducing blade surface pressure data on a more refined version of the Bell AH-1G helicopter operational loads survey. One of the refinements was to make more surface pressure measurements near the blade tip. This improved measurement will enhance the understanding of the flow field near the main rotor blade tip. However, the present numerical experiment shows that, in this case, tip loading has a negligible influence on the predicted sound field. We recommend that the new blade surface pressure data near the blade tip be reviewed before incorporating it into the present noise prediction program. If this new data does not differ substantially from the limit cases in the numerical experiment, it is unlikely that the new data will improve the noise prediction.

2.4 Side Edge Tip Pressure

The calculation of the noise from a helicopter rotor depends on a detailed description of the fluid properties at the blade surface. Originally, we restricted our calculations to the upper and lower surface of the blades. There are two additional surfaces on a blunt tip rotor. These surfaces are the small side edges at either end of the blade. To see if conditions on these edges influenced the sound, the influence of the pressure field on the side edge near the rotor tip was considered.

No good measurements are available to describe this influence. We made two assumptions about the magnitude of these pressures. The first assumption was that this side edge pressure was equal to the minimum measured pressure at the 95.5 percent station and did not vary with azimuth or chordwise position. The second assumption was that this side edge pressure was the average of the upper and lower surface pressures at the 95.5 percent station, the outermost measurement station. Thus, the side edge pressure varied in both the chordwise and azimuthal directions. The calculations based on this second assumption are given in Table 1 and presented in Fig. 7. In this instance, the side edge pressure has almost no influence on the overall sound pressure level.

The tip noise, however, requires further study since in numerical work on hovering rotors the tip noise was found to affect the level of harmonics by several decibels. Of course, any observations are very dependent on the observer location and motion of the vehicle. An effect which is unimportant here may be very important given other circumstances. The intent here is

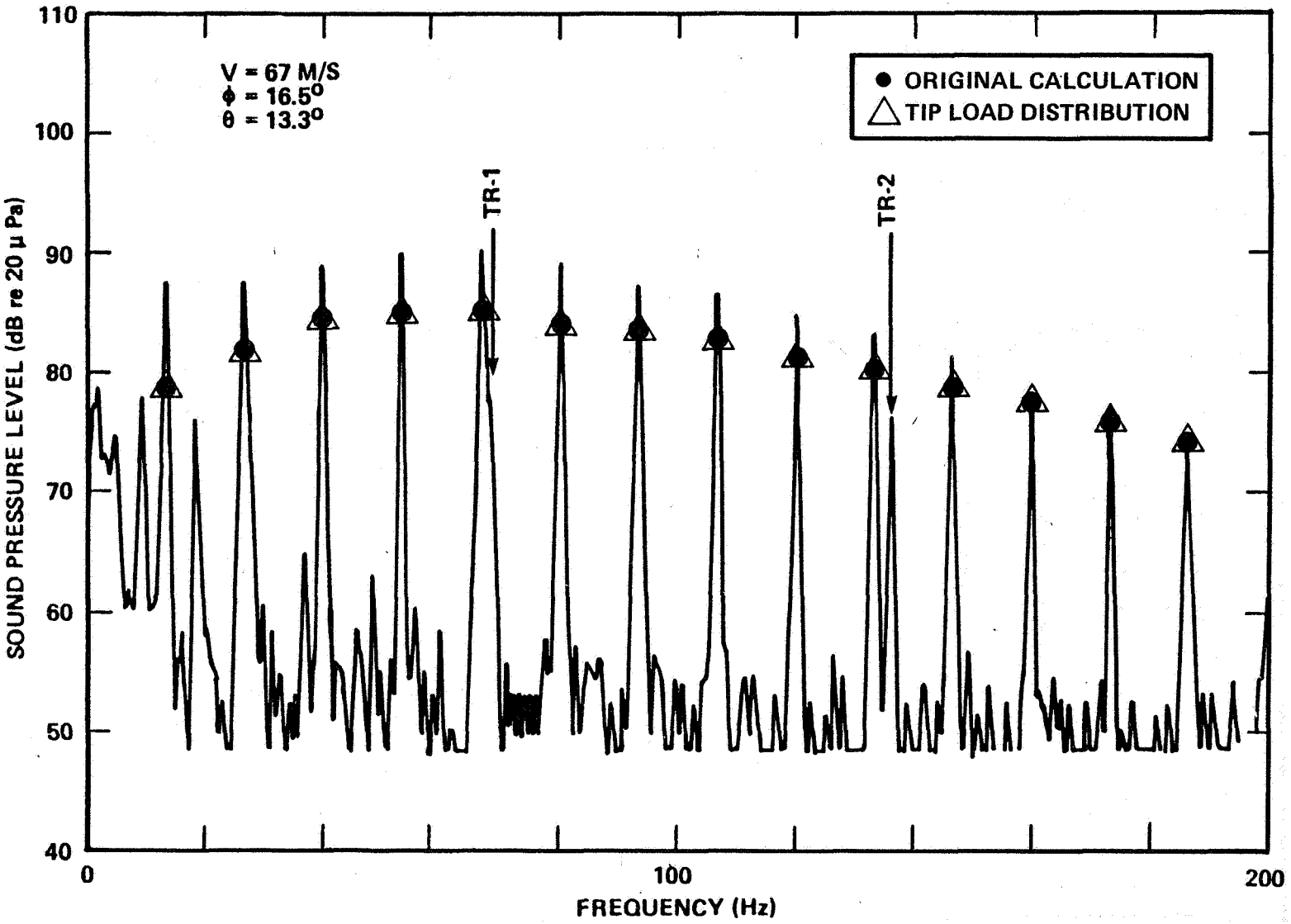

FIG. 6. INFLUENCE OF A MODIFIED TIP LOAD DISTRIBUTION ON THE PREDICTION OF THE ACOUSTIC SPECTRA AT THE POINT OF LEAST ACCURACY.

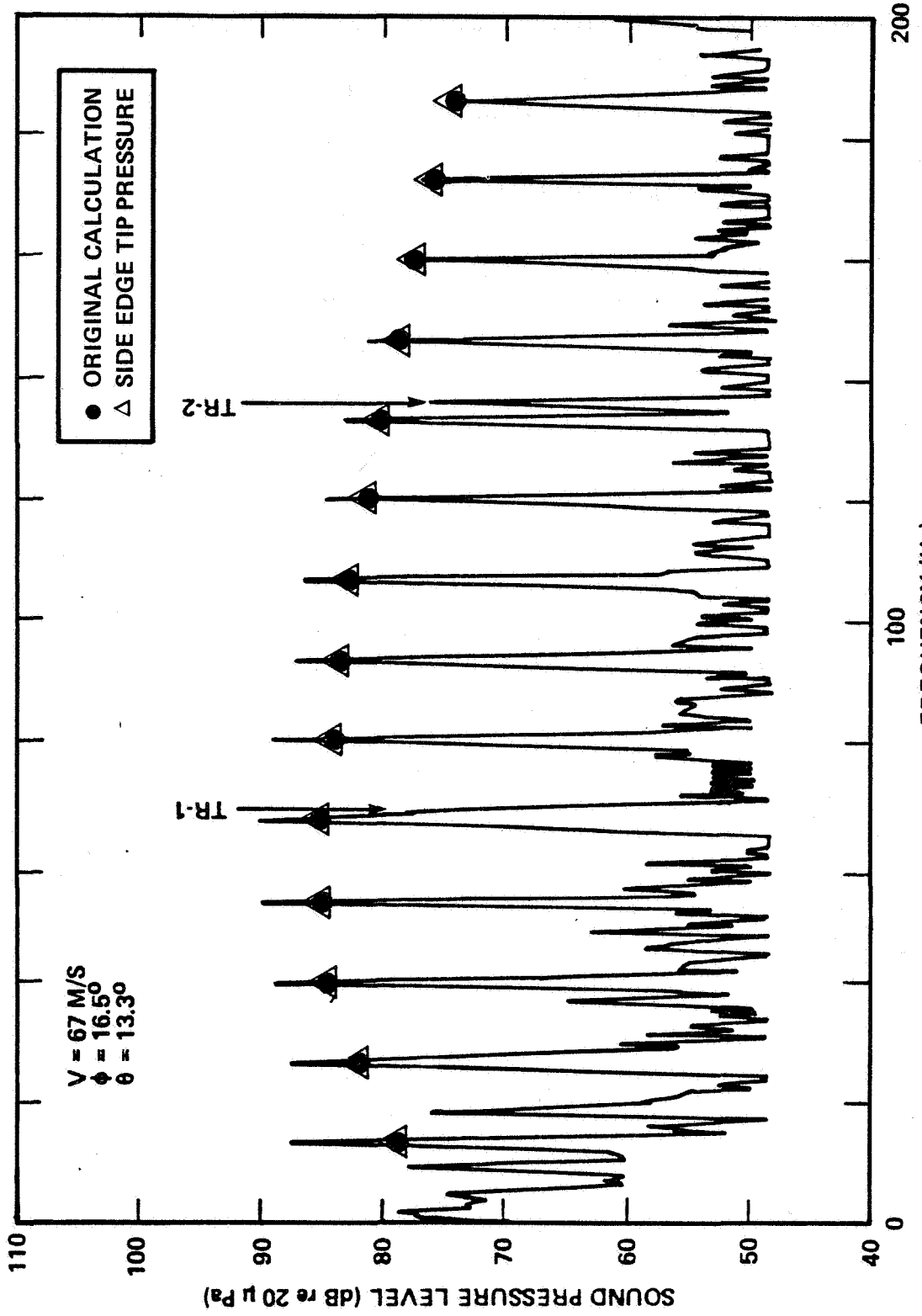

FIG. 7. INFLUENCE OF THE SIDE EDGE STEP PRESSURE ON THE PREDICTION OF THE ACOUSTIC SPECTRA AT THE POINT OF LEAST ACCURACY.

to select the point of worst agreement in the previous study [3] and explore effects which may improve the prediction.

2.5 Combined Effect

The combined effect of the velocity perturbation, chordwise pressures, tip load distribution, and side edge tip pressure are also given in Table 1. This combined effect, which is termed the new calculation, is plotted in Fig. 3. The discrepancy at high speed (67 M/S) does not appear at low speeds (20 M/S), as is evidenced from the comparison made in Fig. 8, which is taken from the original report [3]. Though the prediction is improved, it is still less than the measured noise by 3 dB overall and by 5.7 dB in the first harmonic. That the overall level is closer than the level in any given harmonic indicates compensating errors in the prediction. A discrepancy of 5.7 dB in the first harmonic indicates that we have neglected an important effect in our calculation. The remainder of this section reviews three possible effects: shock noise, quadrupole noise, and skin friction noise.

2.6 Shock Formation

One possible noise source that has been neglected to date is sound emission from a shock located near the tip of the blade. A recent experimental study by Succi has shown that a moving shock can emit a sound pulse equal in magnitude to the rotational noise of the propeller [6]. In this experiment, the shock oscillated at high frequency, thereby allowing its contribution to be easily identified. It is therefore possible that a shock could be a source of noise in helicopters. The first task is to inspect the measured blade loads for evidence of shocks. Figure 9 is a plot of the measured upper and lower surface pressures at the outermost radial stations ($r/R = 95.5\%$) with the rotor located at its point of maximum velocity ($\psi = 90^0$). Each point in the plot corresponds to an instantaneous measurement. No interpolation is made.

There are two aspects of this plot to notice. First, note that the upper and lower surface pressures are nearly the same. This indicates that the blade element is at approximately zero angle of attack. Next note that a strong discontinuity in pressure is evident on both the upper and lower surfaces. The measurement stations at either side of this discontinuity are at the 25 percent and 35 percent blade stations. The maximum blade thickness is at the 30 percent station. Thus the shock occurs near the point of greatest thickness on the blade. Another feature is that the shock on the lower surface is stronger than the shock on the upper surface.

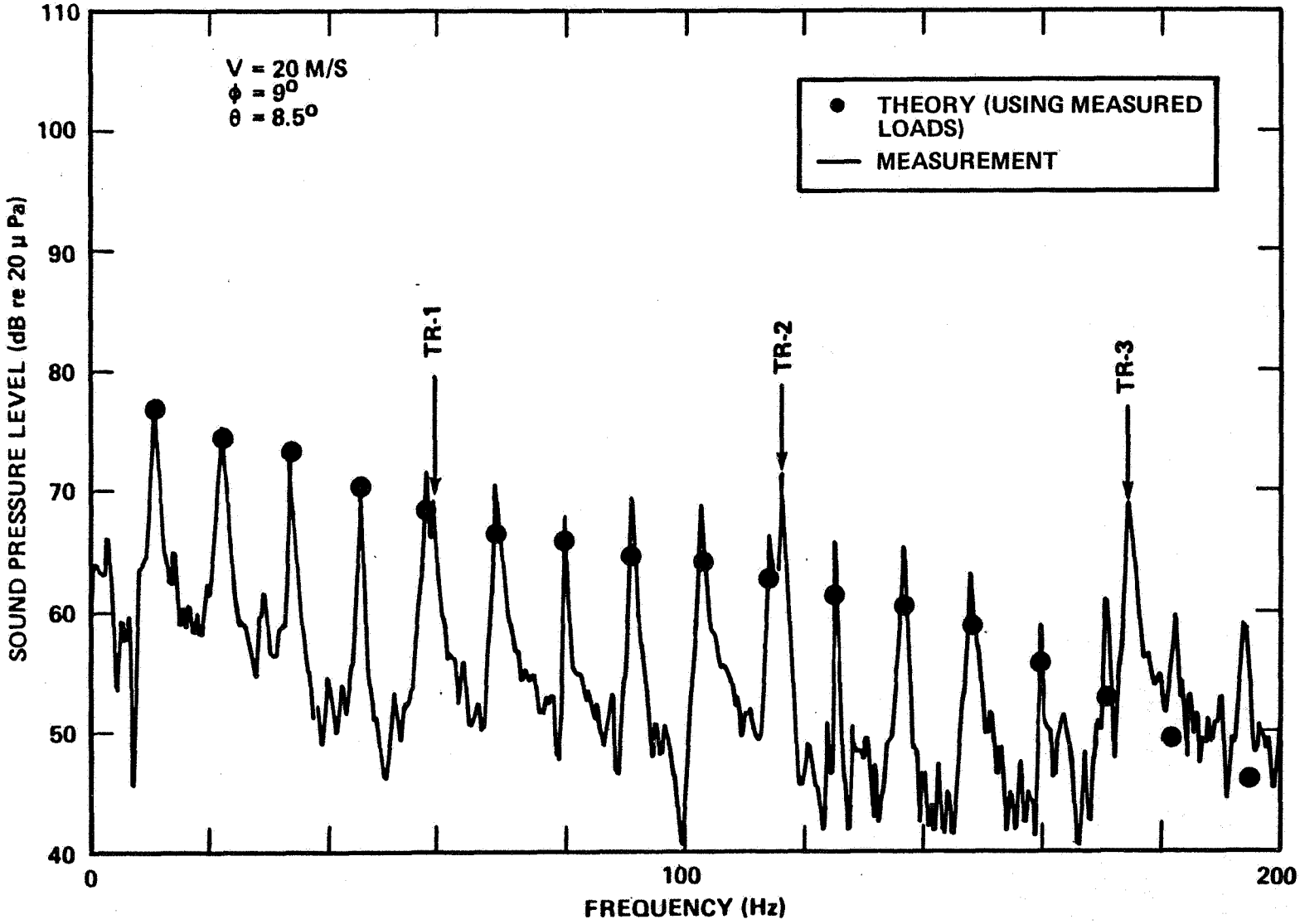

FIG. 8. ILLUSTRATION OF THE GOOD PREDICTION ATTAINABLE FOR LOW SPEED FLIGHT AT AN OBSERVATION ANGLE SIMILAR TO THAT ILLUSTRATED AT HIGH SPEEDS IN FIG. 3.

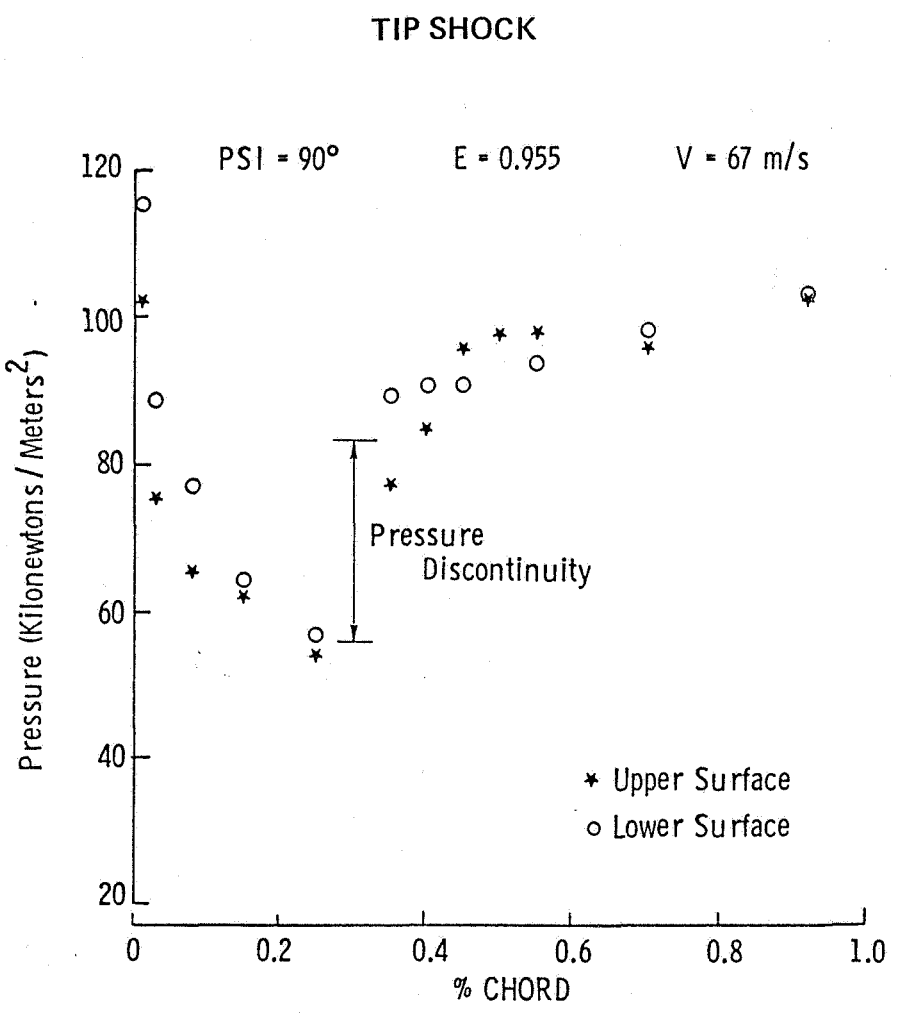

FIG. 9. MEASURED SURFACE PRESSURE DATA INDICATING A SHOCK ON THE UPPER AND LOWER SURFACE NEAR THE TIP OF THE ADVANCING BLADE DURING HIGH SPEED LEVEL FLIGHT.

Though we cannot conclude that the excess noise is due to shocks on the blade tip, the experimental evidence of these shocks does indicate that shocks should be studied as a possible source of noise in helicopter rotors. A theoretical work on this subject is by Kitaplioglu and George [7]. One can formally apply the acoustic analogy to calculate the noise from moving shocks. The discontinuities in the Lighthill stress tensor act like sources on the shock surface [8].

Care must be taken to account for compensating terms when applying this model. For example, the discontinuity in pressure across the shock is balanced by the discontinuity in velocity normal to the shock. Though each discontinuity can influence the sound field, the effects may cancel one another. One possible shock noise source, which has not yet been explored in detail, is the entropy generated at the shock surface. In Lighthill's [9] formulation this entropy source might be represented as $(c^2 - c_0^2)\ \rho_0\ \delta_{ij}$ where ρ_0 is the air density, c is the local speed of sound and c_0 the speed of sound at infinity. In Howe's [10] formulation this source is described directly as T grad S where T is the temperature and S the entropy.

2.7 Quadrupole Noise

The effects of quadrupole noise have been discussed at length by Hanson and Fink [11]. They identify the velocity perturbation along the blade chord as the most important term. The observation is that the Reynolds' stresses are convected with the blade element section and it is the periodic variation of the direction of these stresses at high rates of speed which generates the noise. An important observation of Hanson and Fink is that, for nonlifting parabolic arc blades, the thickness and quadrupole terms are of equal importance between the section critical Mach number and Mach 1. Outside of this range, the quadrupole terms are unimportant. This section critical Mach number is that Mach number at which the flow is locally transonic. It is possible that these conditions are met near the tip of the rotor on the advancing blade ($\psi = 90^0$). One indication is that the maximum value of the tip speed, which is the sum of the rotational and forward speeds of the rotor, is Mach .87. The rotor blades on this helicopter are modified NACA 0012 airfoils and the flow is locally transonic when these airfoils have kinematic Mach numbers as small as Mach .87.

Another strong indicator of transonic flow is the evidence of a shock wave on the 95.5 percent radial station. Thus, on the advancing blade at high forward speeds, the blade elements near the rotor tip move at speeds between the section critical Mach number and Mach 1. Therefore, the criteria of Hanson and Fink is

met and quadrupole noise should be considered as a possible source of the excess noise. At present, the computer code developed at Langley is being modified to include a part of the quadrupole sources described earlier.

2.8 Skin Friction

We have not considered the effect of skin friction in detail. Qualitatively, it will have roughly the same influence as the addition of forces due to the chordwise component of pressure. That is, it is an additional force whose direction is parallel to the blade element velocity. Quantitatively, the drag on a stationary airfoil is about 80 percent skin friction and 20 percent chordwise pressure distribution. Thus, from an acoustical standpoint, the magnitude of skin friction effects will also be about the same as the magnitude of the chordwise contribution of the pressure distribution.

SECTION 3.
CONCLUSIONS

Recent methods developed for the prediction of helicopter noise are based wholly on fundamental acoustic principles. This paper describes a study of the analysis developed by Farassat which requires detailed input specifications of the rotor characteristics, operating conditions, and rotor blade surface pressure distribution. This present study uses measured data for an AH-1G helicopter from the extensive database of the Operational Loads Survey [2]. The study is a continuation of a previous study at BBN using the Farassat noise prediction based on the measured loads on the AH-1G helicopter main rotor[3]. Discrepancies between the measured and predicted noise field were evident in the previous study, particularly at high forward flight speeds.

The goal of the present study is to further refine the inputs to Farassat's prediction in an attempt to alleviate these errors. However, at present, Farassat's model can only account for the thickness and loading noise sources (although improvements are presently underway at NASA Langley). If noise sources other than the thickness and loading are important then no amount of refinement in the description of these terms will make the predictions accurate. We found that refinements in this description improved the prediction; however, discrepancies between the measured and predicted noise field remain. These discrepancies are most likely due to sources located in the convected fluid perturbations in the immediate vicinity of the main rotor blade. Detailed review of the blade surface pressure data (Appendix A) indicated shocks near the tip of the main rotor during high speed flights. The influence of these shocks cannot be predicted if only surface sources (thickness and loading terms) are used.

REFERENCES

1. Shockey, G.A., Williamson, J.W., and Cox, C.R., "AH-1G Helicopter Aerodynamic and Structural Loads Survey," USAAMRDL-TR-76-39, Bell Helicopter Textron, February 1977.

2. Brieger, J.T., "Validation of Helicopter Noise Prediction Techniques - Data Base," Bell Helicopter Textron Report 699-099-119, February 1980.

3. Succi, G.P., "Validation of Helicopter Noise Prediction Techniques," NASA CR 165715, April 1981.

4. Chigier, N.A., and Corsiglia, V.R., "Tip Vortices - Velocity Distributions," NASA TM X-62087, 1971. (Also Preprint #522, 27th Ann. National V/STOL Forum of the AHS, May 1971.

5. Spivey, R.F., "Blade Tip Aerodyanmics - Profile and Planform Effects," 25th Annual National Forum, AHS, Washington, DC, May 1968.

6. Succi, G.P., Munro, D.H., and Ingard, U.K., "Propeller Tone Bursts," accepted by Journal of Sound and Vibration, to be published in February 1983.

7. Kitaplioglu, C., and George, A.R., "Study of the Far-Field Sound Due to Unsteady Shocks on Helicopter Rotors, AIAA Paper 77-1360, 1977.

8. Farassat, F., "The Acoustic Far-Field of Rigid Bodies in Arbitrary Motion," Journal of Sound and Vibration, 32, 1974, pp. 387-405.

9. Lighthill, M.J., Proc. Roy. Soc. A211, 1952.

10. Howe, M.S., "Contributing to the Theory of Aerodynamic Sound with Application to Excess Jet Noise and the Theory of the Flute," J. Fluid Mech., Vol. 71, Part 4, 1975.

11. Hanson, D.B., and Fink, M.R. "The Importance of Quadrupole Sources in Prediction of Transonic Tip Speed Propeller Noise," Journal of Sound and Vibration, 62(1), 1979, pp. 19-38.

LIST OF SYMBOLS

c	=	local speed of sound
c_0	=	speed of sound in ambient medium
M_r	=	relative Mach number of flow at blade tip
r	=	radial distance
R	=	radius of blade
TR-i	=	i^{th} harmonic of tail rotor blade passing frequency
V	=	forward speed

GREEK

θ	=	emission angle
ψ	=	observation angle
ρ	=	air density

APPENDIX A
PLOTS OF BLADE PRESSURES

APPENDIX A

PLOTS OF BLADE PRESSURES

In this appendix, plots are presented of the detailed blade surface pressure data. The intent was to locate those instances in which shocks may have occurred. One such case was discovered ($V = 67$ M/S, $\psi = 90^0$, $r/R = 95.5\%$) and is presented as Fig. 9 in the text. Herein, a systematic presentation of the measured blade surface pressure is given in graphical form. Each graph represents the measured blade surface pressures as the ordinate and the chordwise location as the abcissa. Stars indicate measurements on the upper surface and circles measurements on the lower surface. A series of graphs is given representing changes in velocity (V = 20, 41, and 67 M/S), radial station (E = 40, 60, 75, 86.4, and 95.5% position) and azimuth (psi = 90, 180, 270, and 360°). In the usual manner, 90° represents the advancing blade position at its maximum kinematic velocity, at 180° the blade is in front of the helicopter, at 270° the blade is on the retreating side, and at 360° (or, equivalently, at 0°) the blade is pointing toward the tail. The graphs are organized so that the azimuthal index varies most rapidly, the radial station less rapidly, and the velocity least rapidly.

Beside the indication of shock, the only point of note is the bad measurement on the lower surface of the blade at the 86.4% radial station and 59.95% chordwise station (the transducer was not working and only measured atmospheric pressure, which was 108.2 KN/M^2 on the day of the test). Altering the computer program to interpret the load data linearly between the two adjacent measurement stations had no measurable effect on the noise prediction.

The data presented here are the actual measurements used by BBN as input to the Farassat computer program. This data may be normalized in the usual aerodynamic manner by the transform $P_{normalized} = (P_{measured} - P_0)/P_0$, where $P_0 = 108.2$ KN/M^2. The data is presented in the order given in Table A-1.

TABLE A-1

Figure	Velocity (M/S)	Radius (%)	Azimuth (degrees)
A-1	20	40.0	90
A-2	20	40.0	180
A-3	20	40.0	270
A-4	20	40.0	360
A-5	20	60.0	90
A-6	20	60.0	180
A-7	20	60.0	270
A-8	20	60.0	360
A-9	20	75.0	90
A-10	20	75.0	180
A-11	20	75.0	270
A-12	20	75.0	360
A-13	20	86.4	90
A-14	20	86.4	180
A-15	20	86.4	270
A-16	20	86.4	360
A-17	20	95.5	90
A-18	20	95.5	180
A-19	20	95.5	270
A-20	20	95.5	360
A-21	41	40.0	90
A-22	41	40.0	180
A-23	41	40.0	270
A-24	41	40.0	360
A-25	41	60.0	90
A-26	41	60.0	180
A-27	41	60.0	270
A-28	41	60.0	360
A-29	41	75.0	90
A-30	41	75.0	180
A-31	41	75.0	270
A-32	41	75.0	360*

*Because of computer printing errors, the last 15% of the data near the blade trailing edge is missing from this graph.

TABLE A-1 (Cont.)

Figure	Velocity (M/S)	Radius (%)	Azimuth (degrees)
A-33	41	86.4	90
A-34	41	86.4	180
A-35	41	86.4	270
A-36	41	86.4	360
A-37	41	95.5	90
A-38	41	95.5	180
A-39	41	95.5	270
A-40	41	95.5	360
A-41	67	40.0	90
A-42	67	40.0	180
A-43	67	40.0	270
A-44	67	40.0	360
A-45	67	60.0	90
A-46	67	60.0	180
A-47	67	60.0	270
A-48	67	60.0	360
A-49	67	75.0	90
A-50	67	75.0	180
A-51	67	75.0	270
A-52	67	75.0	360
A-53	67	86.4	90
A-54	67	86.4	180
A-55	67	86.4	270
A-56	67	86.4	360
A-57	67	95.5	90
A-58	67	95.5	180
A-59	67	95.5	270
A-60	67	95.5	360

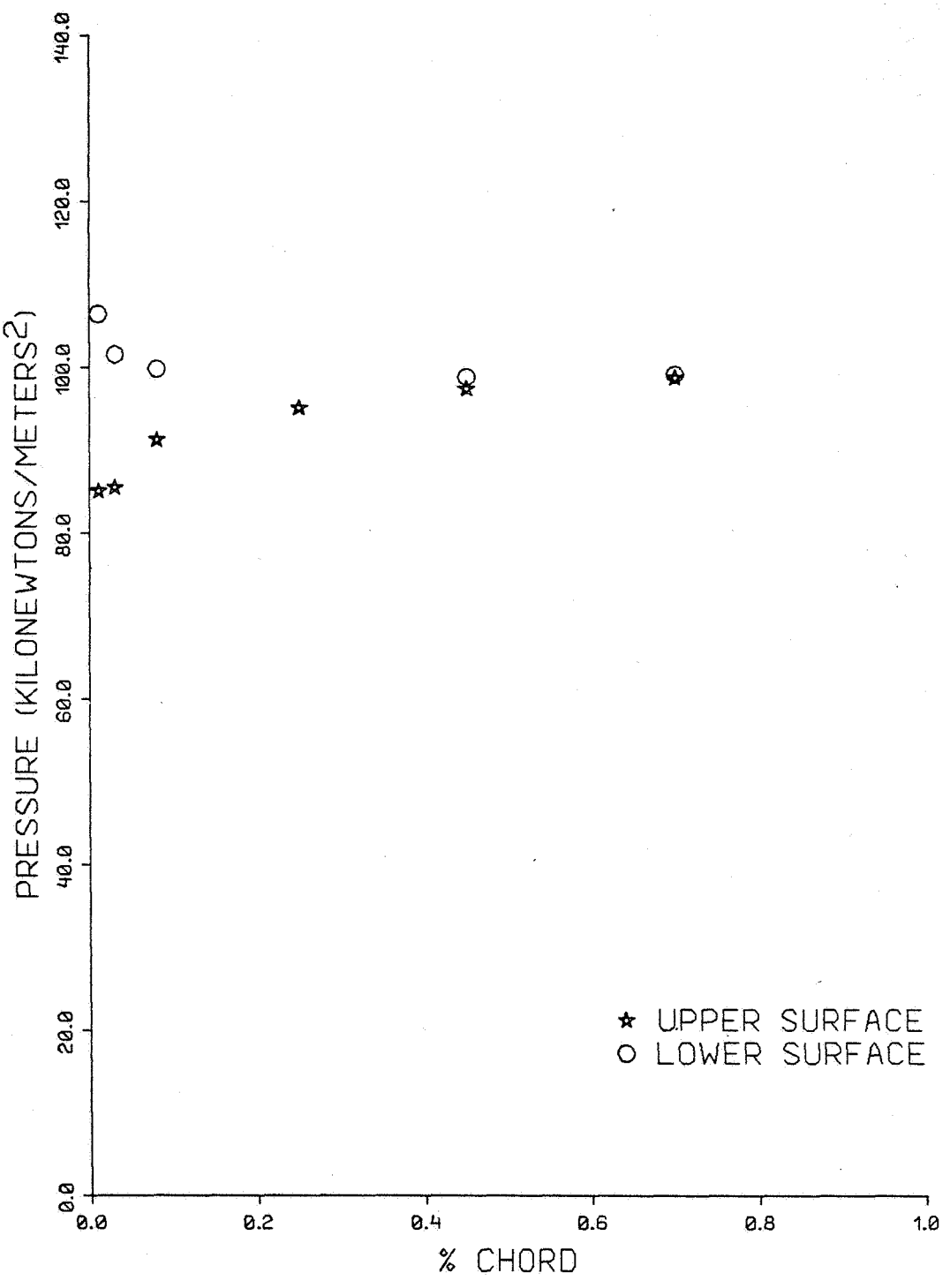

FIG. A-1. SUCCI-BBN

MEASURED BLADES SURFACE PRESSURES

PHI = 180 deg E = 0.400 V = 20 m/s

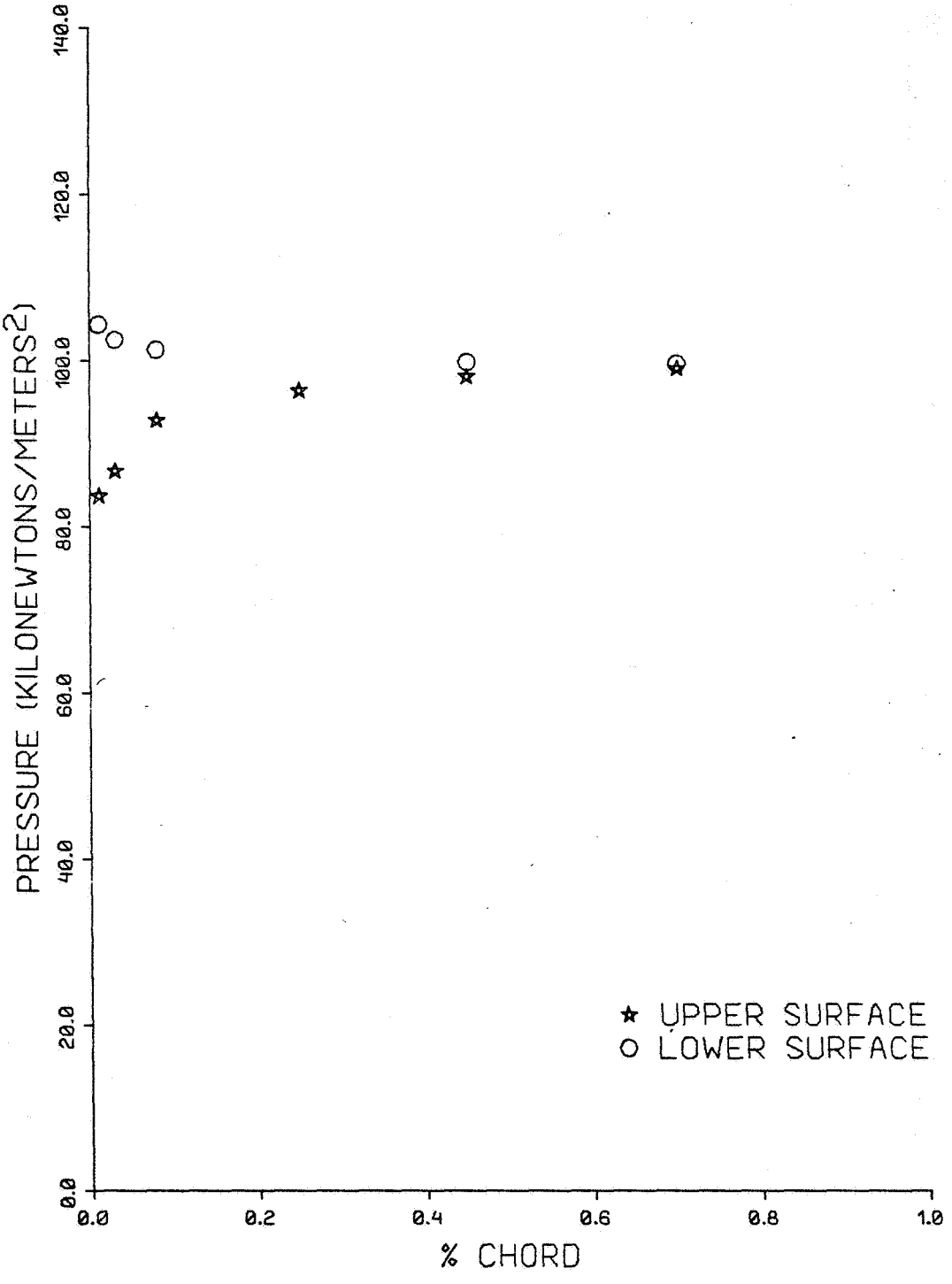

FIG. A-2.

SUCCI-BBN

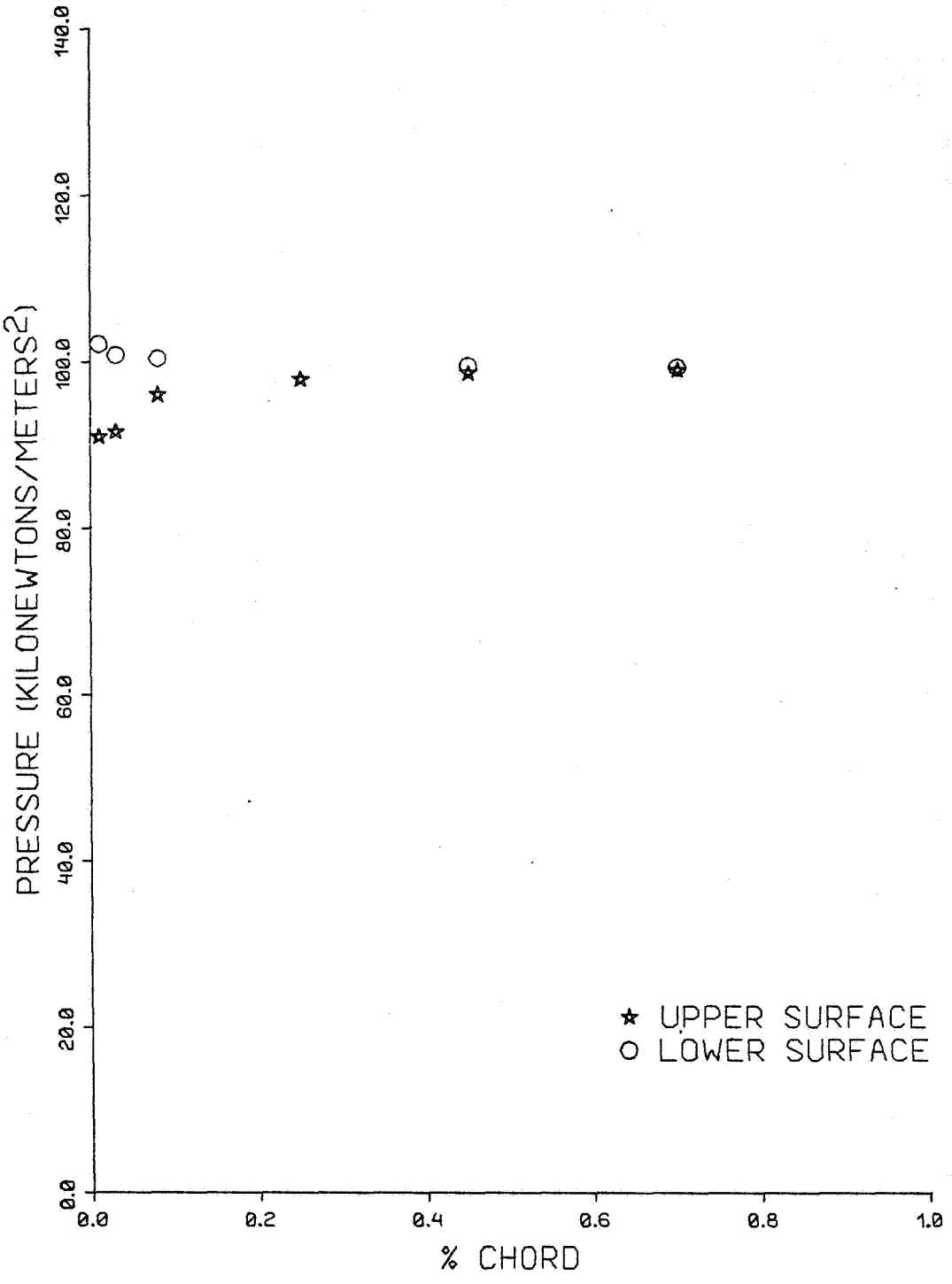

FIG. A-3. SUCCI-BBN

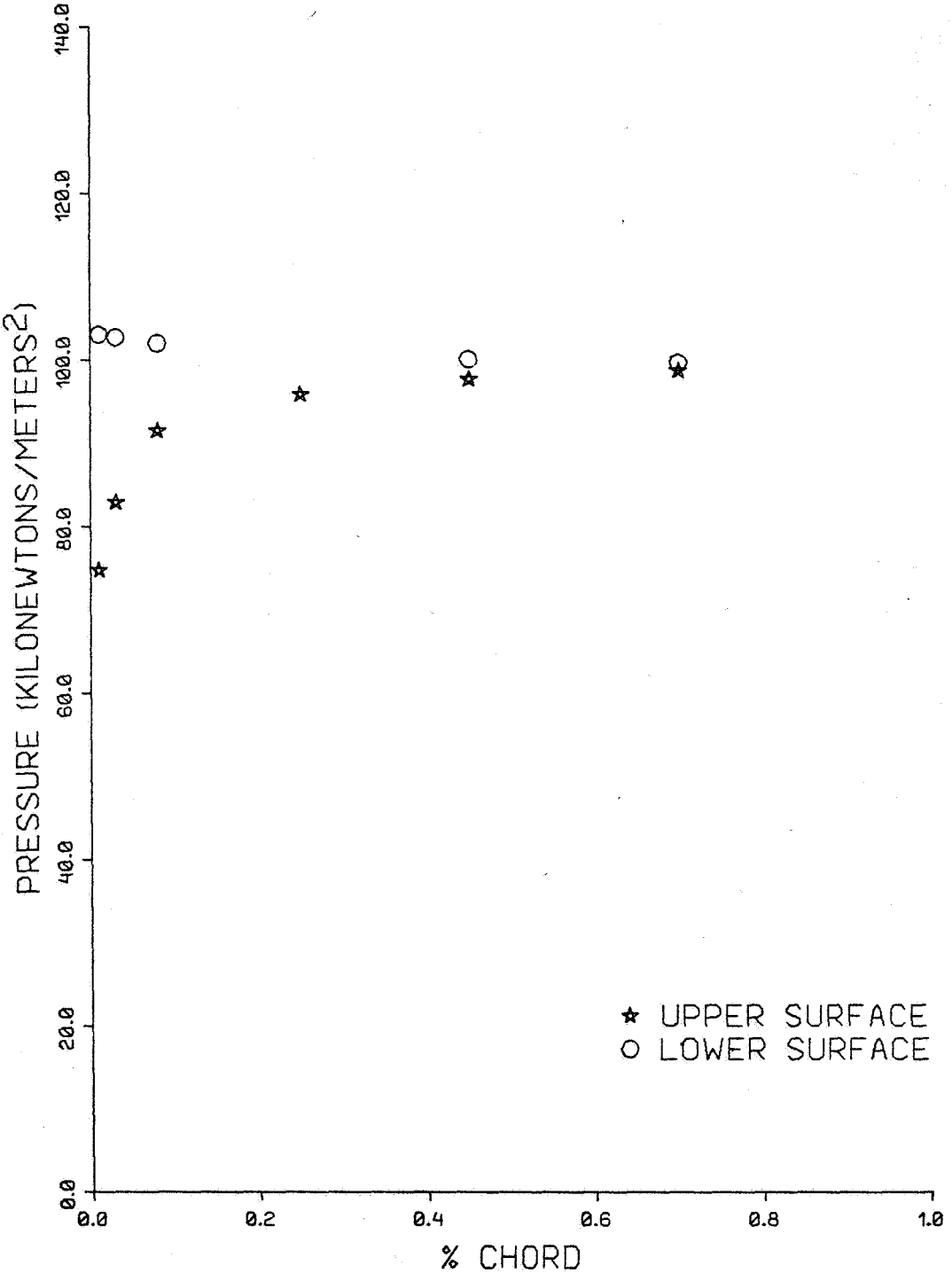
MEASURED BLADES SURFACE PRESSURES
PHI = 360 deg E = 0.400 V = 20 m/s
PRESSURE (KILONEWTONS/METERS2)
140.0
120.0
100.0
80.0
60.0
40.0
20.0
0.0
0.0
0.2
0.4
0.6
0.8
1.0
% CHORD
UPPER SURFACE
LOWER SURFACE
SUCCI-BBN

FIG. A-4.

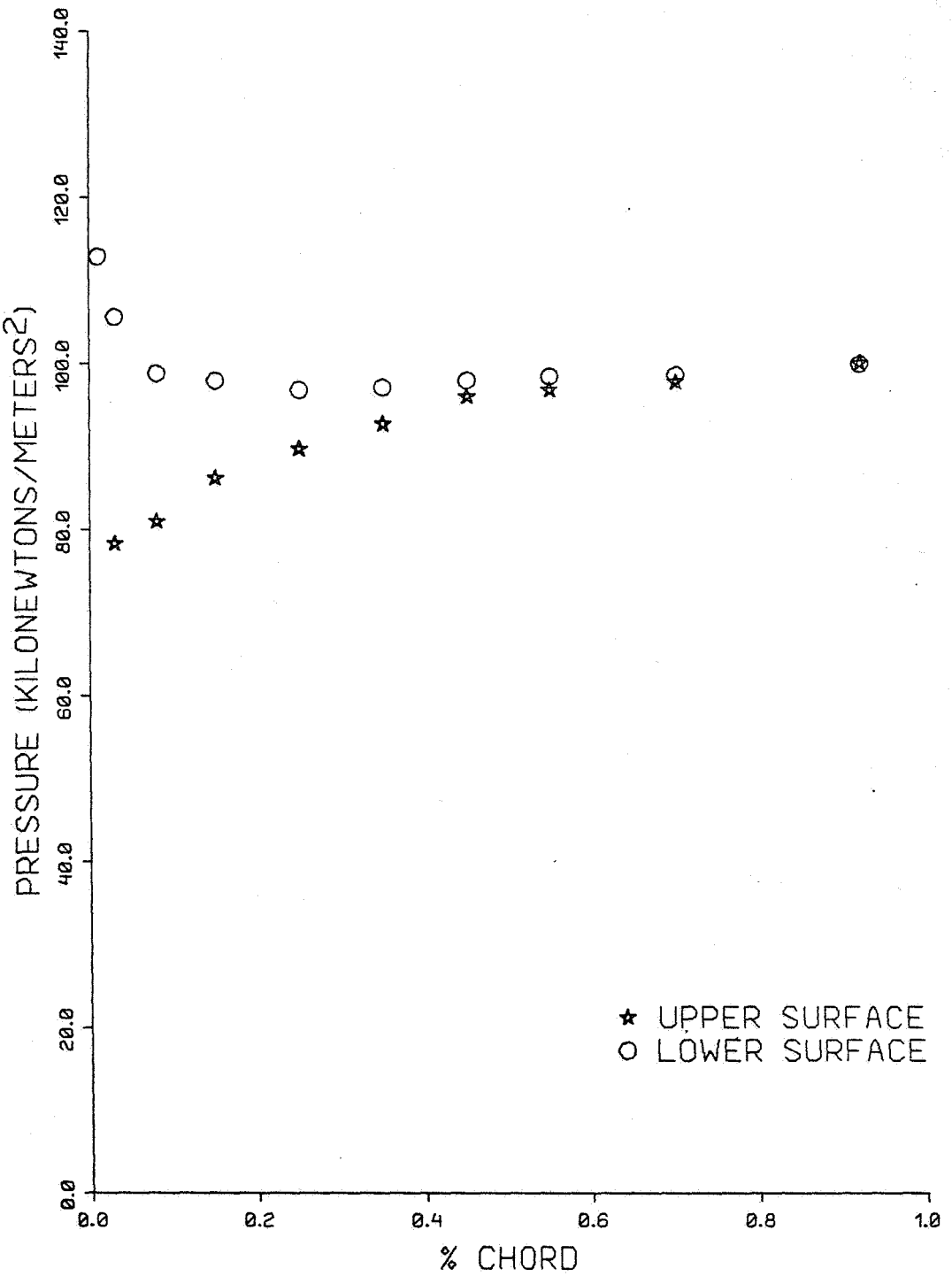

FIG. A-5.

SUCCI-BBN

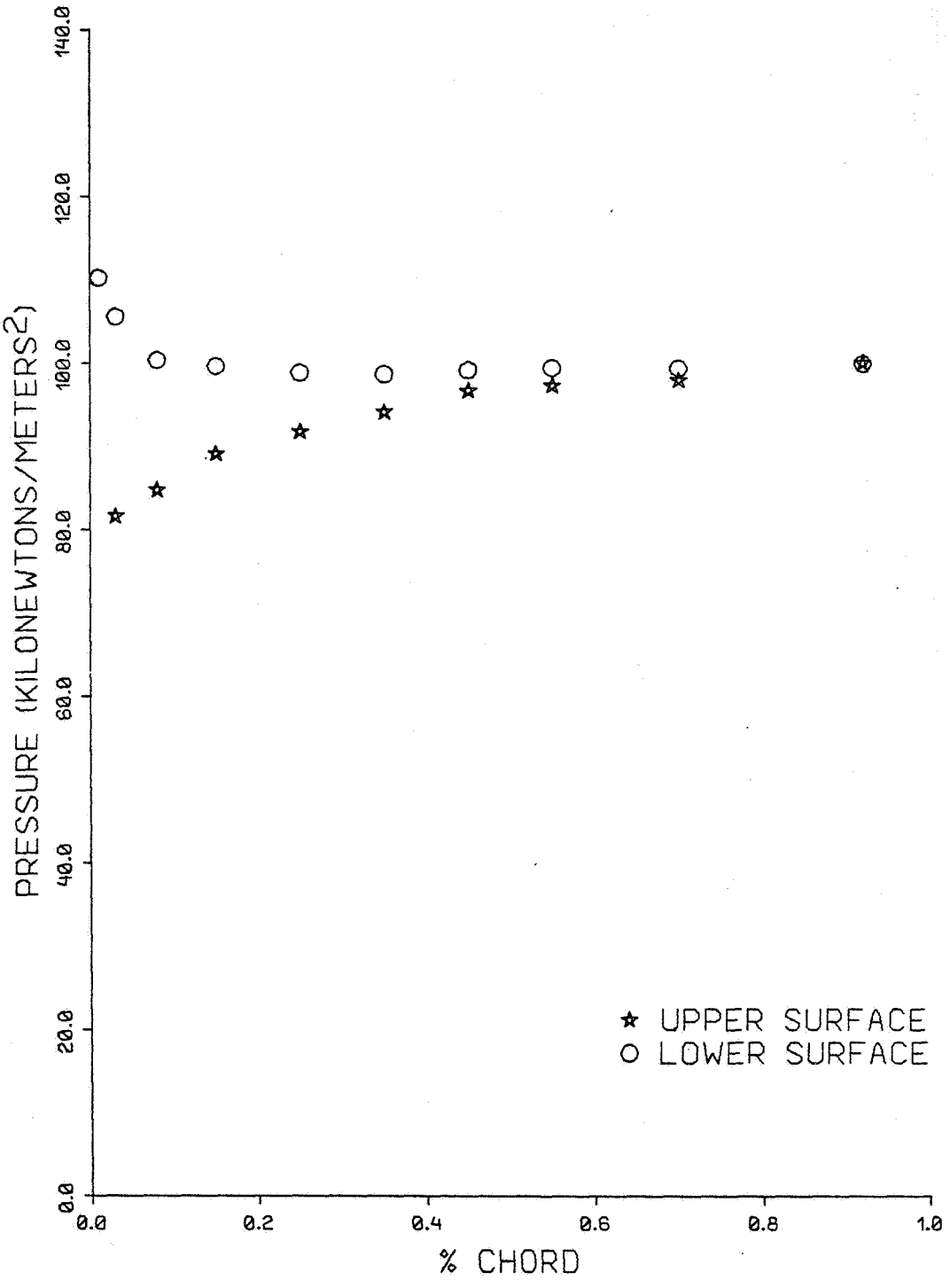

FIG. A-6.

SUCCi-BBN

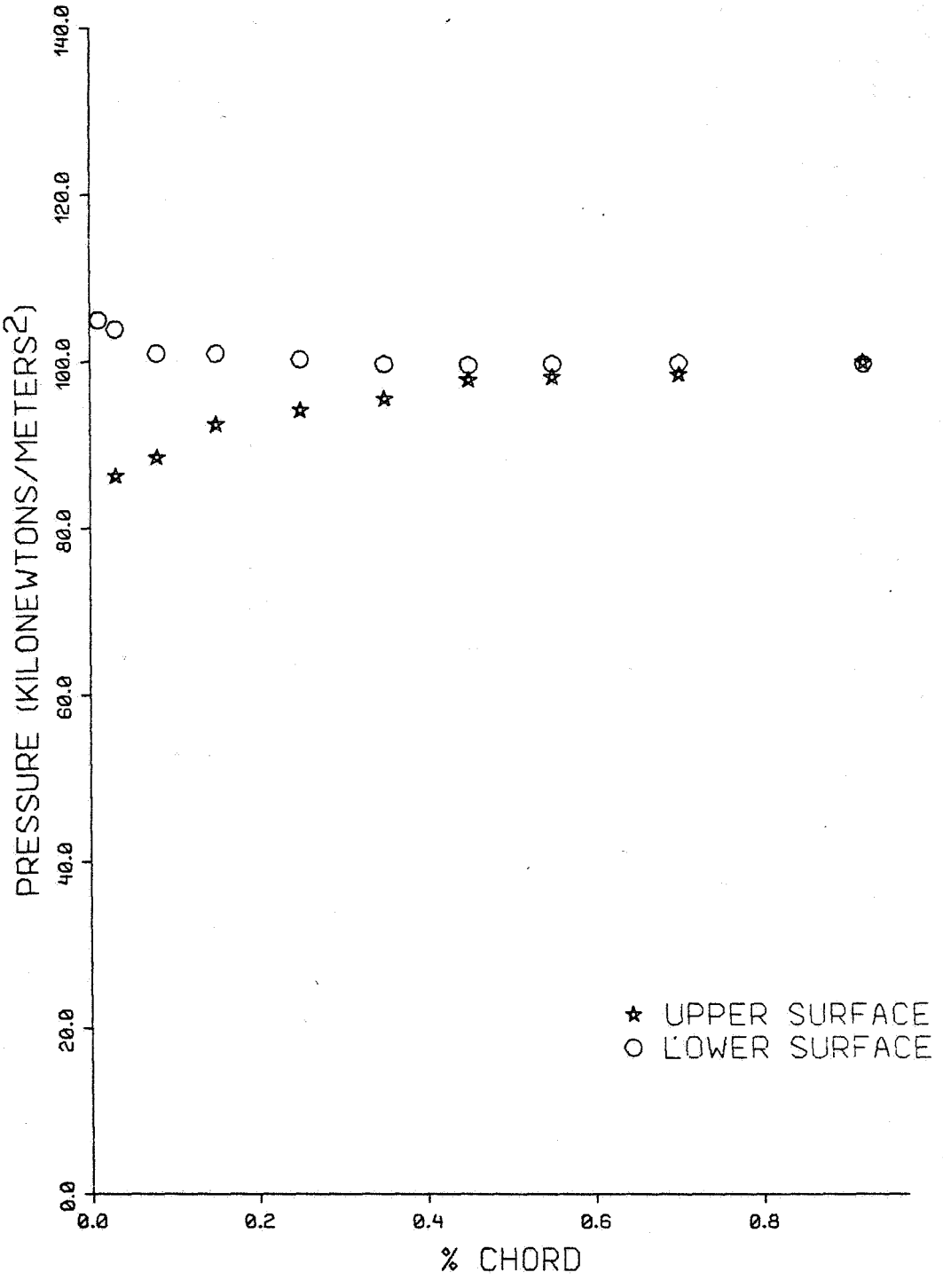

FIG. A-7.

SUCCI-BB

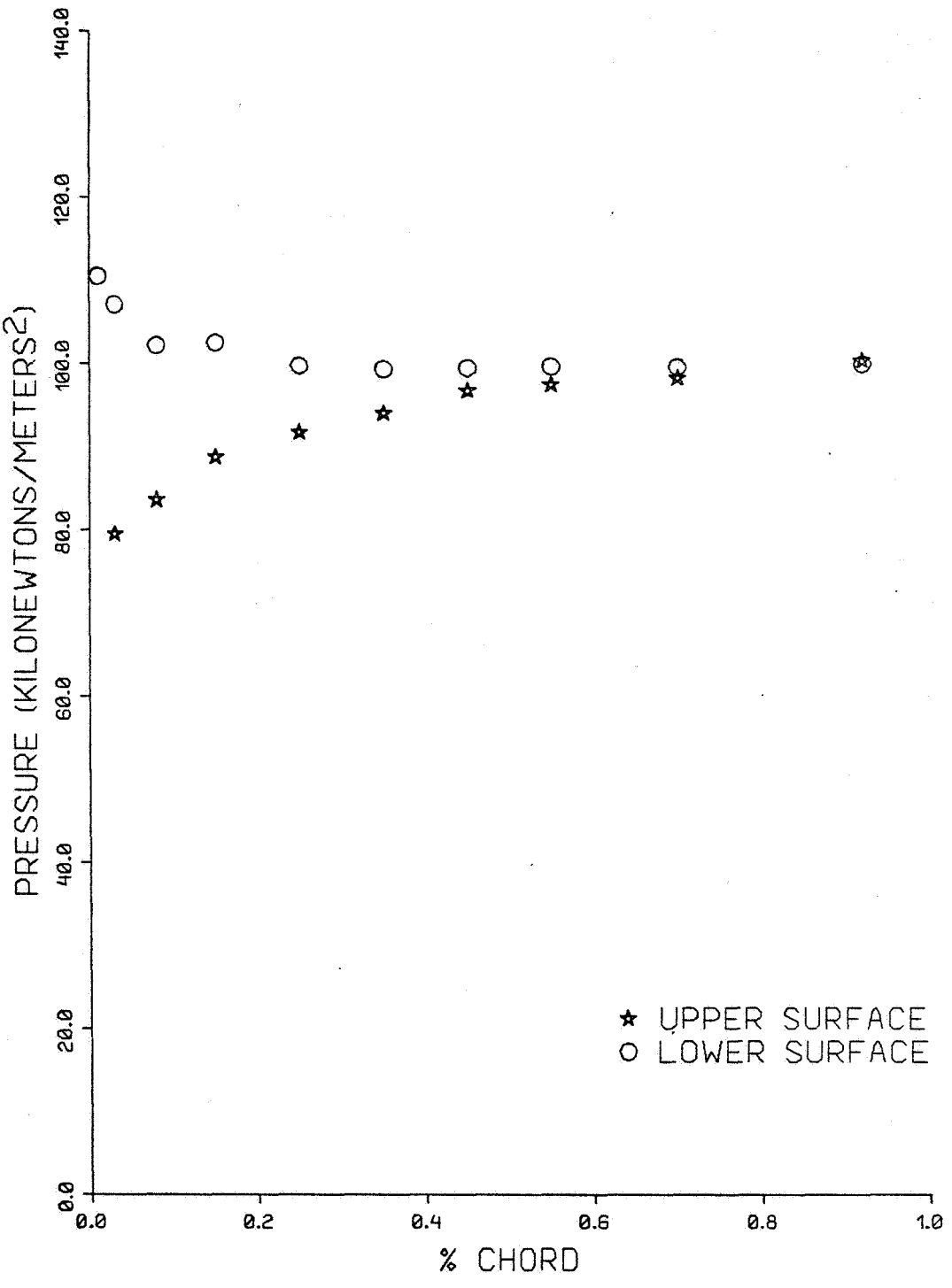

FIG. A-8.

SUCCI-BBN

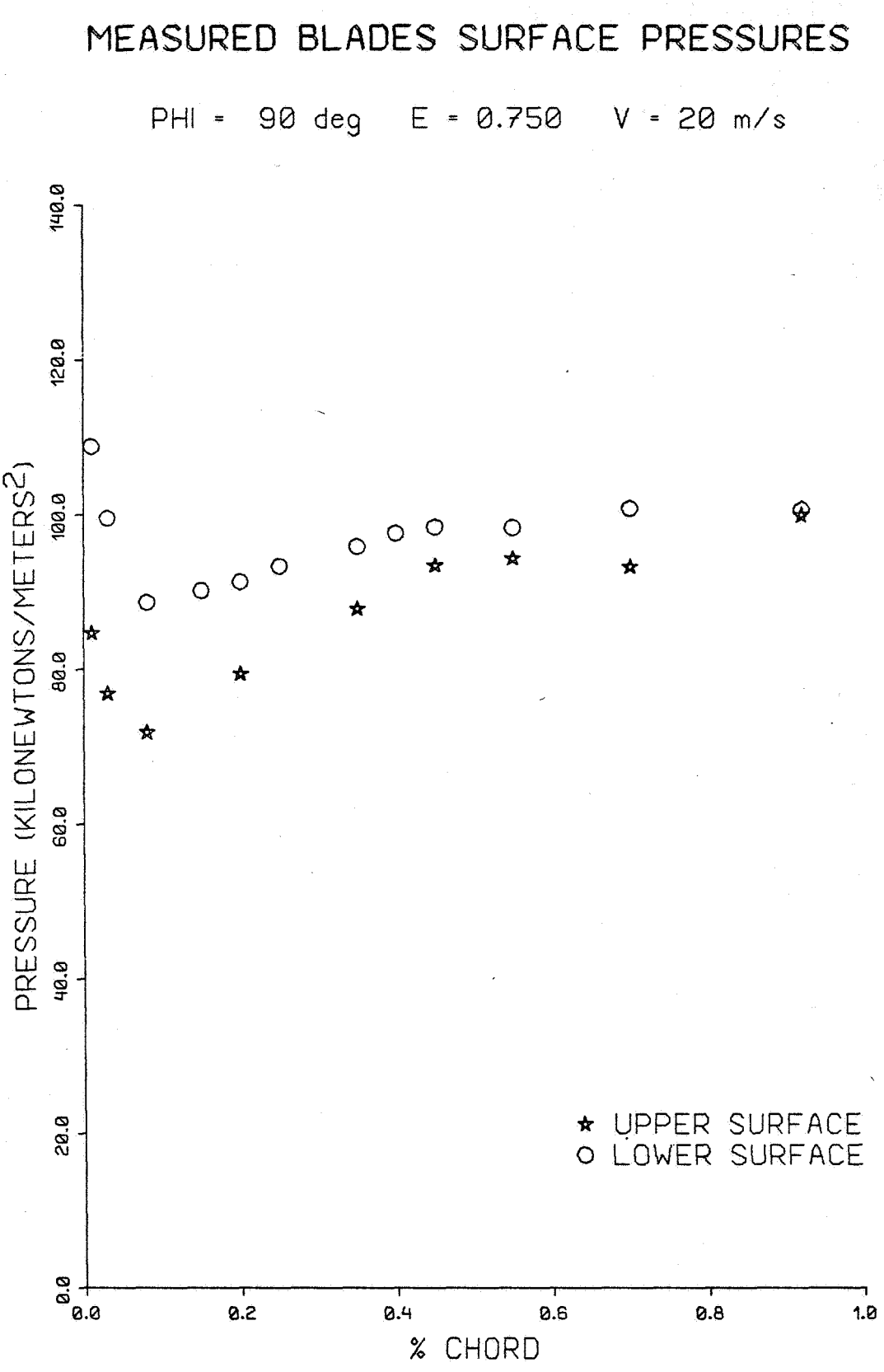

FIG. A-9.

SUCCI-BBN

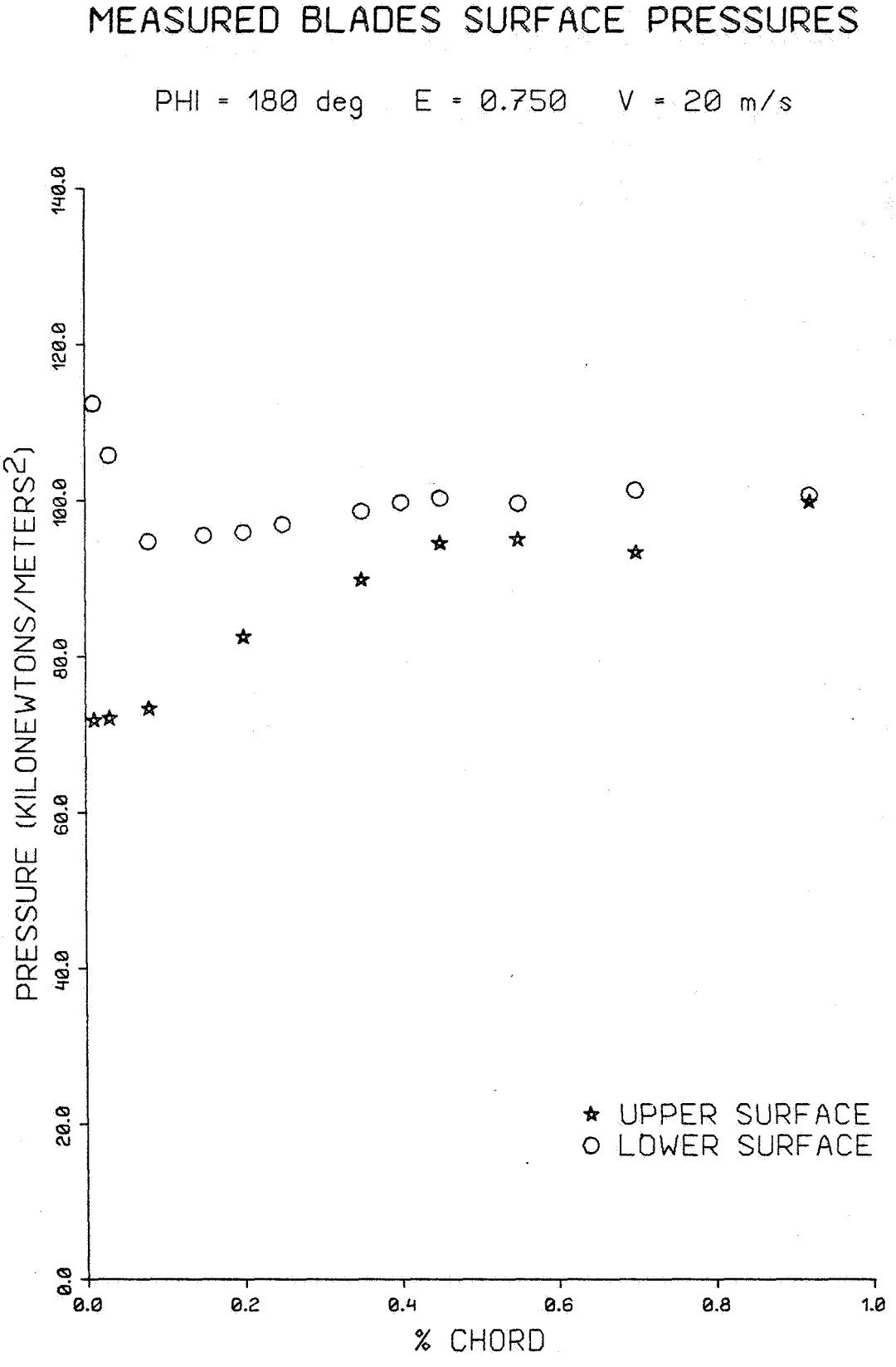

FIG. A-10.

SUCCI-BBN

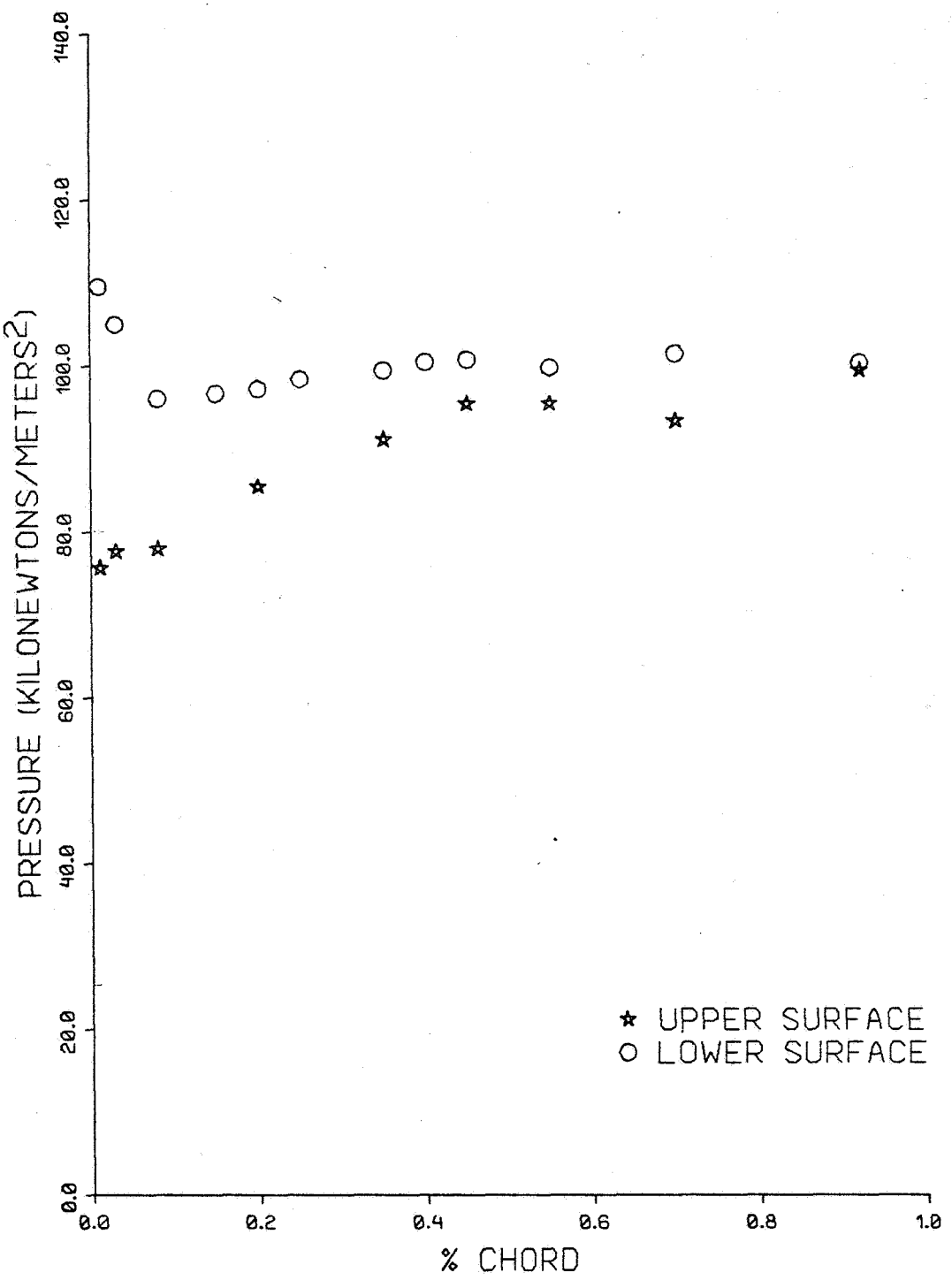

FIG. A-11.

SUCCI-BBN

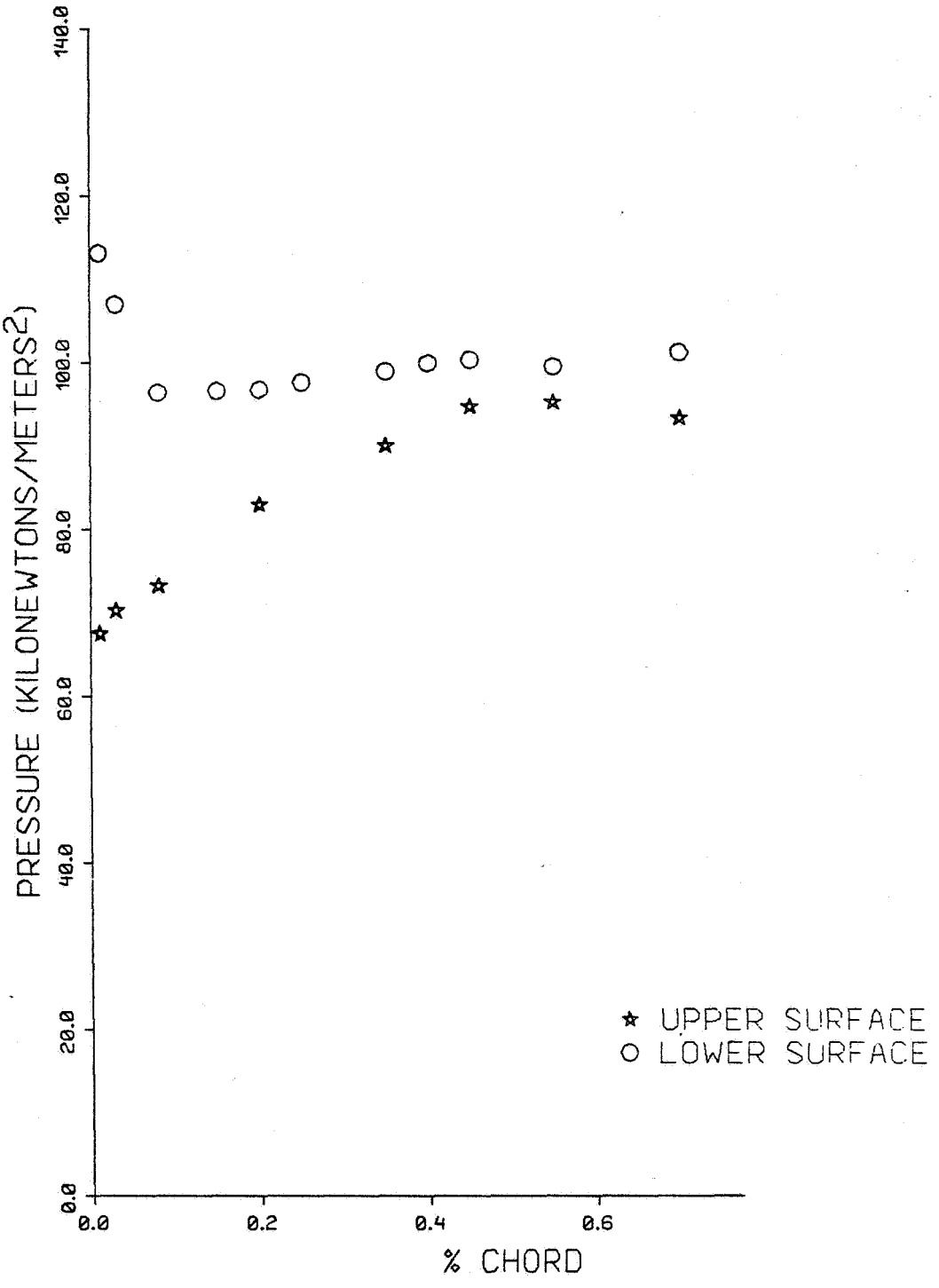
MEASURED BLADES SURFACE PR
PHI = 360 deg E = 0.750 V = 20 m/s
PRESSURE (KILONEWTONS/METERS2)
140.0
120.0
100.0
80.0
60.0
40.0
20.0
0.0
0.0
0.2
0.4
0.6
% CHORD
UPPER SURFACE
LOWER SURFACE

FIG. A-12.

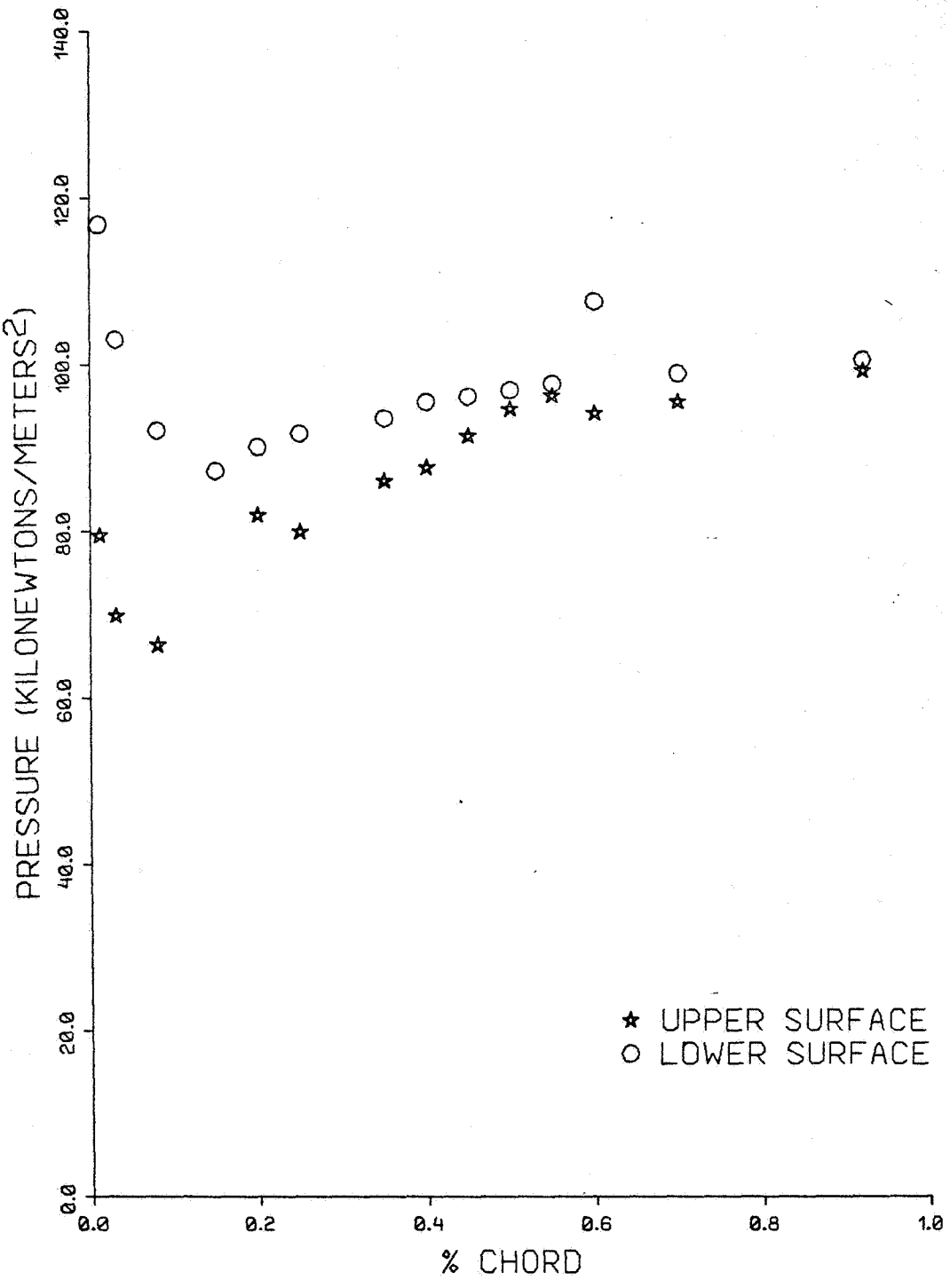

FIG. A-13.

SUCCI-BBN

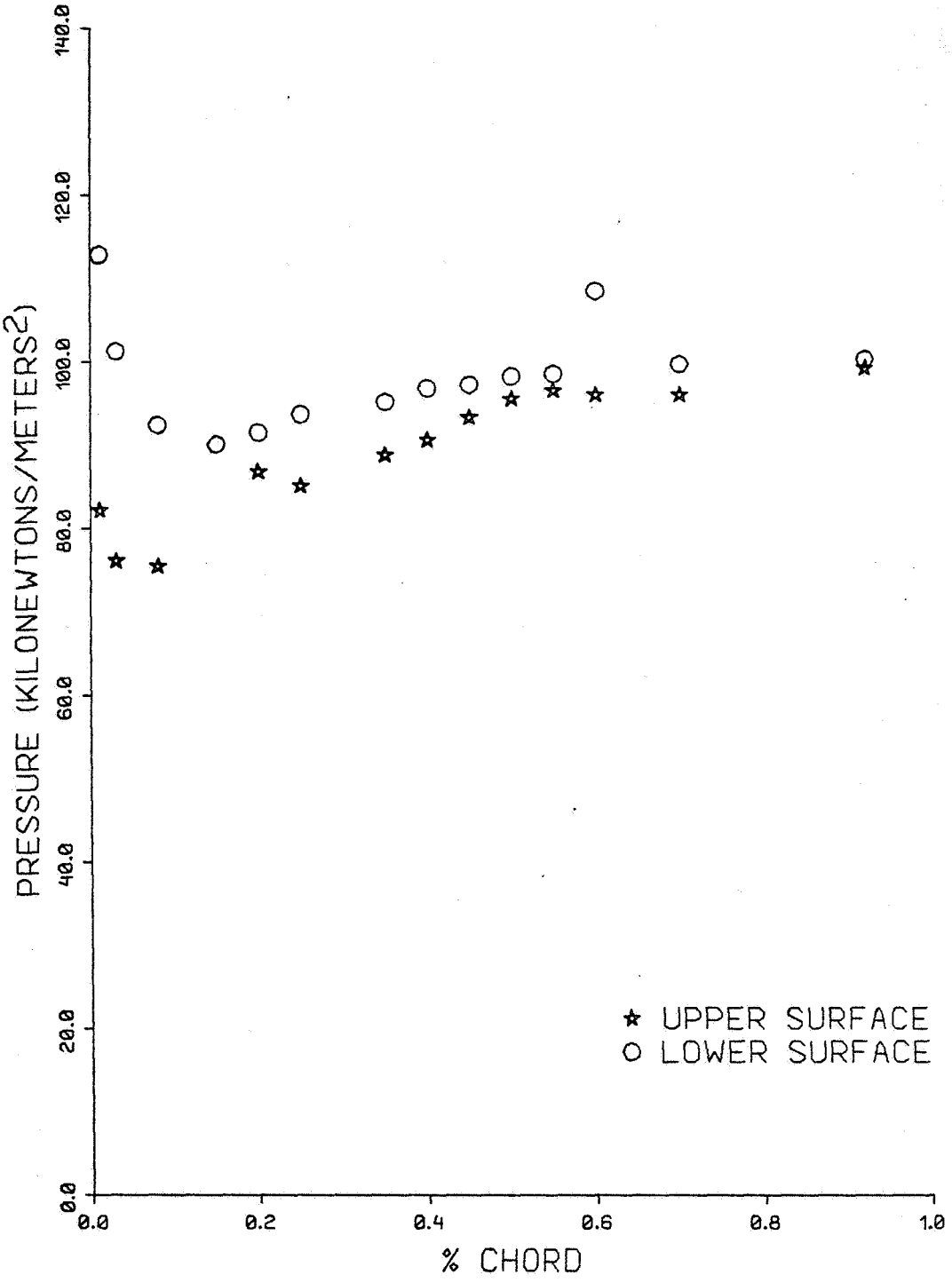
MEASURED BLADES SURFACE PRESSURES
PHI = 180 deg E = 0.864 V = 20 m/s
PRESSURE (KILONEWTONS/METERS2)
140.0
120.0
100.0
80.0
60.0
40.0
20.0
0.0
0.0
0.2
0.4
0.6
0.8
1.0
% CHORD
UPPER SURFACE
LOWER SURFACE
SUCCI-BBN

FIG. A-14.

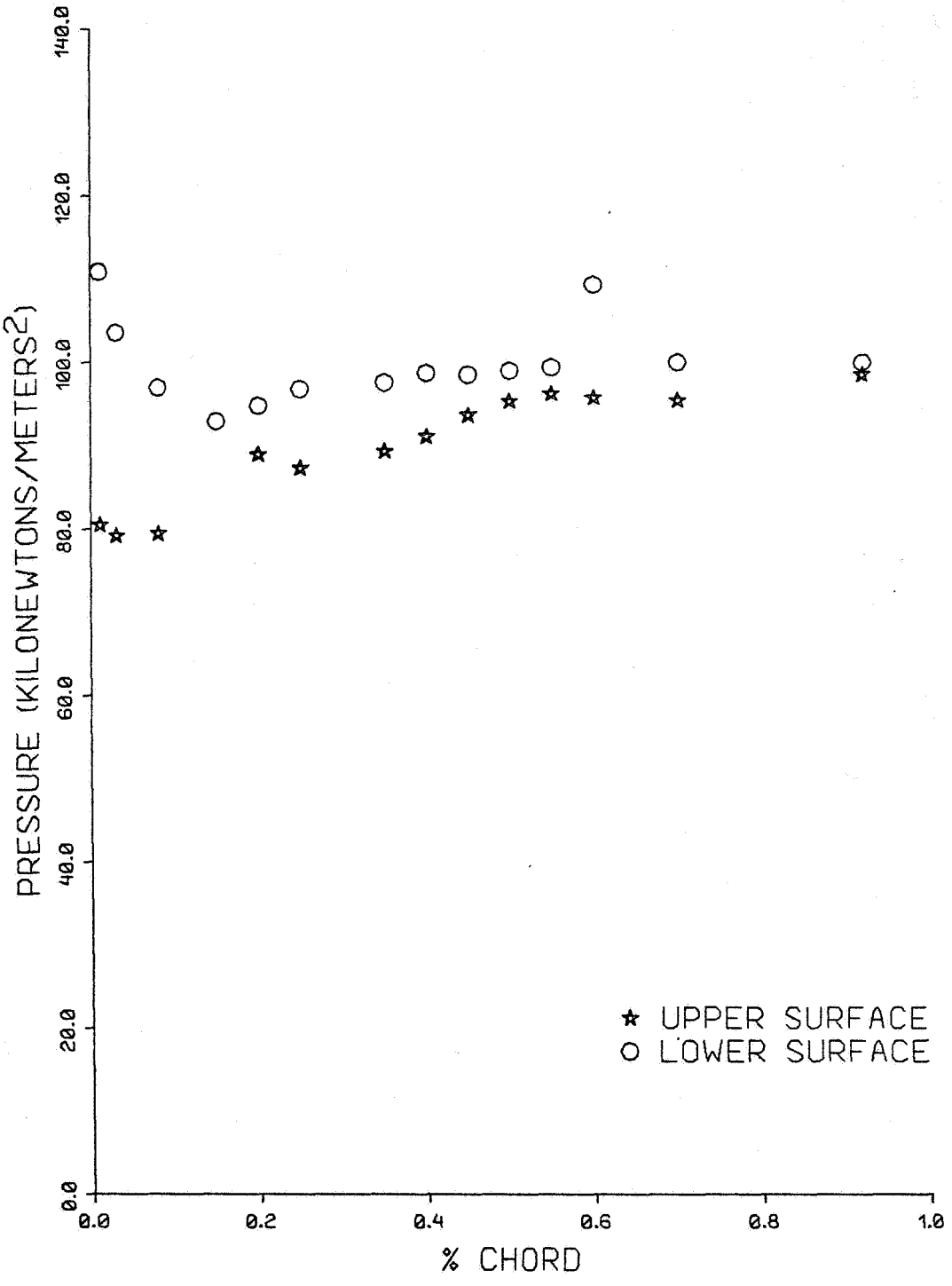

FIG. A-15.

SUCCI-BBN

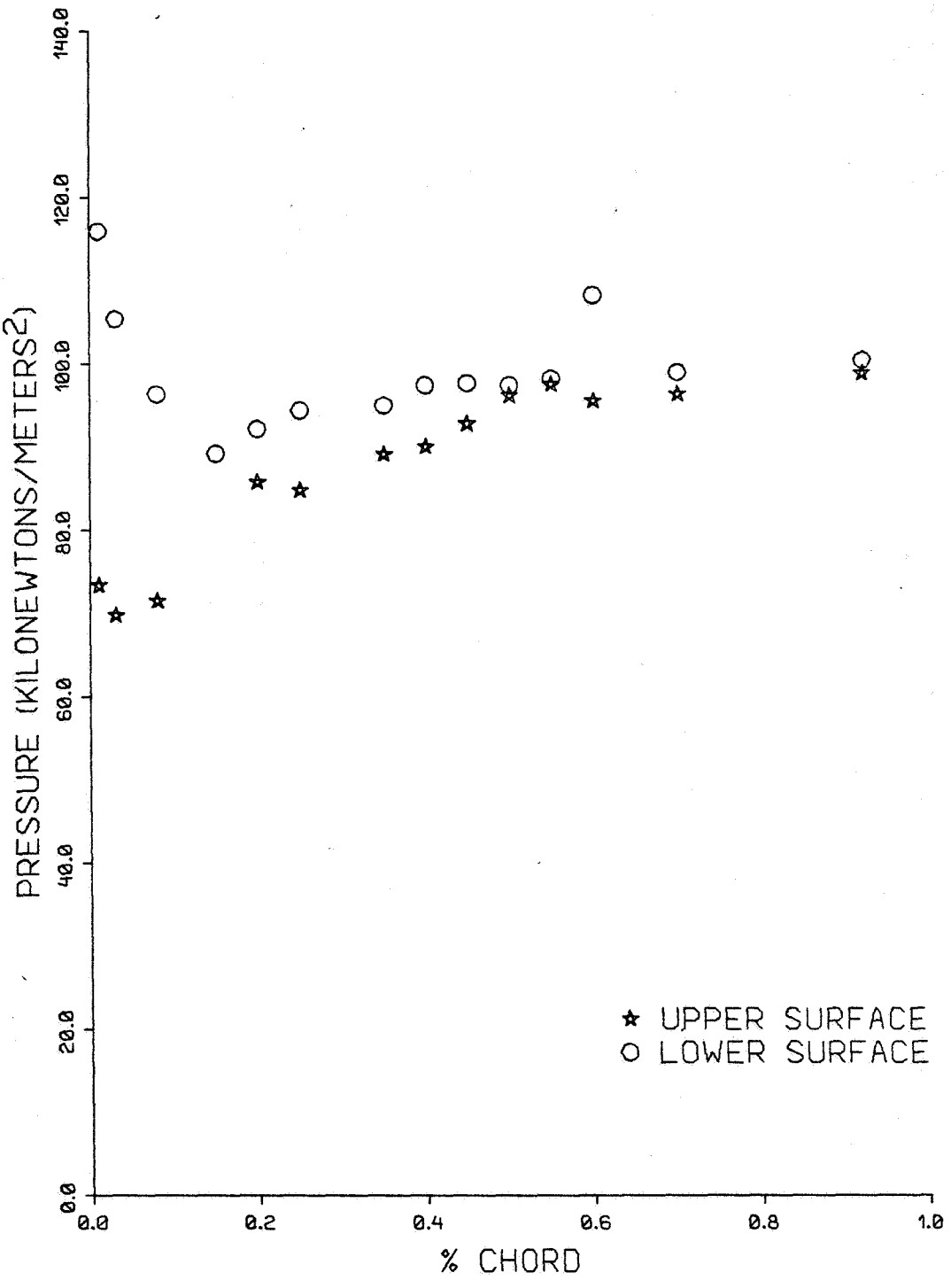

FIG. A-16.

SUCCI-BBN

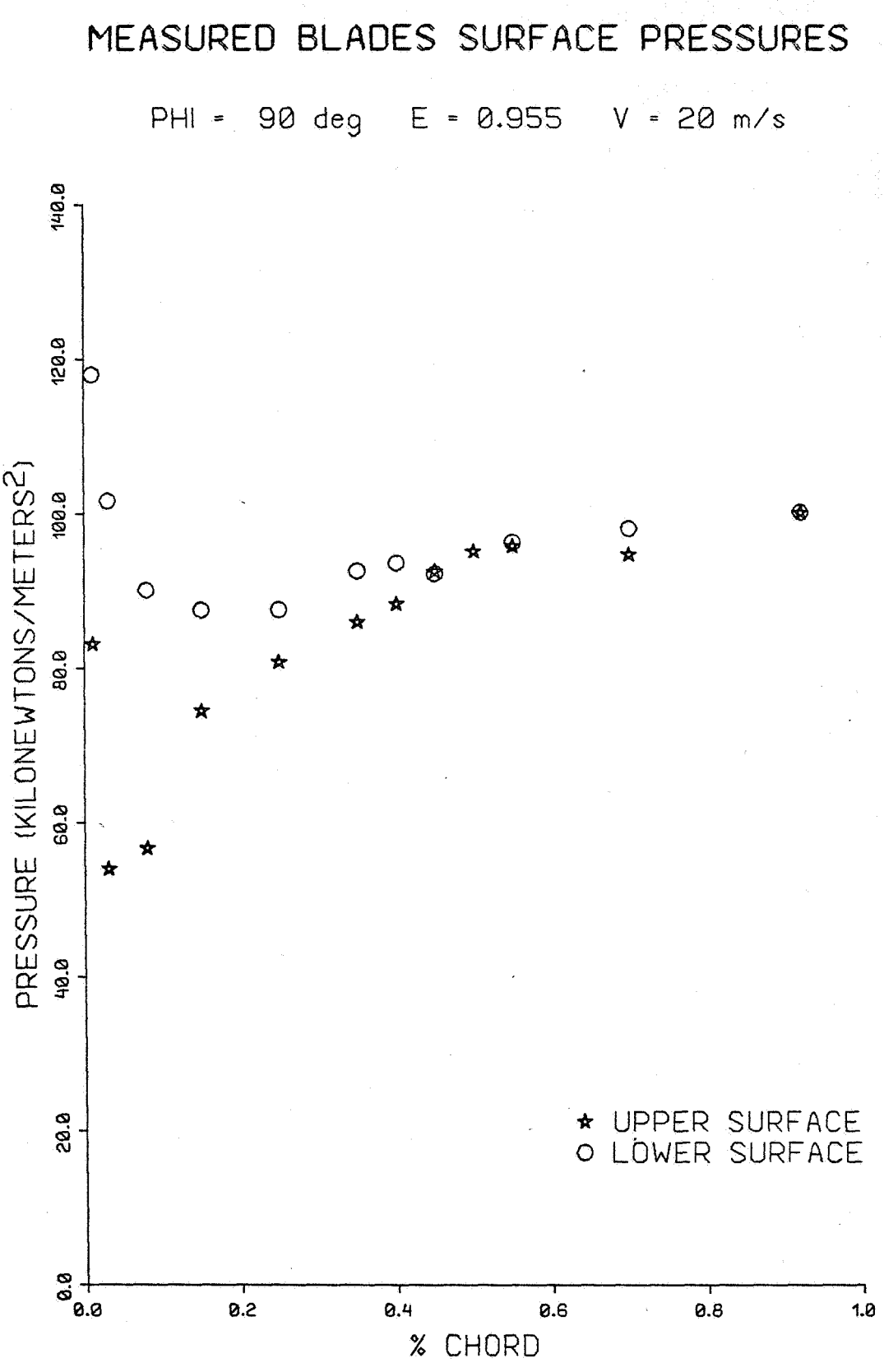

FIG. A-17. SUCCI-BBN

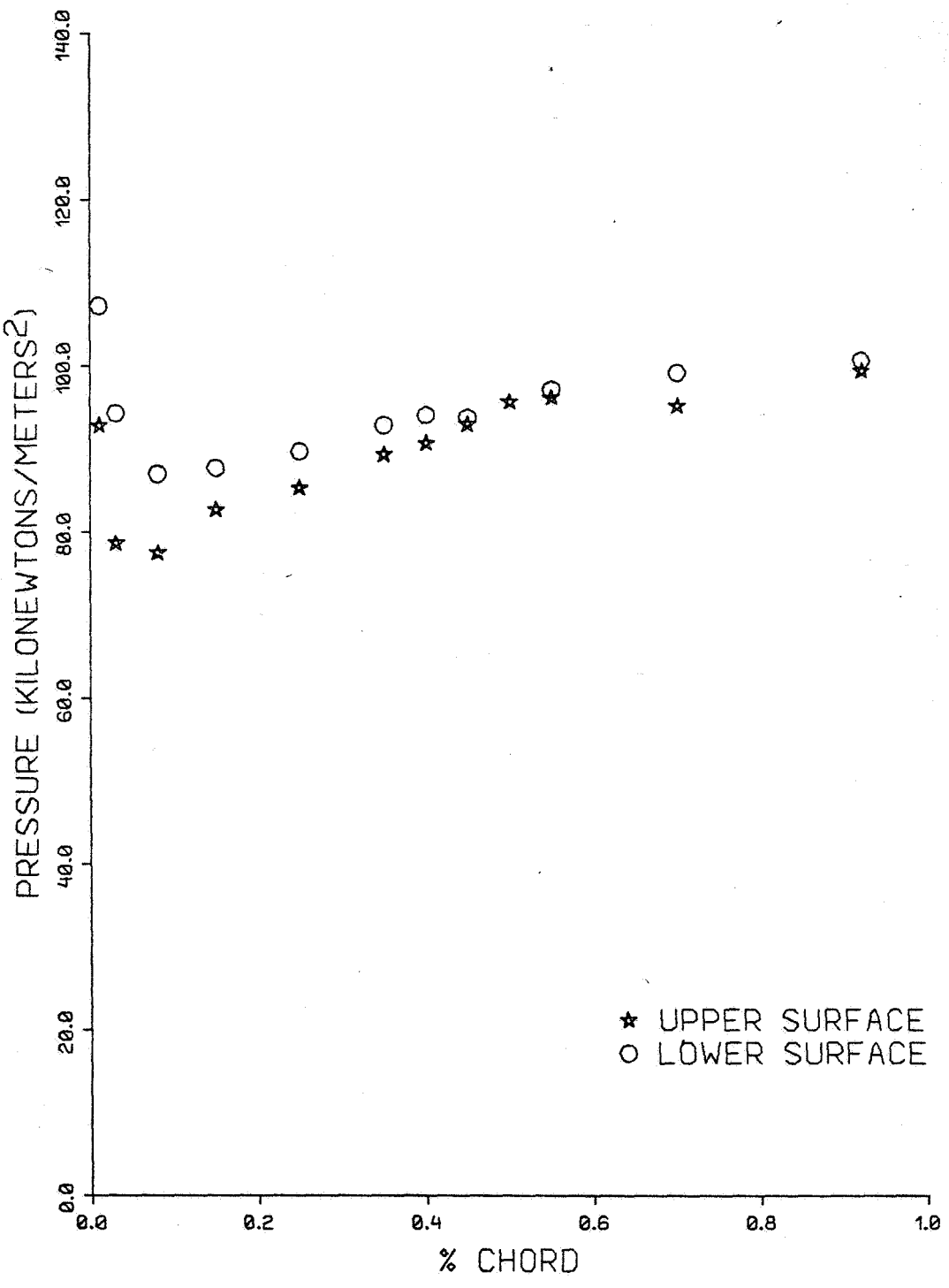
MEASURED BLADES SURFACE PRESSURES
PHI = 180 deg E = 0.955 V = 20 m/s
PRESSURE (KILONEWTONS/METERS2)
140.0
120.0
100.0
80.0
60.0
40.0
20.0
0.0
0.0
0.2
0.4
0.6
0.8
1.0
% CHORD
UPPER SURFACE
LOWER SURFACE
SUCCI-BBN

FIG. A-18.

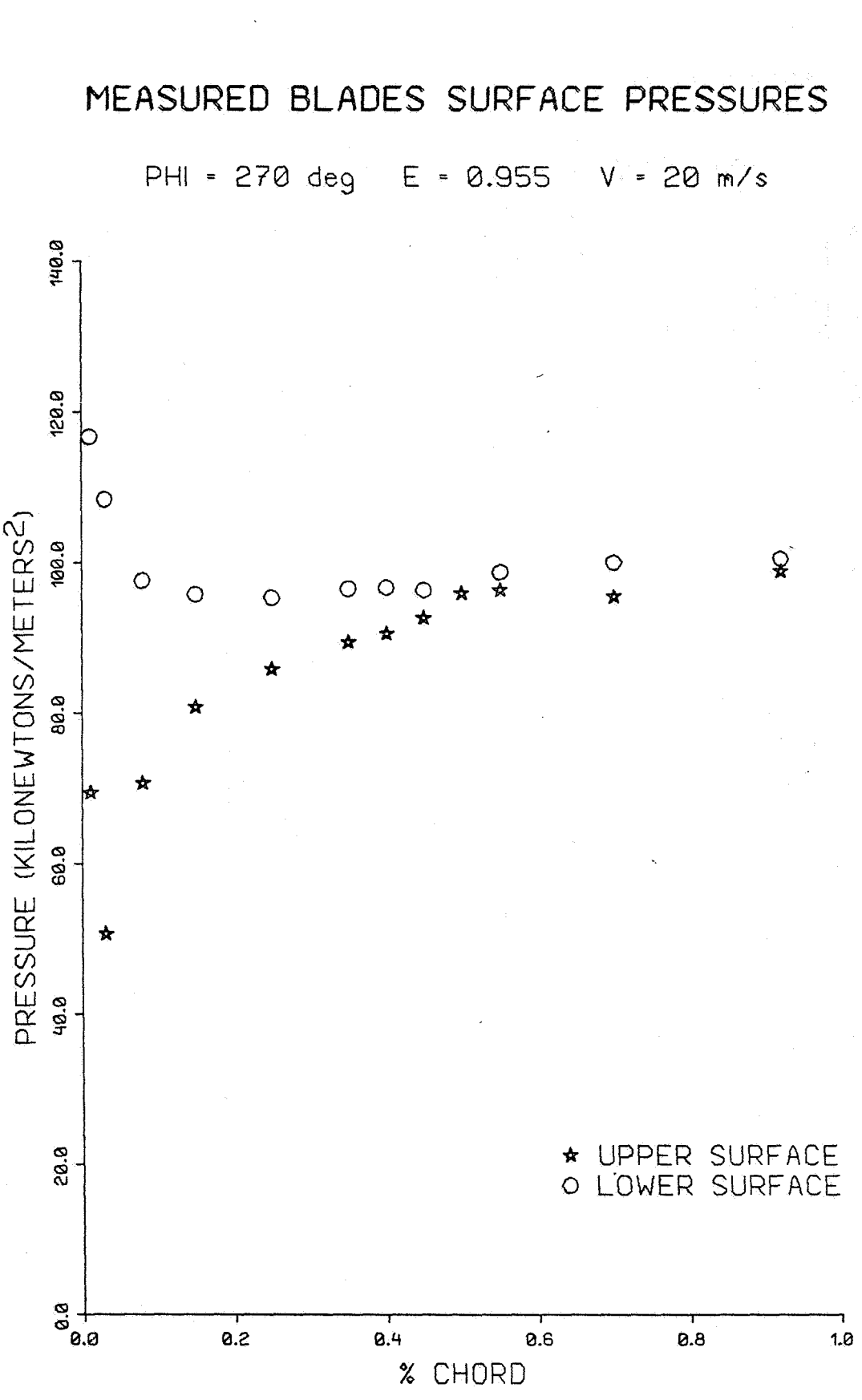

FIG. A-19.

SUCCI-BBN

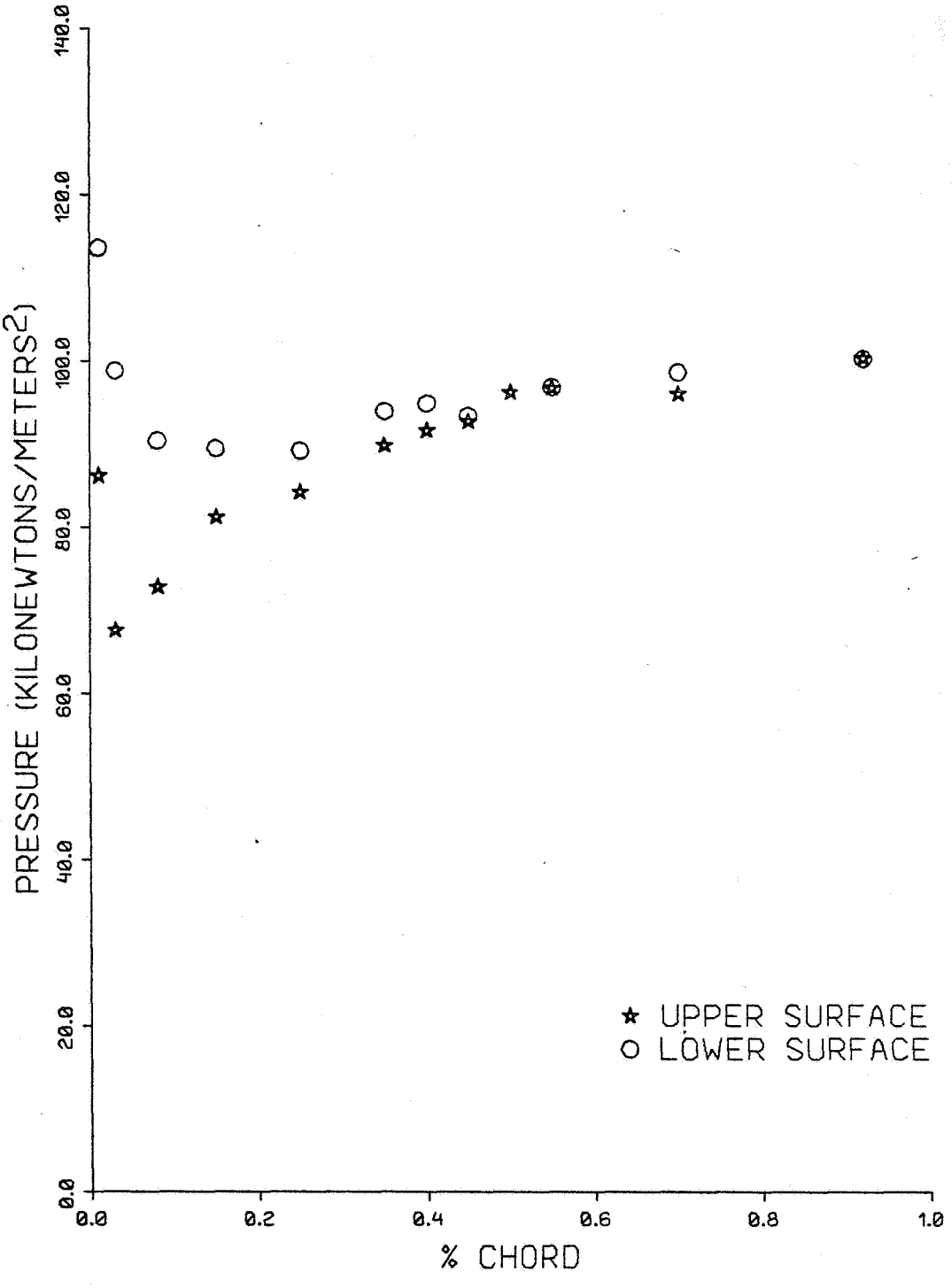

FIG. A-20.

SUCCI-BBN

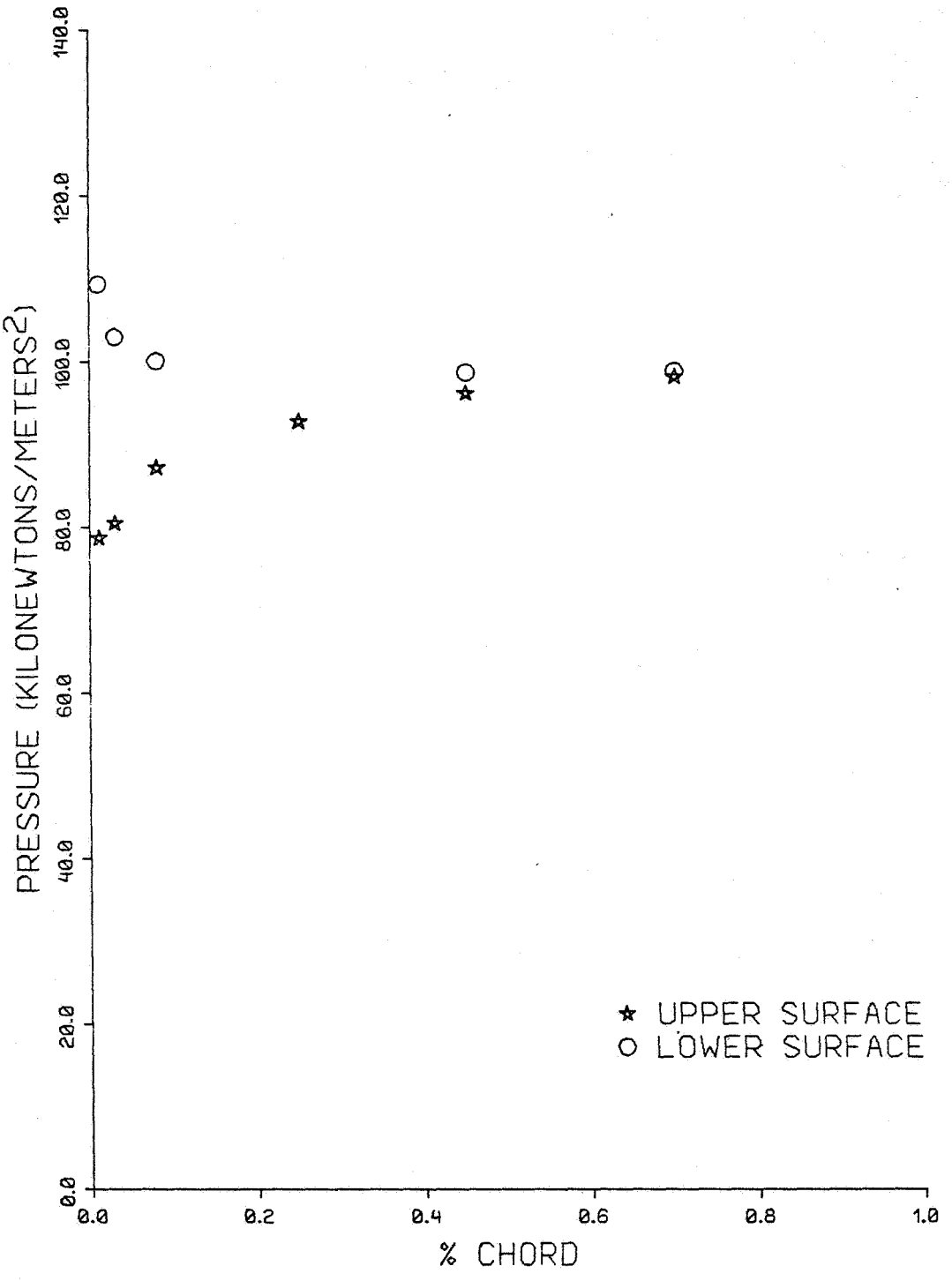

FIG. A-21.

SUCCI-BBN

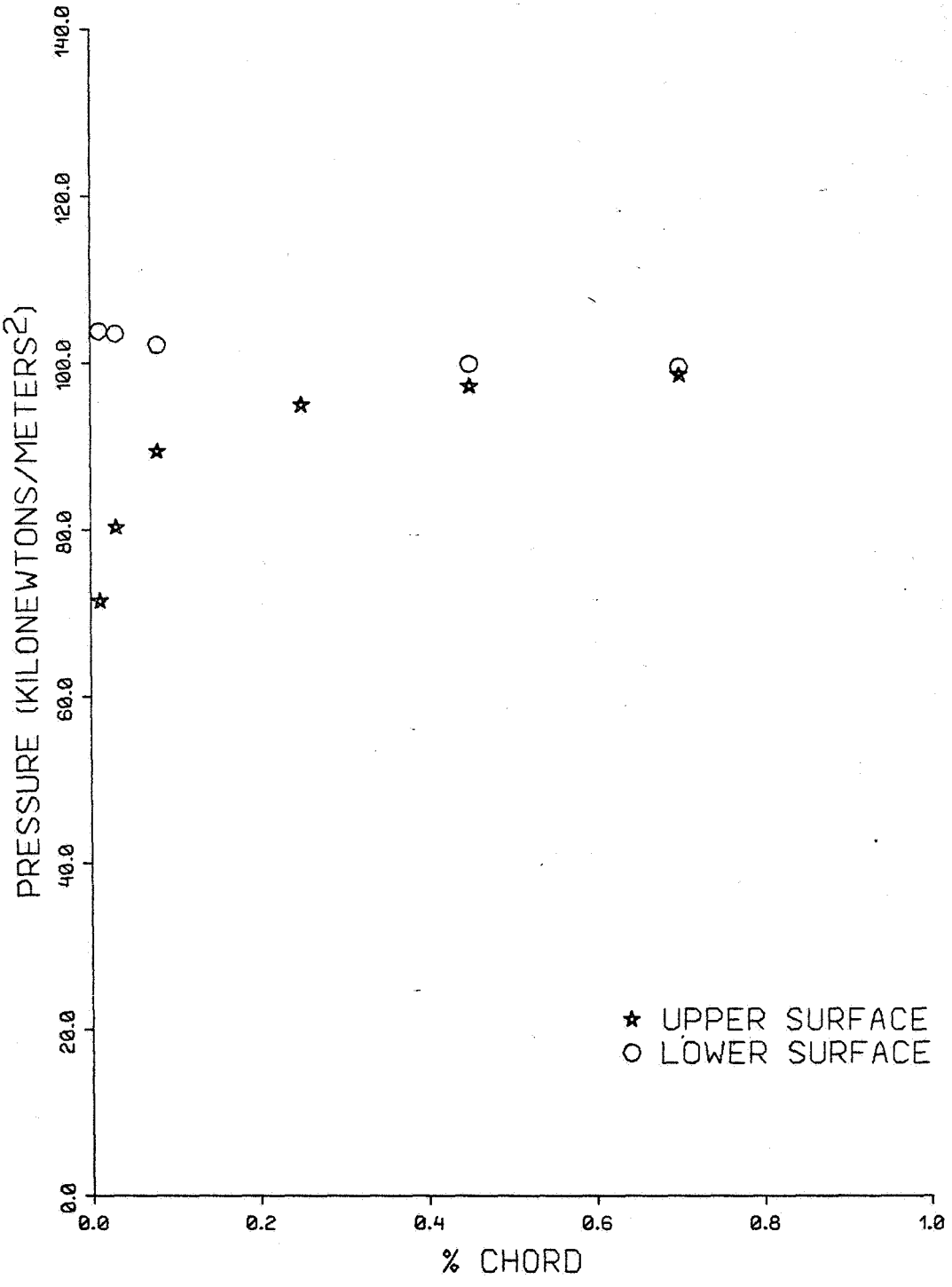

FIG. A-22.

SUCCI-BBN

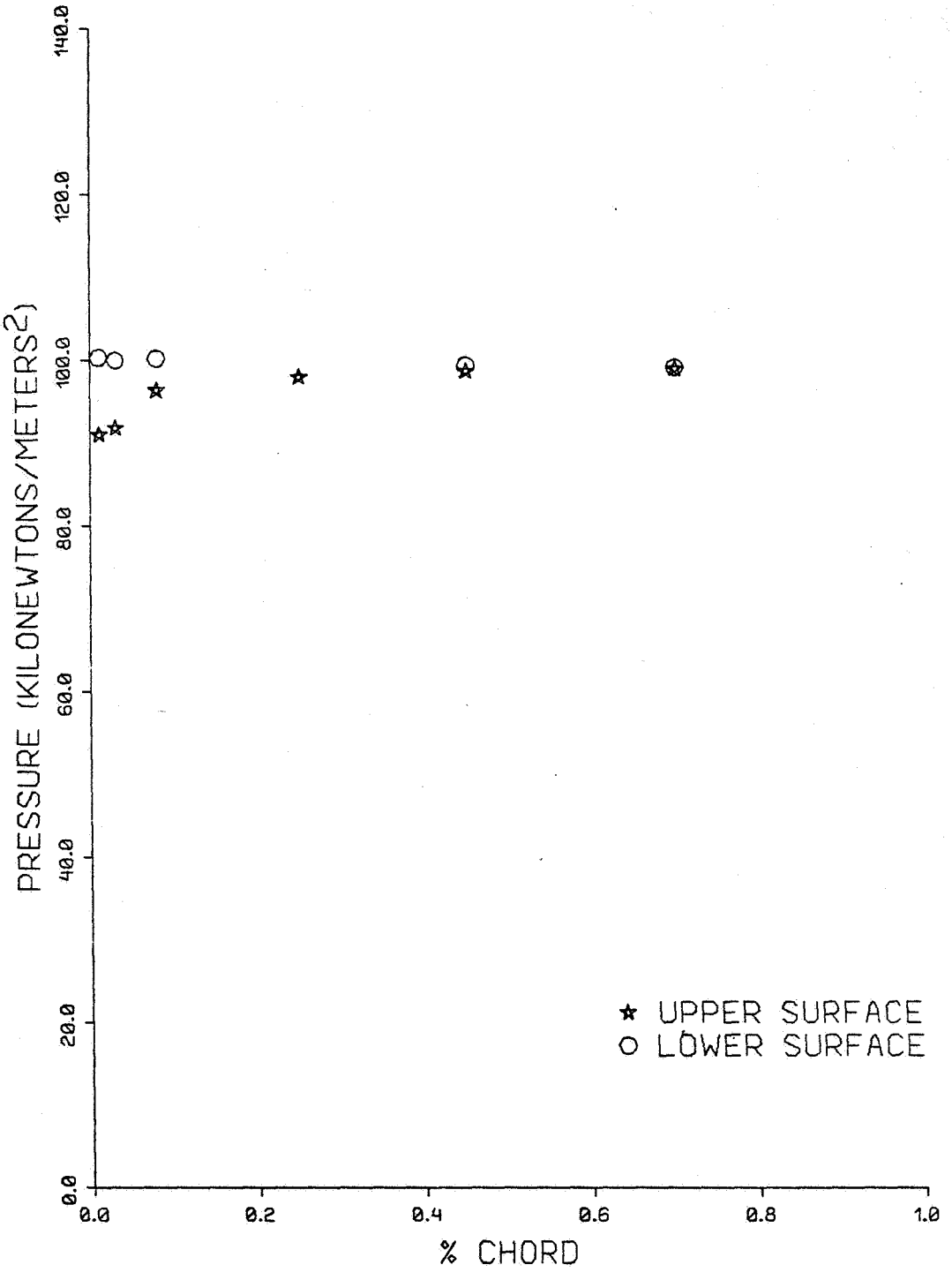

FIG. A-23.

SUCCI-BBN

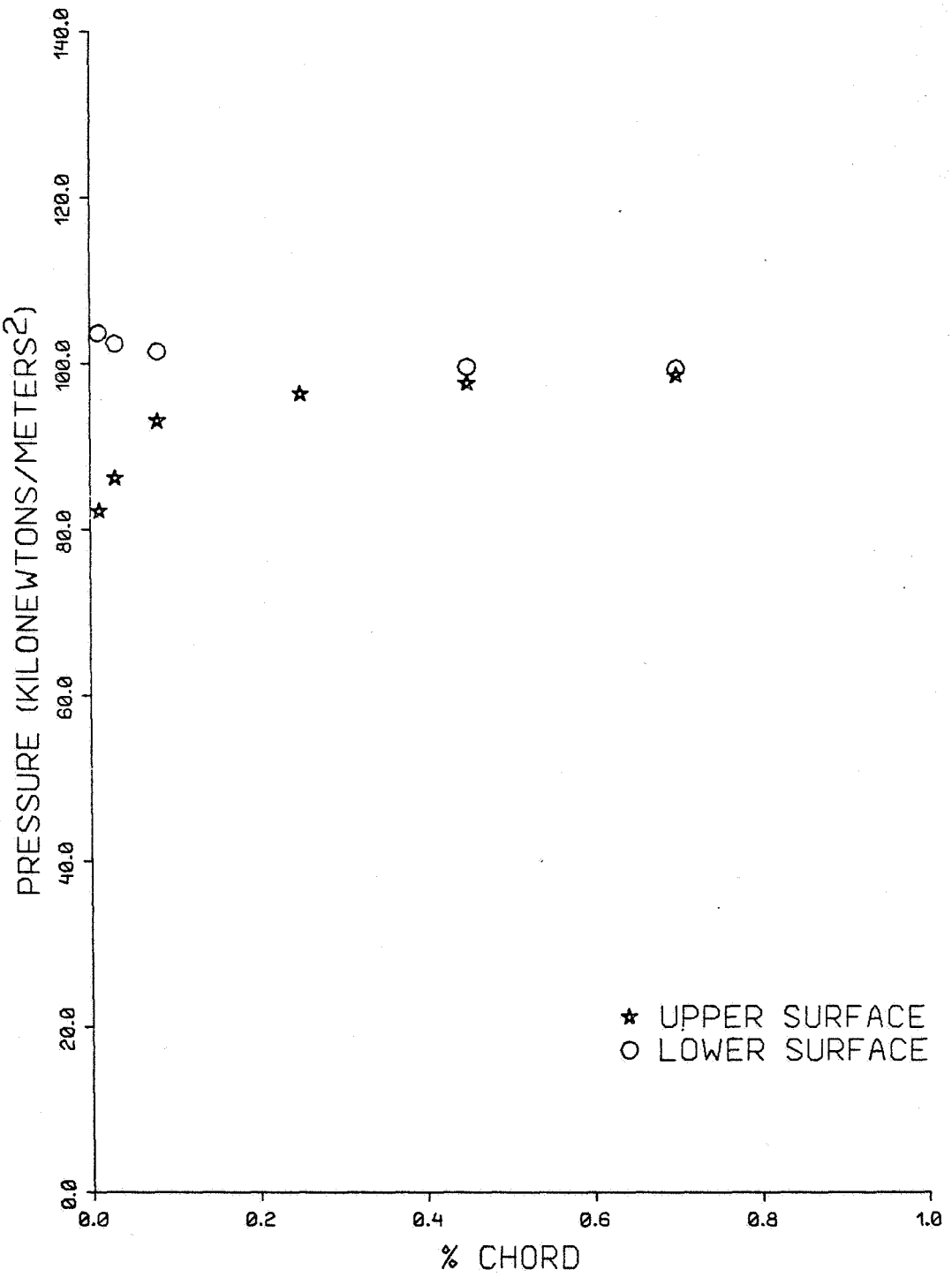

FIG. A-24.

SUCCI-BBN

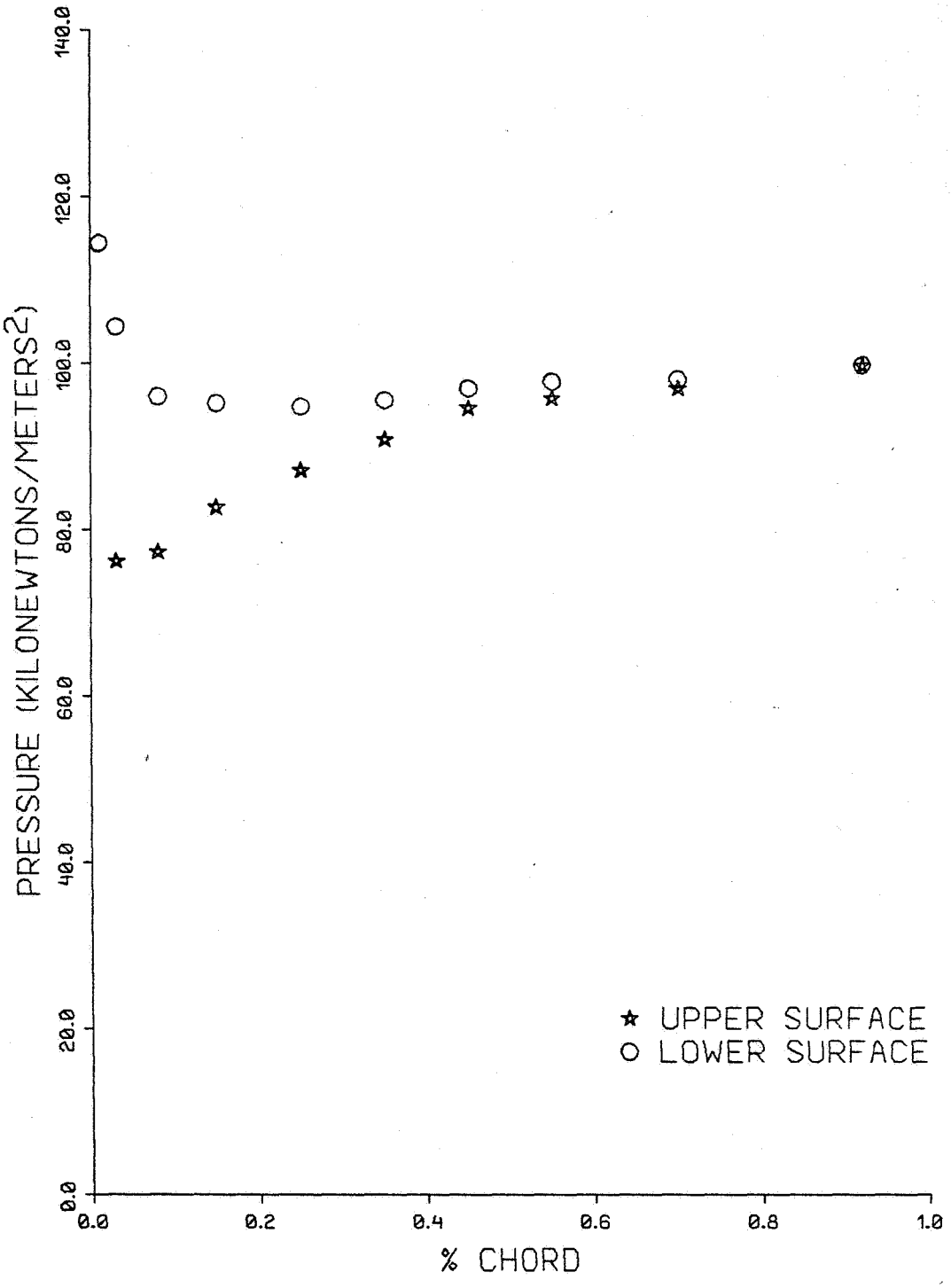

FIG. A-25.

SUCCI-BBN

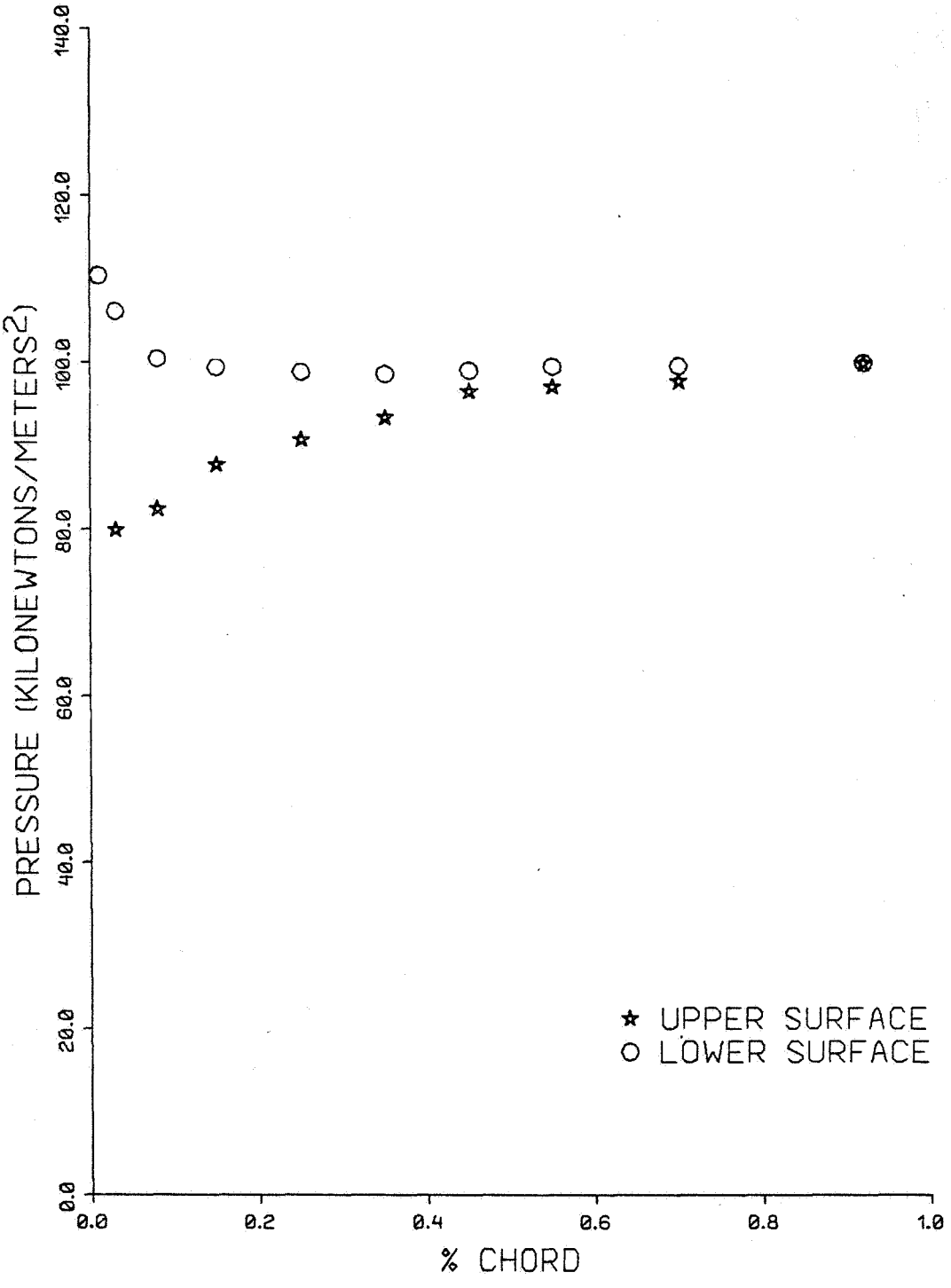

FIG. A-26.

SUCCI-BBN

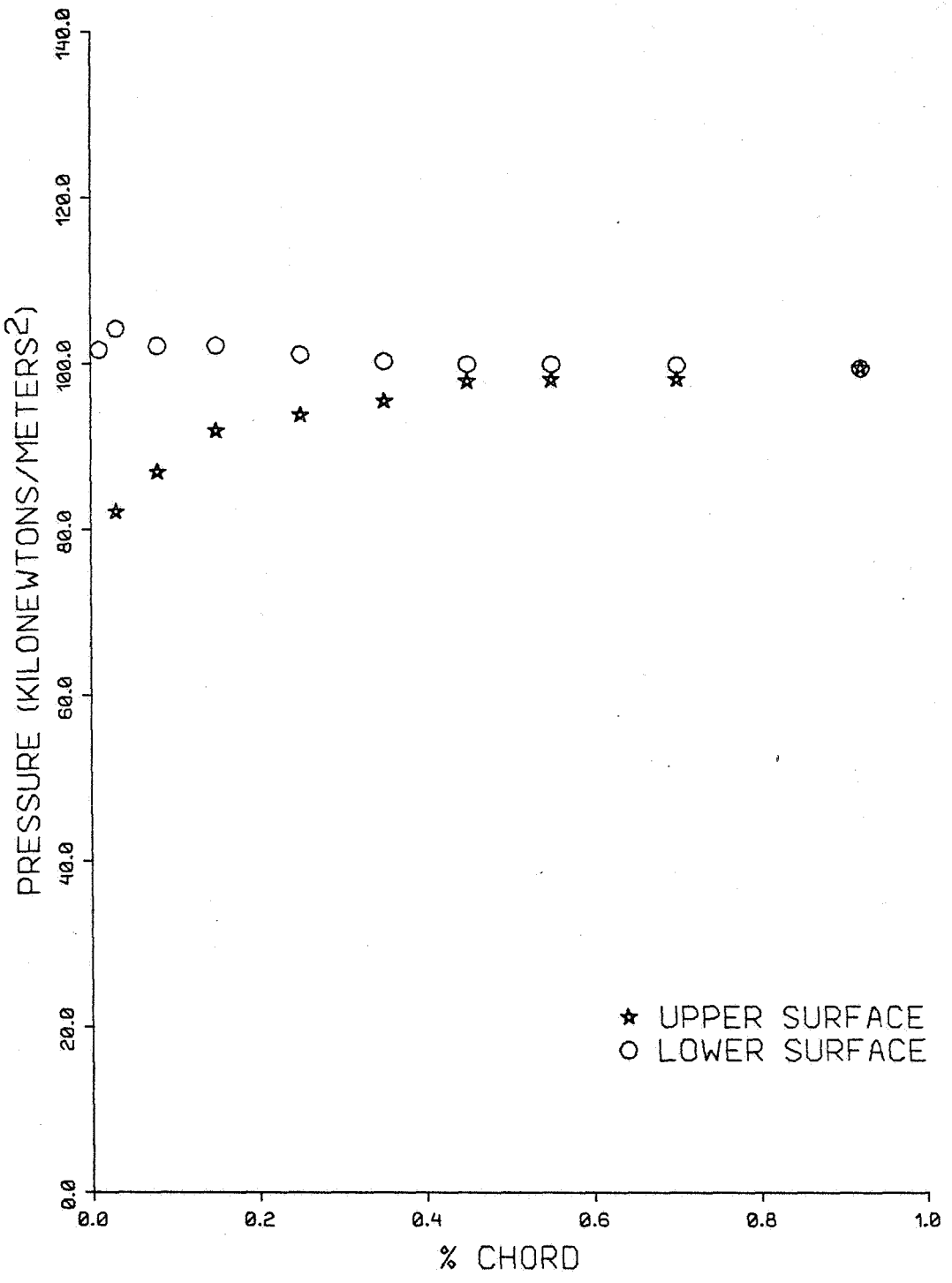

FIG. A-27. SUCCI-BBN

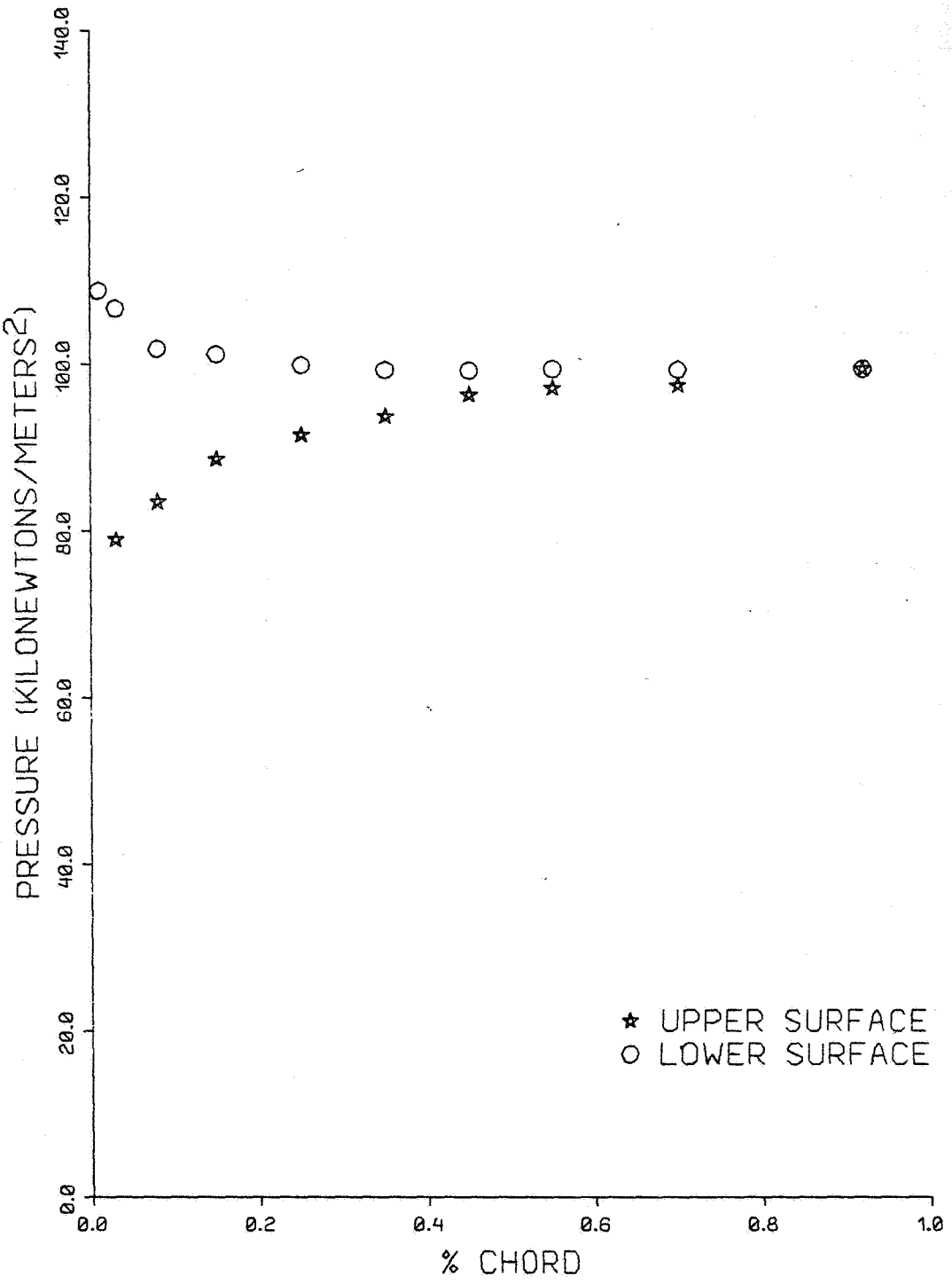

FIG. A-28. SUCCI-BBN

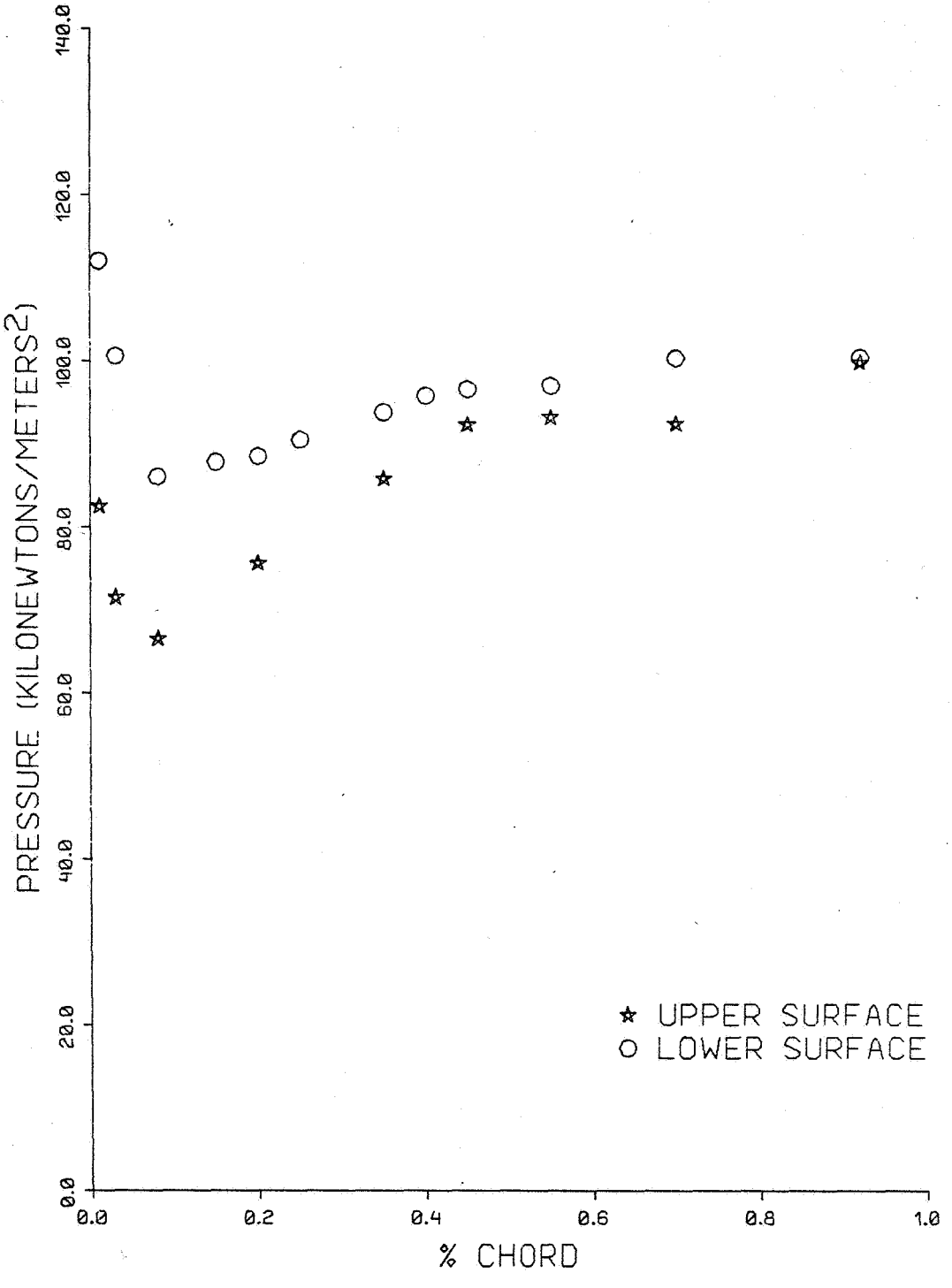

FIG. A-29.

SUCCI-BBN

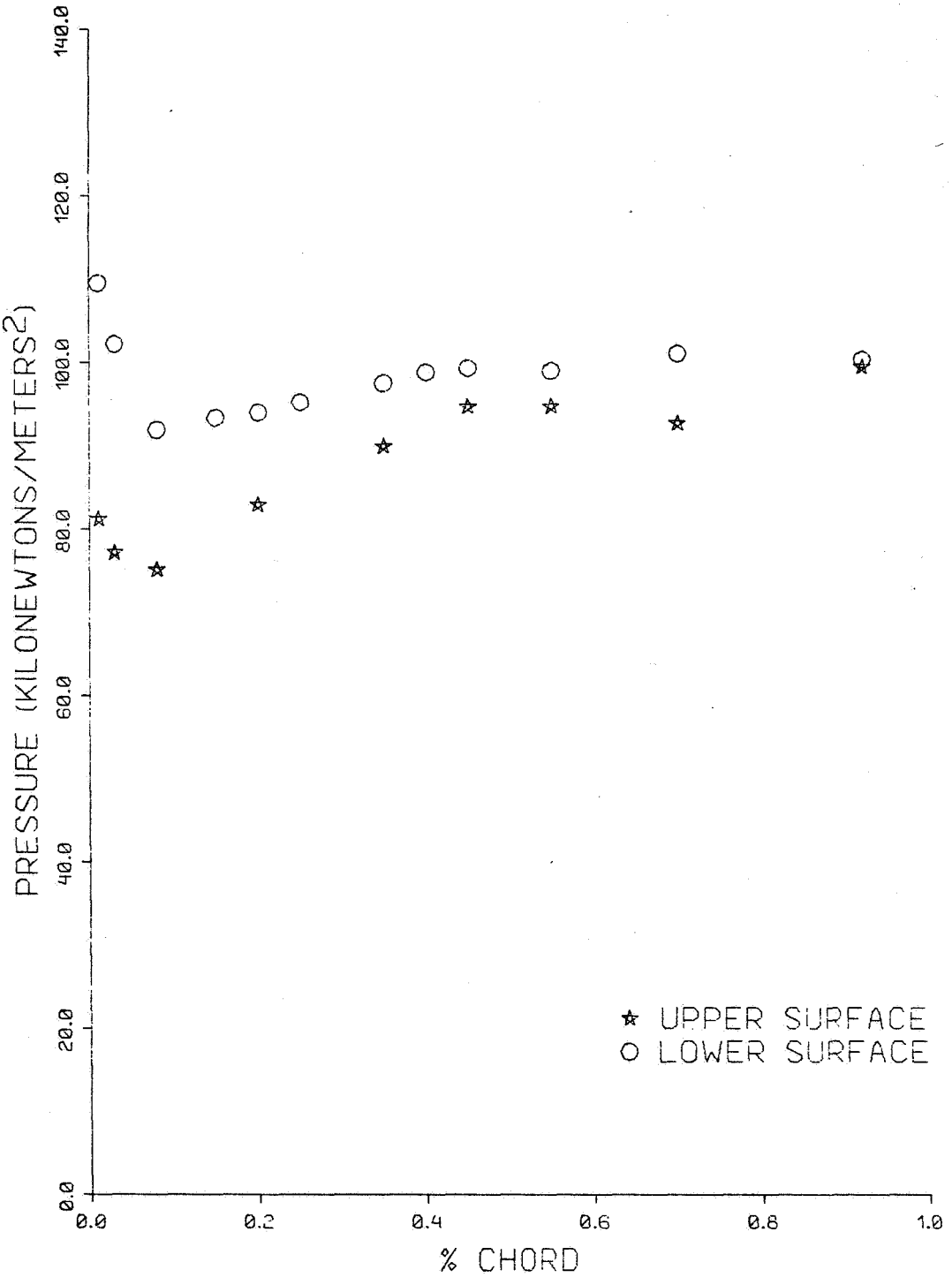

FIG. A-30.

SUCCI-BBN

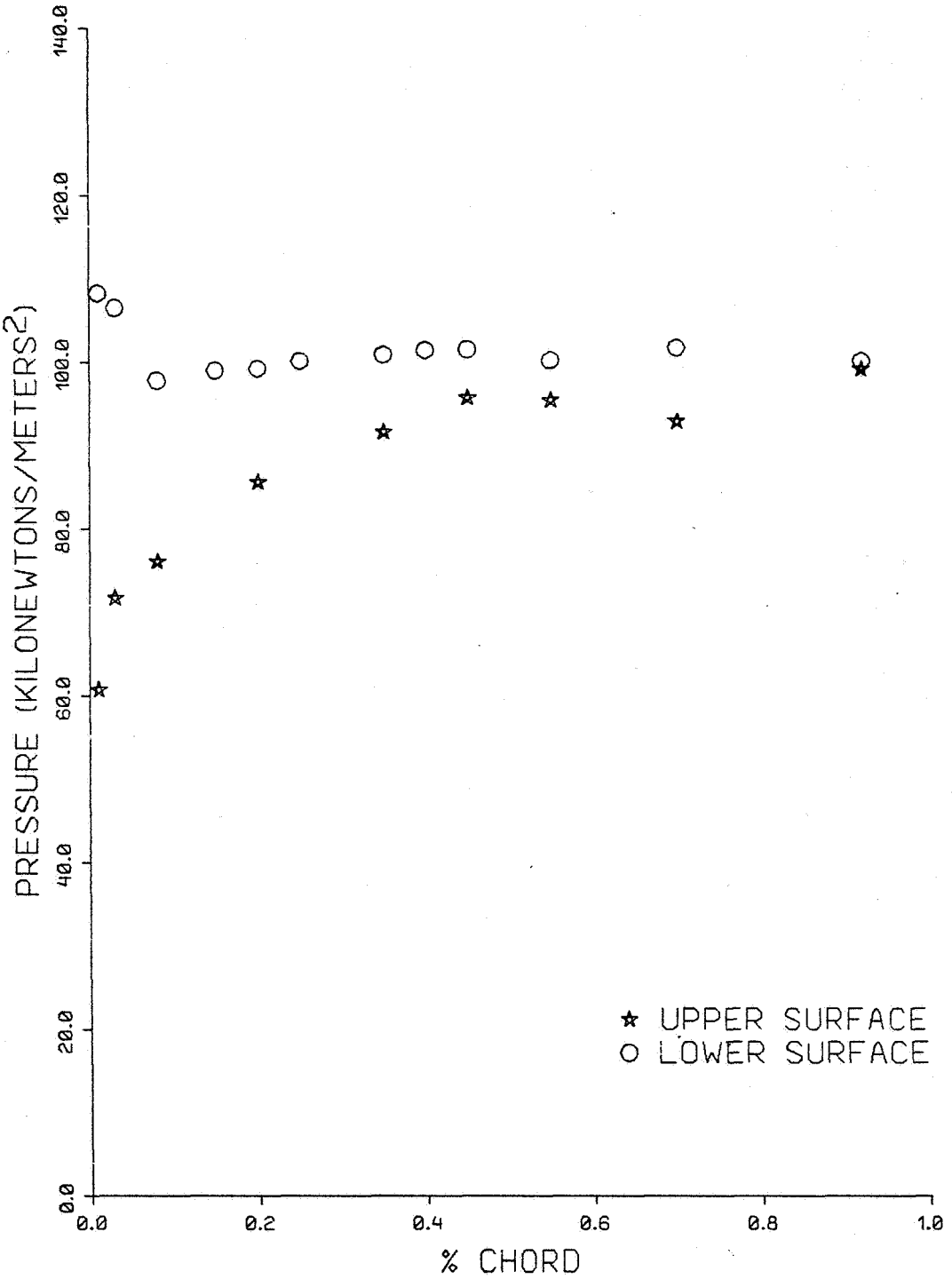

FIG. A-31.

SUCCI-BBN

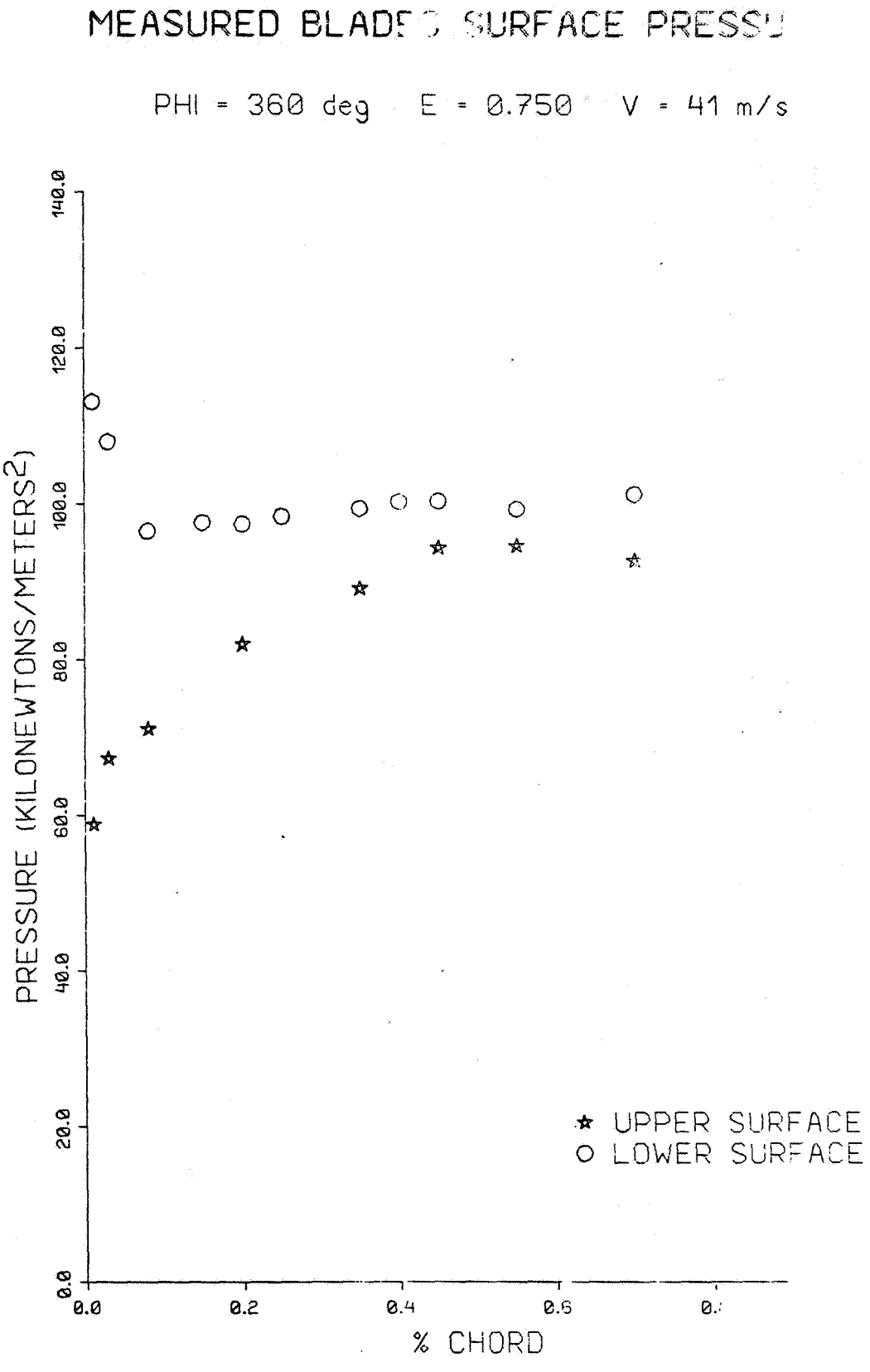
MEASURED BLADE SURFACE PRESSU
PHI = 360 deg E = 0.750 V = 41 m/s
PRESSURE (KILONEWTONS/METERS2)
140.0
120.0
100.0
80.0
60.0
40.0
20.0
0.0
0.0
0.2
0.4
0.6
% CHORD
UPPER SURFACE
LOWER SURFACE

FIG. A-32.

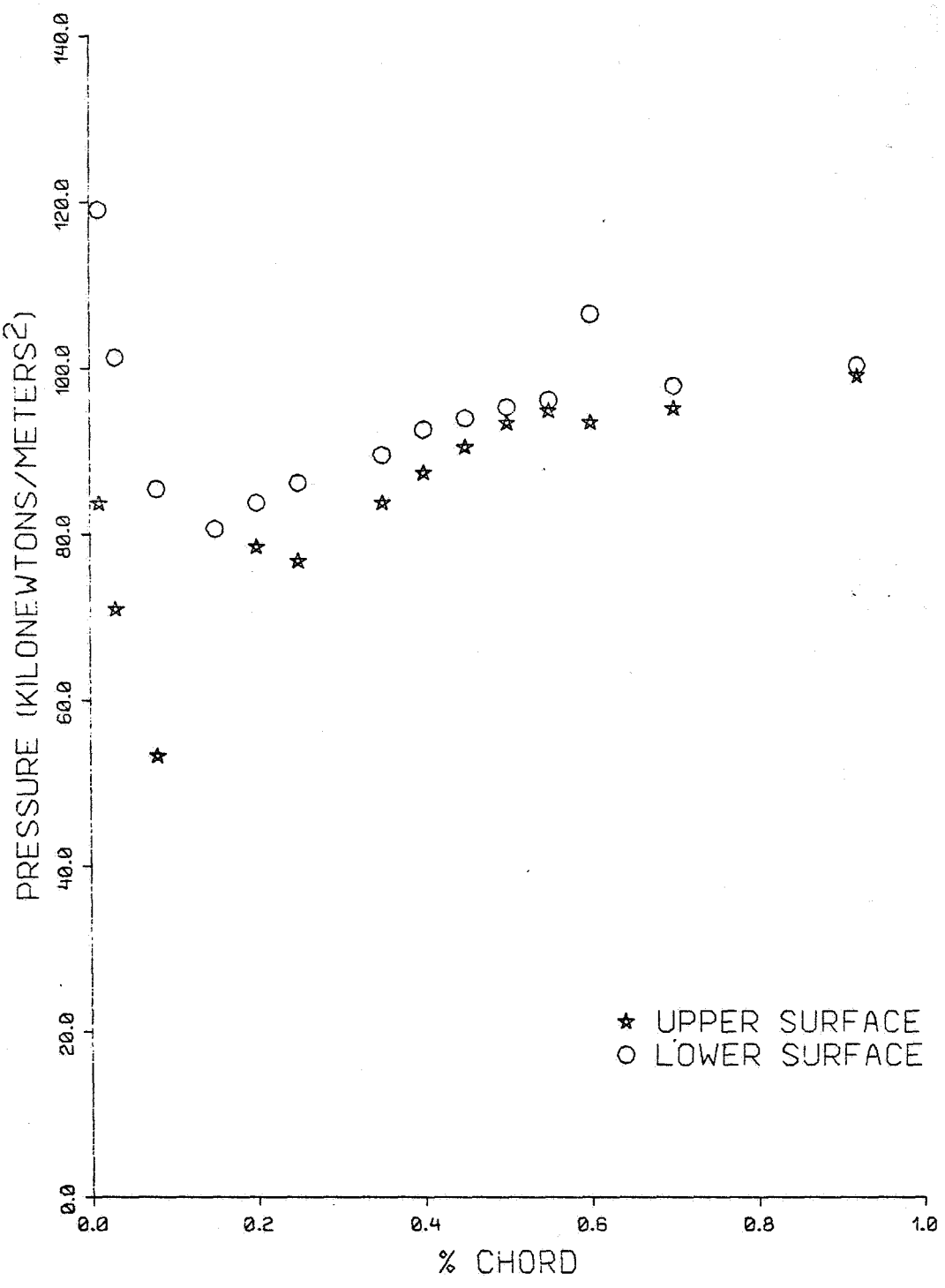

FIG. A-33.

SUCCI-BBN

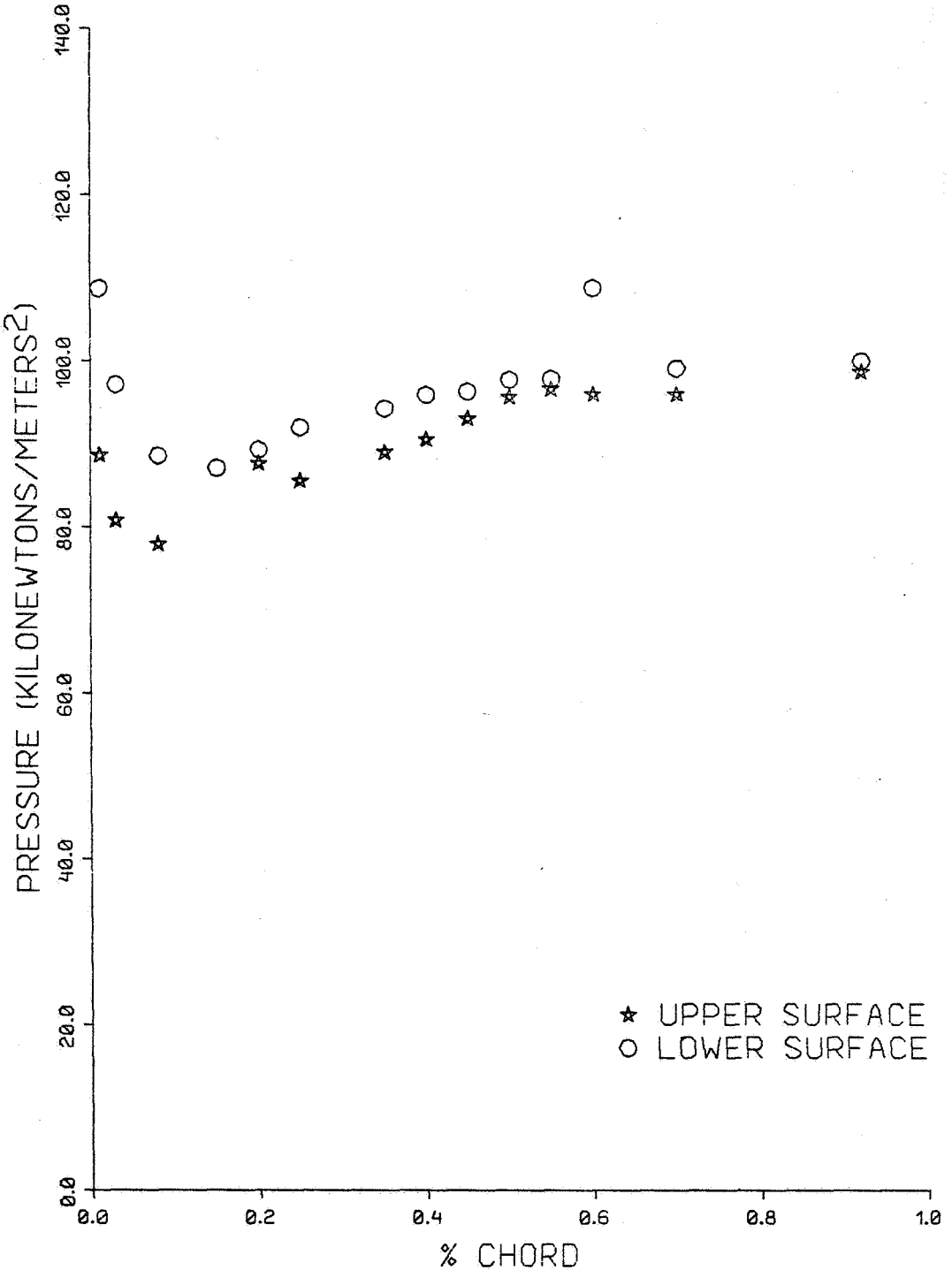

FIG. A-34.

SUCCI-BBN

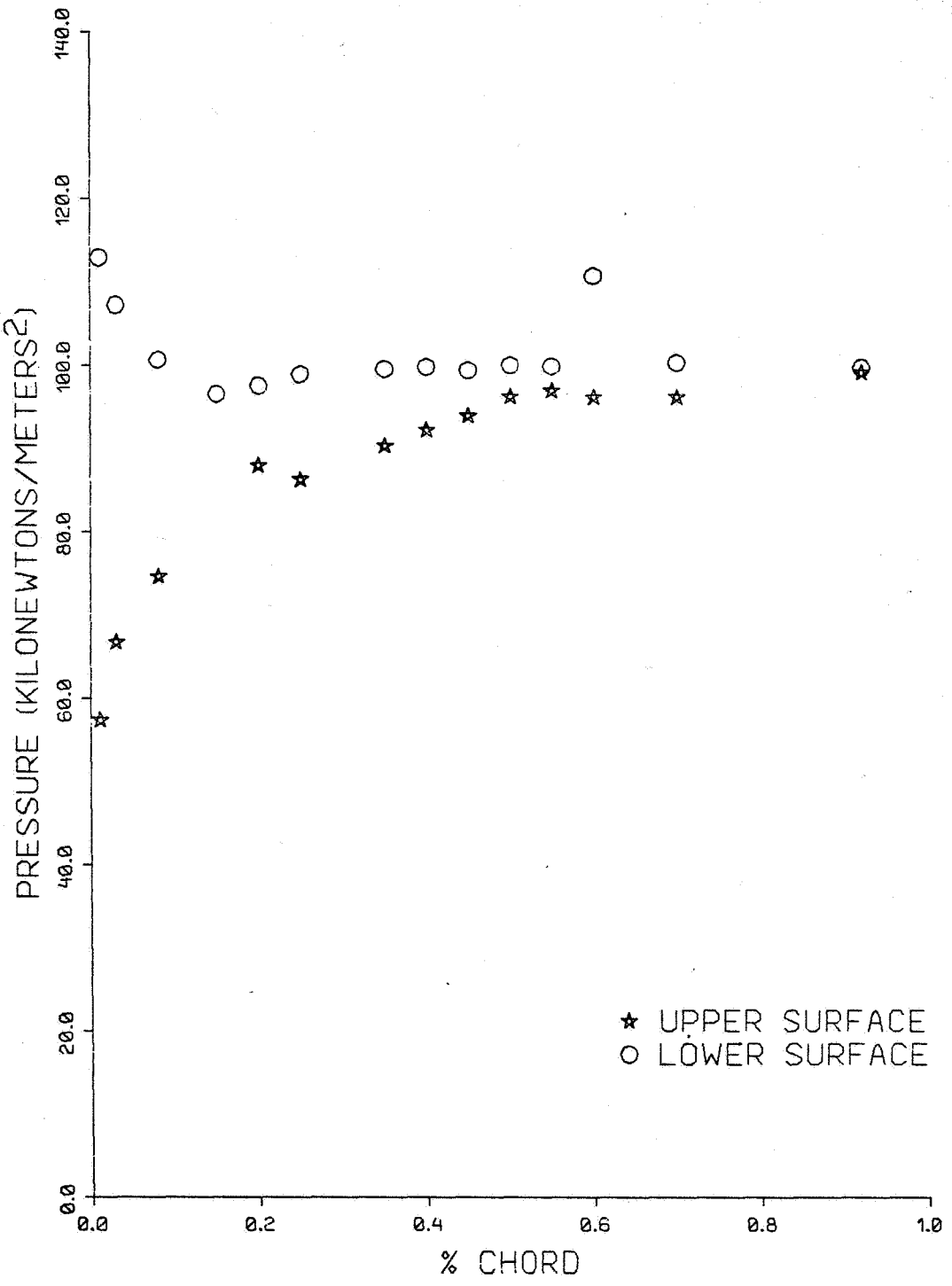

FIG. A-35.

SUCCI-BBN

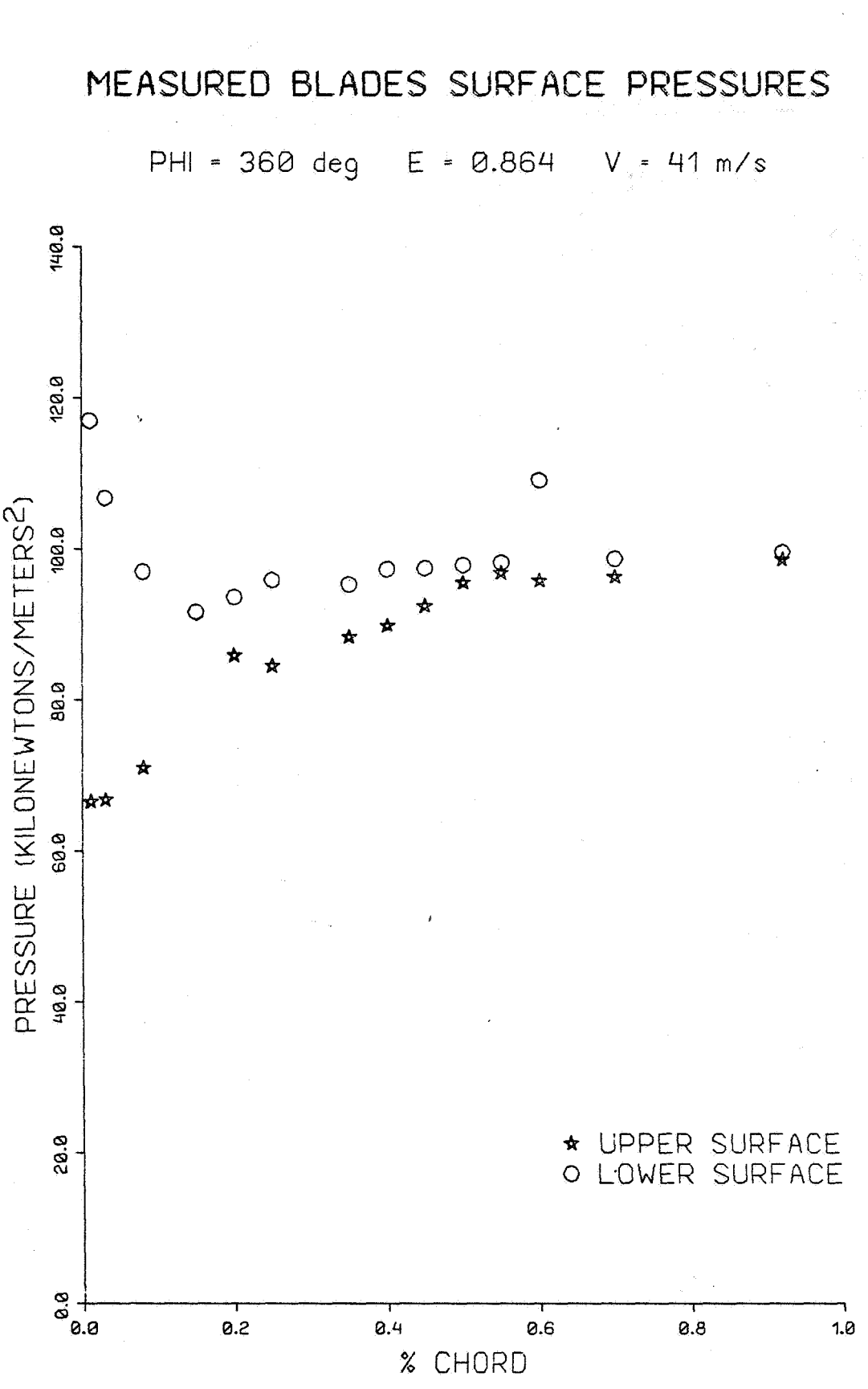

FIG. A-36.

SUCCI-BBN

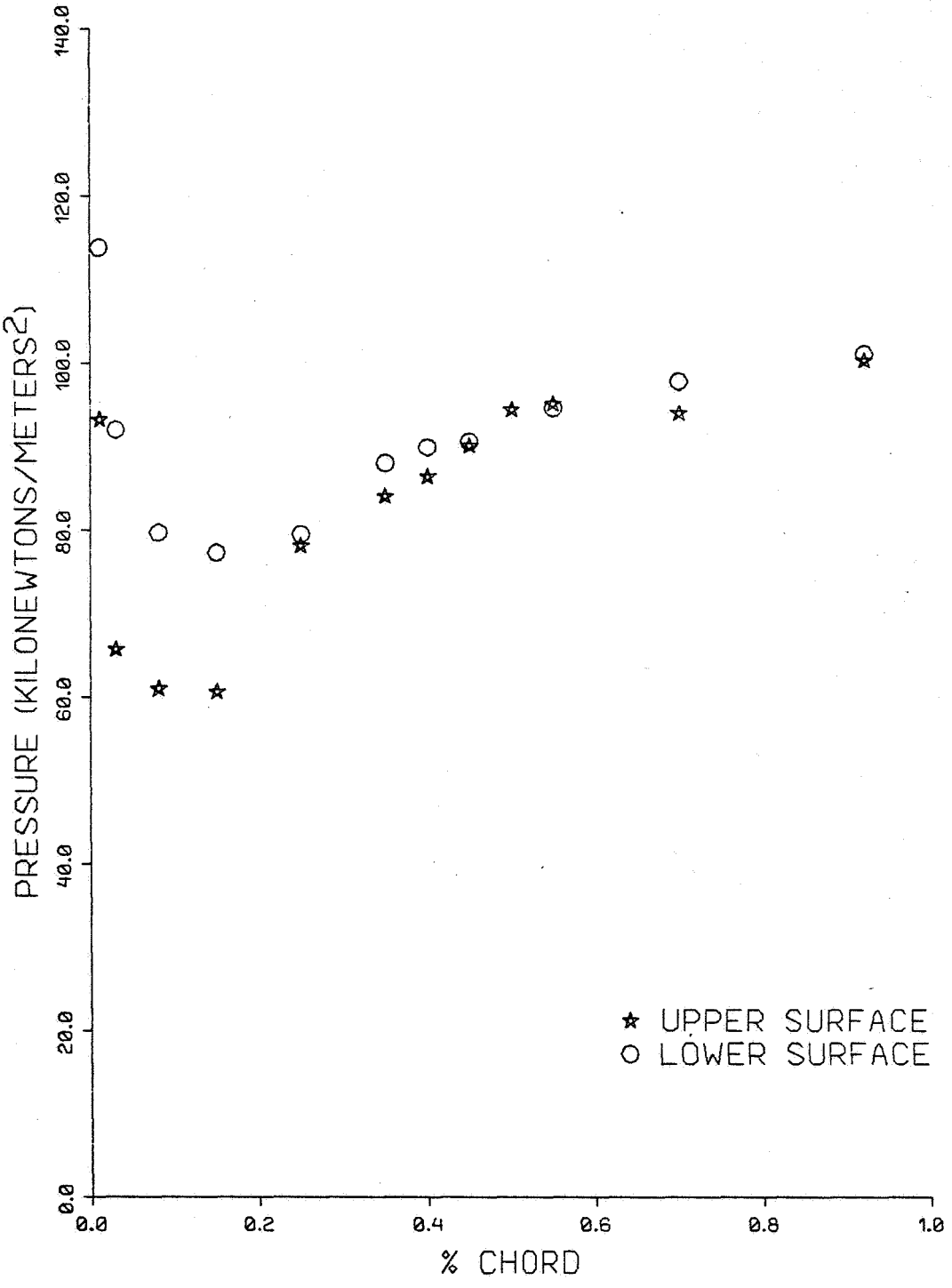

FIG. A-37.

SUCCI-BBN

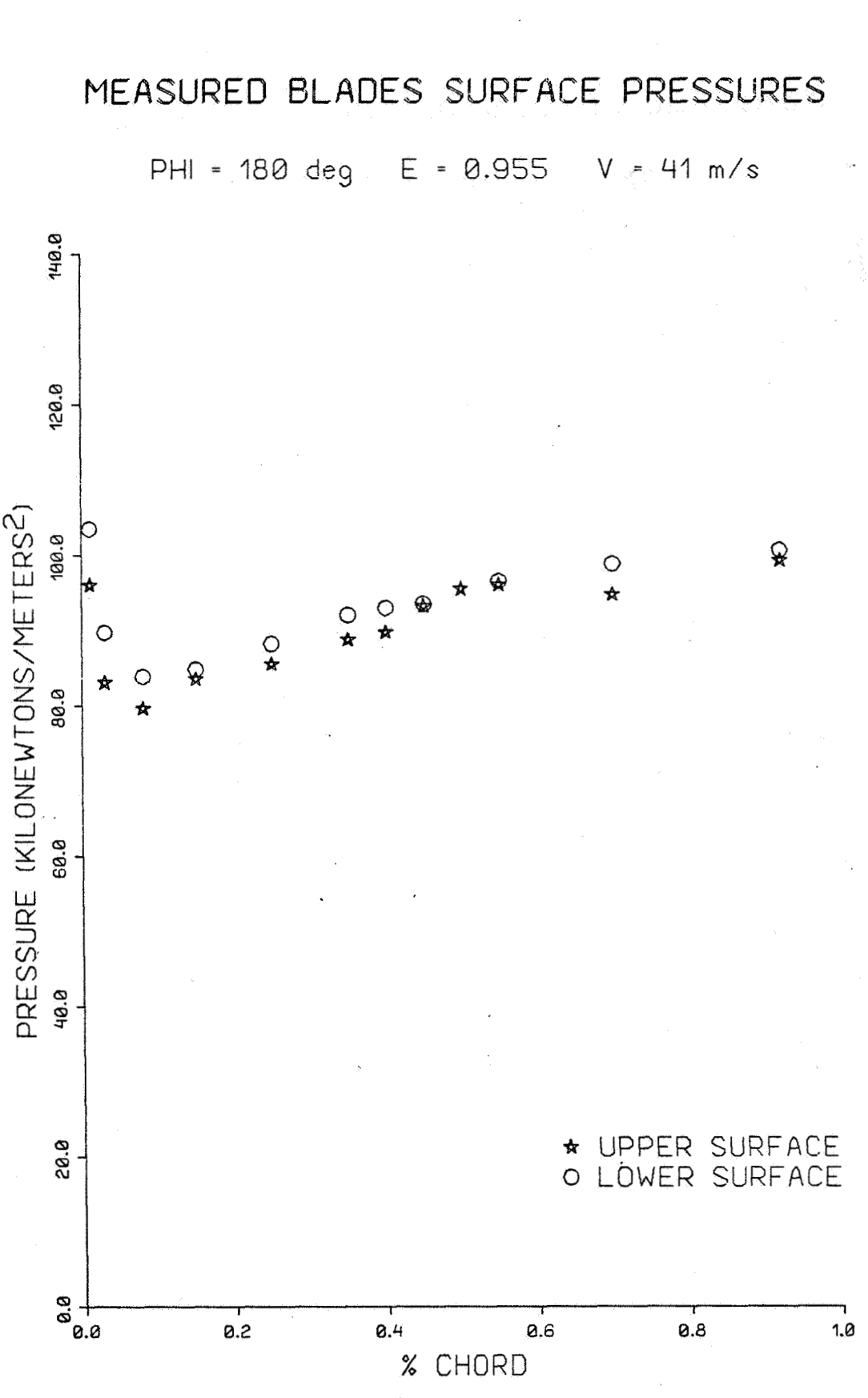

FIG. A-38.

SUCCI-BBN

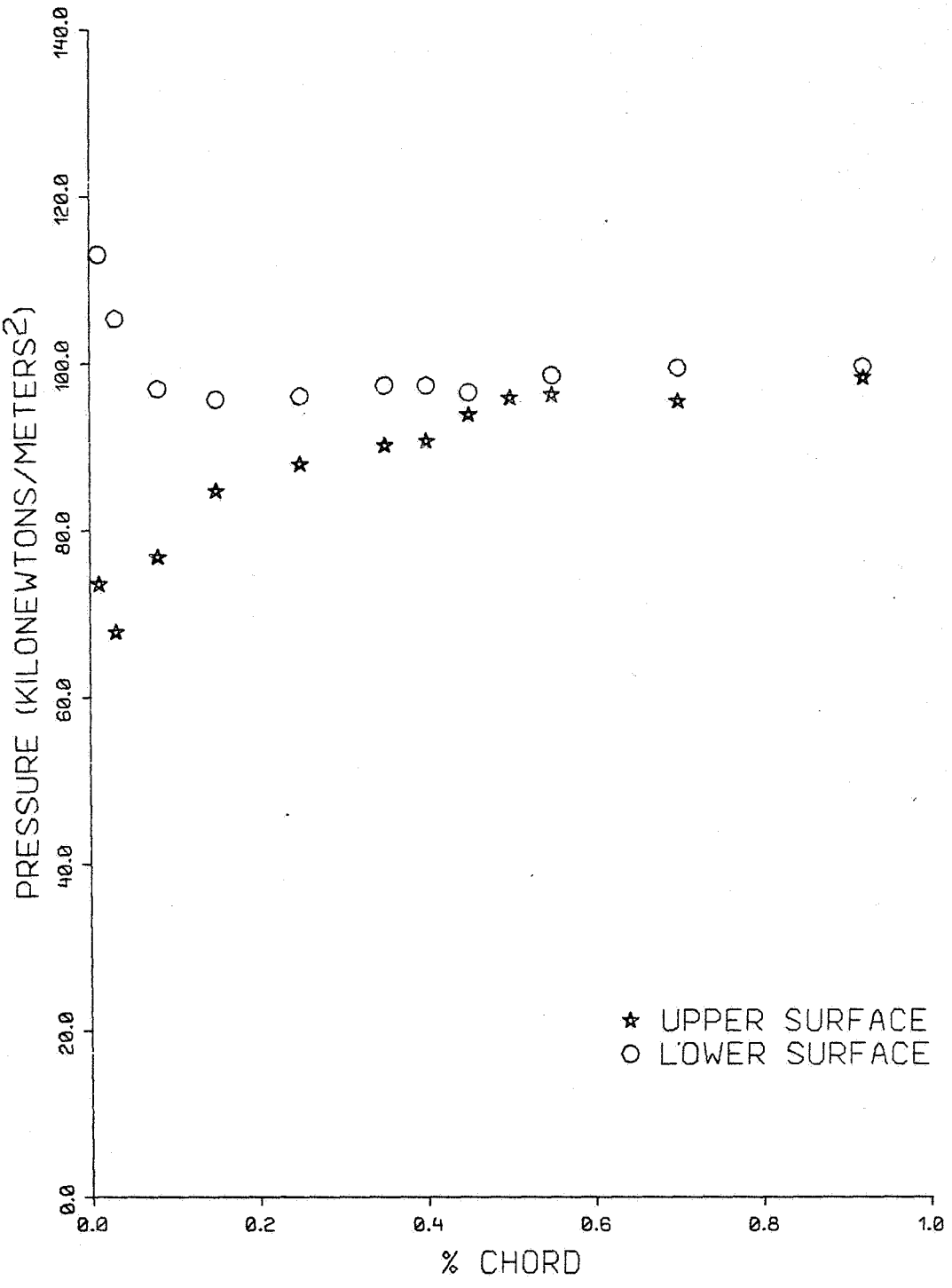

FIG. A-39.

SUCCI-BBN

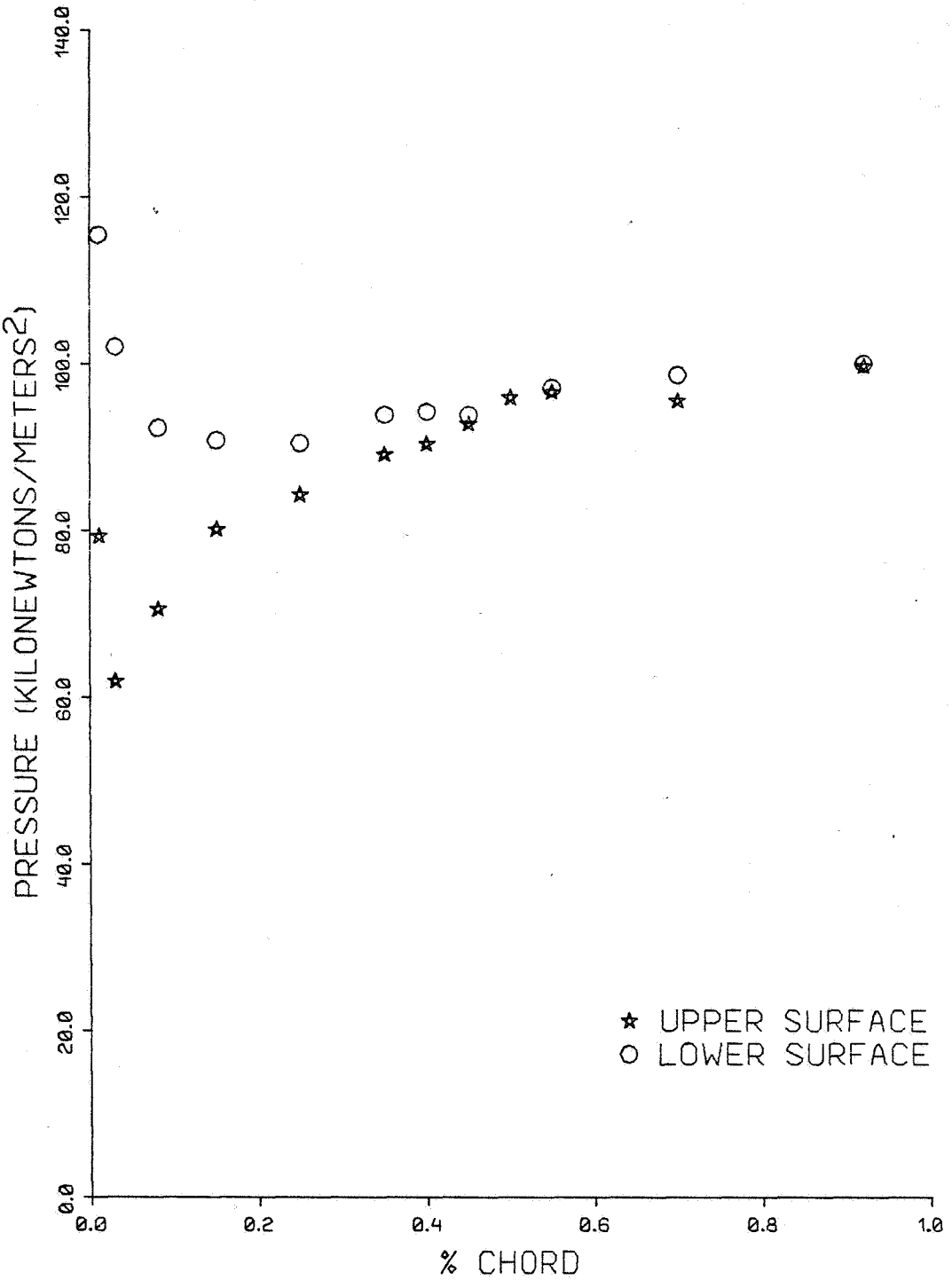

FIG. A-40.

SUCCI-BBN

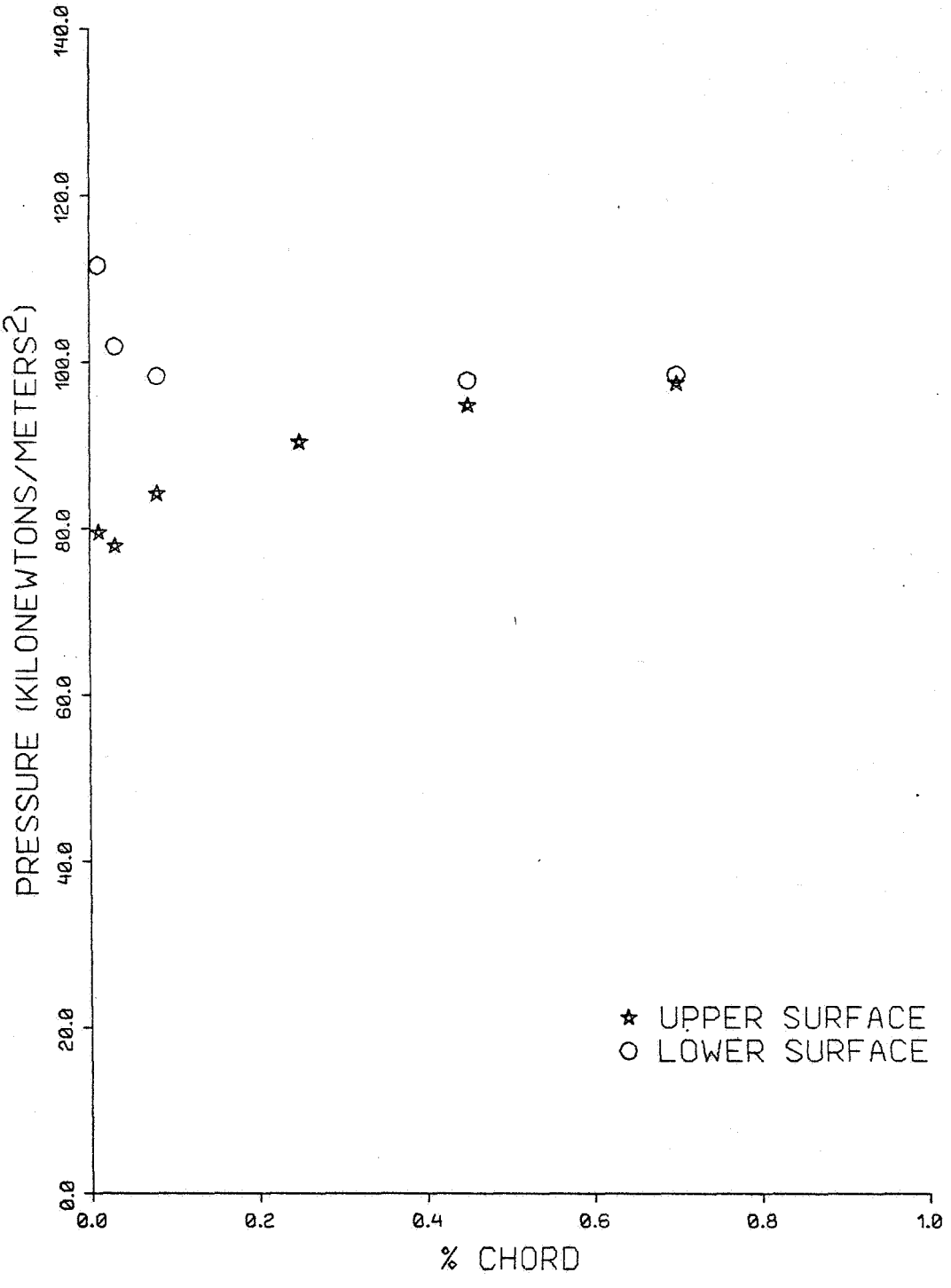

FIG. A-41.

SUCCI-BBN

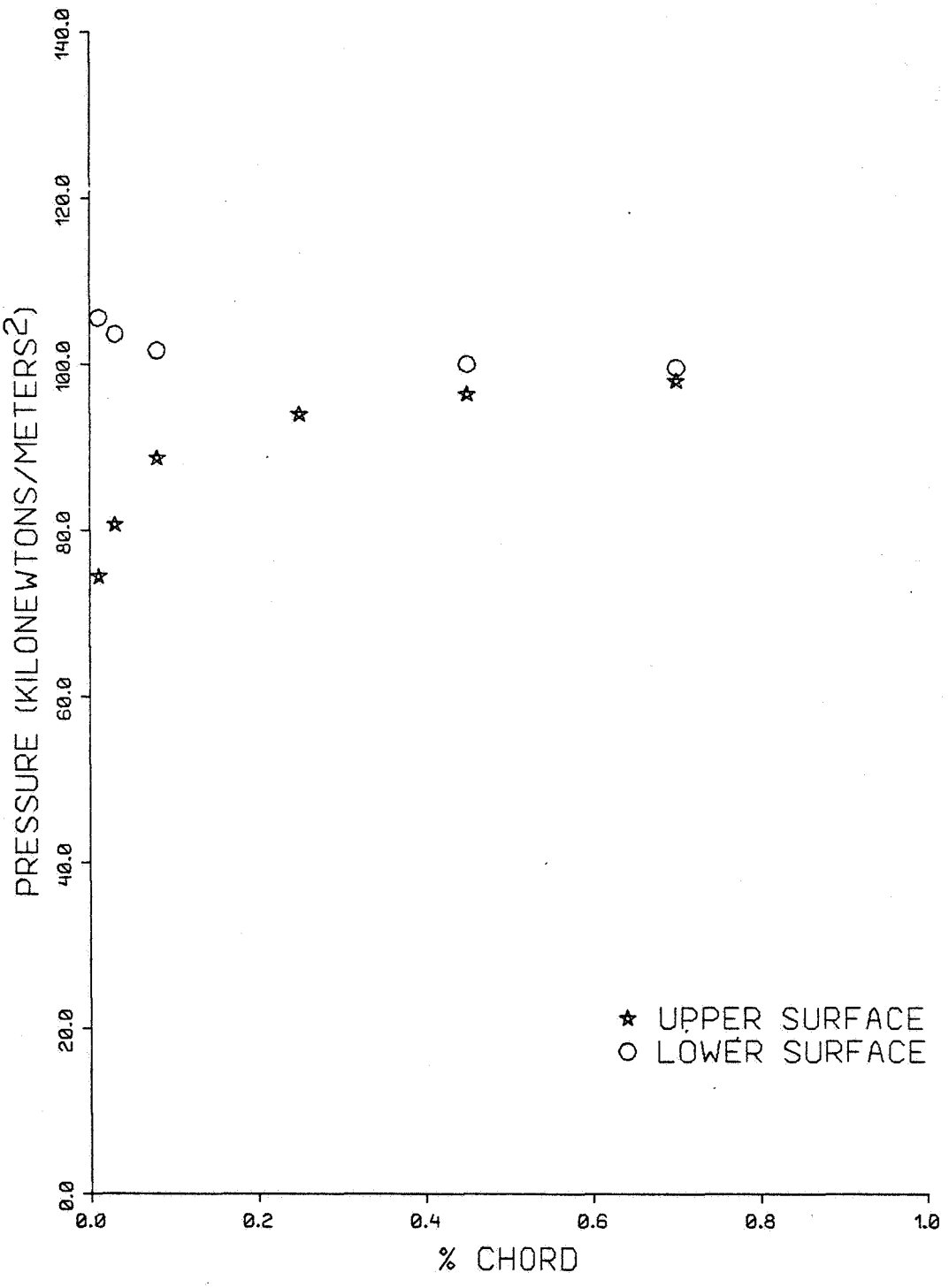

FIG. A-42.

SUCCI-BBN

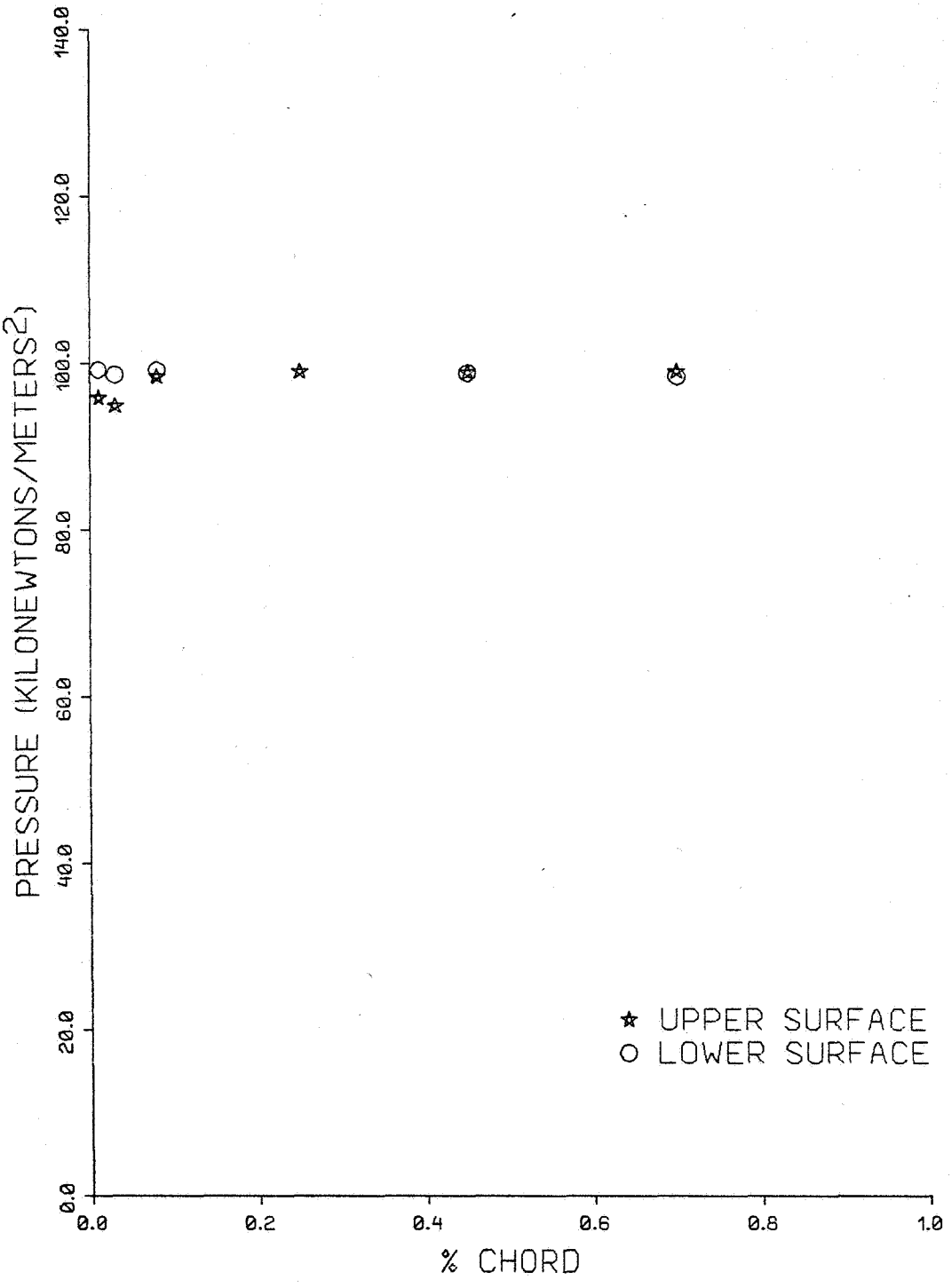

FIG. A-43.

SUCCI-BBN

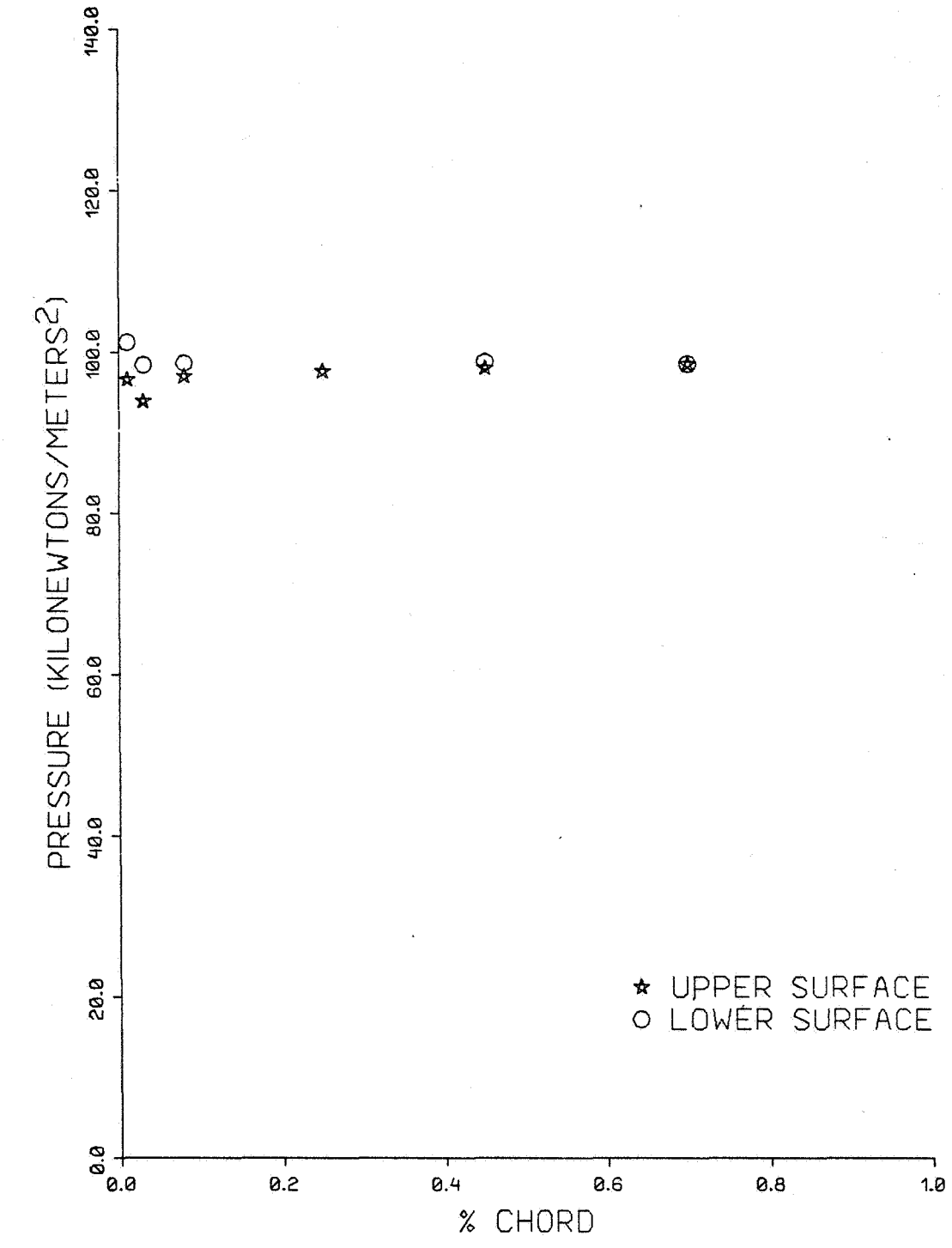

FIG. A-44.

SUCCI-BBN

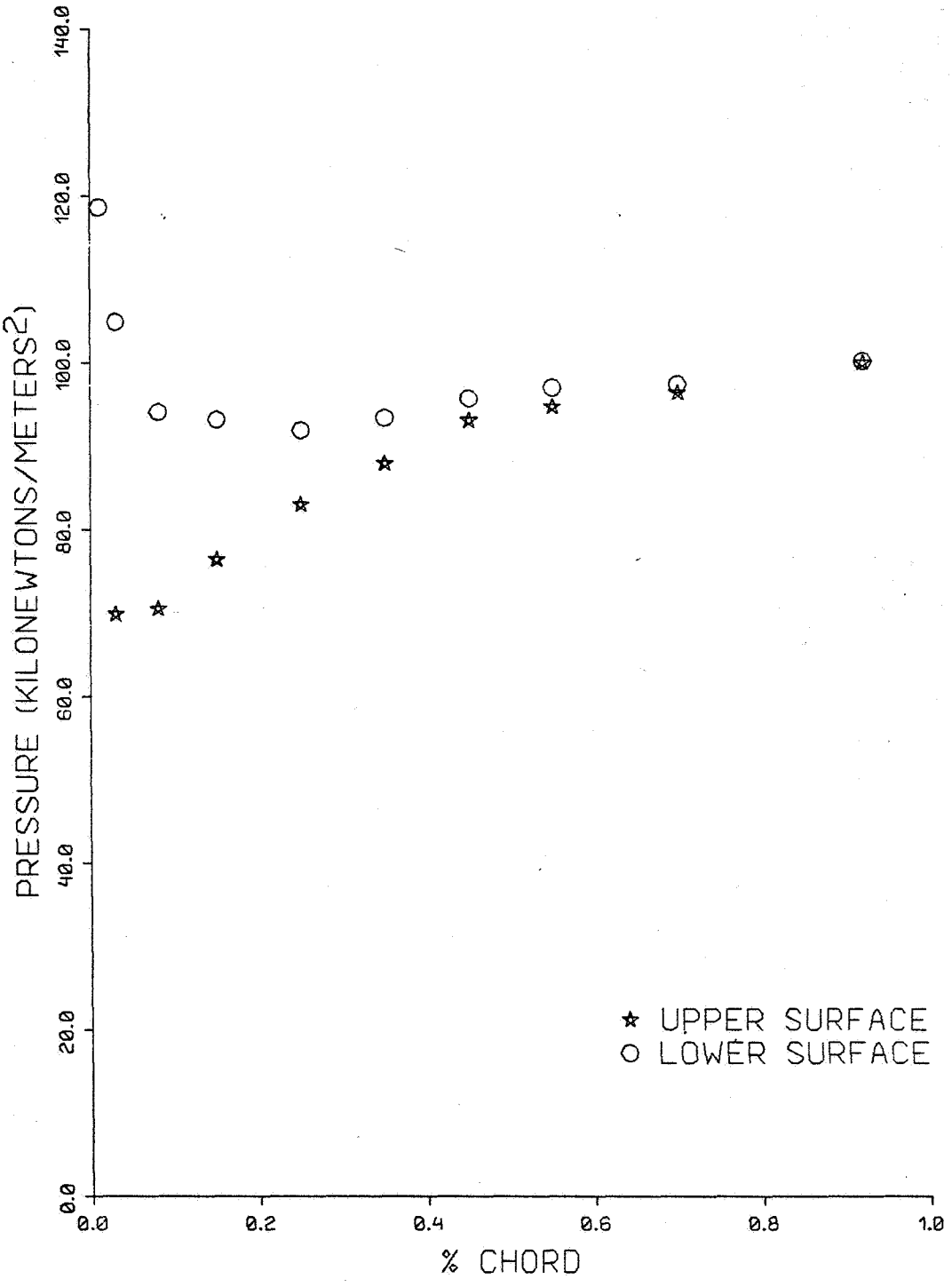

FIG. A-45. SUCCI-BBN

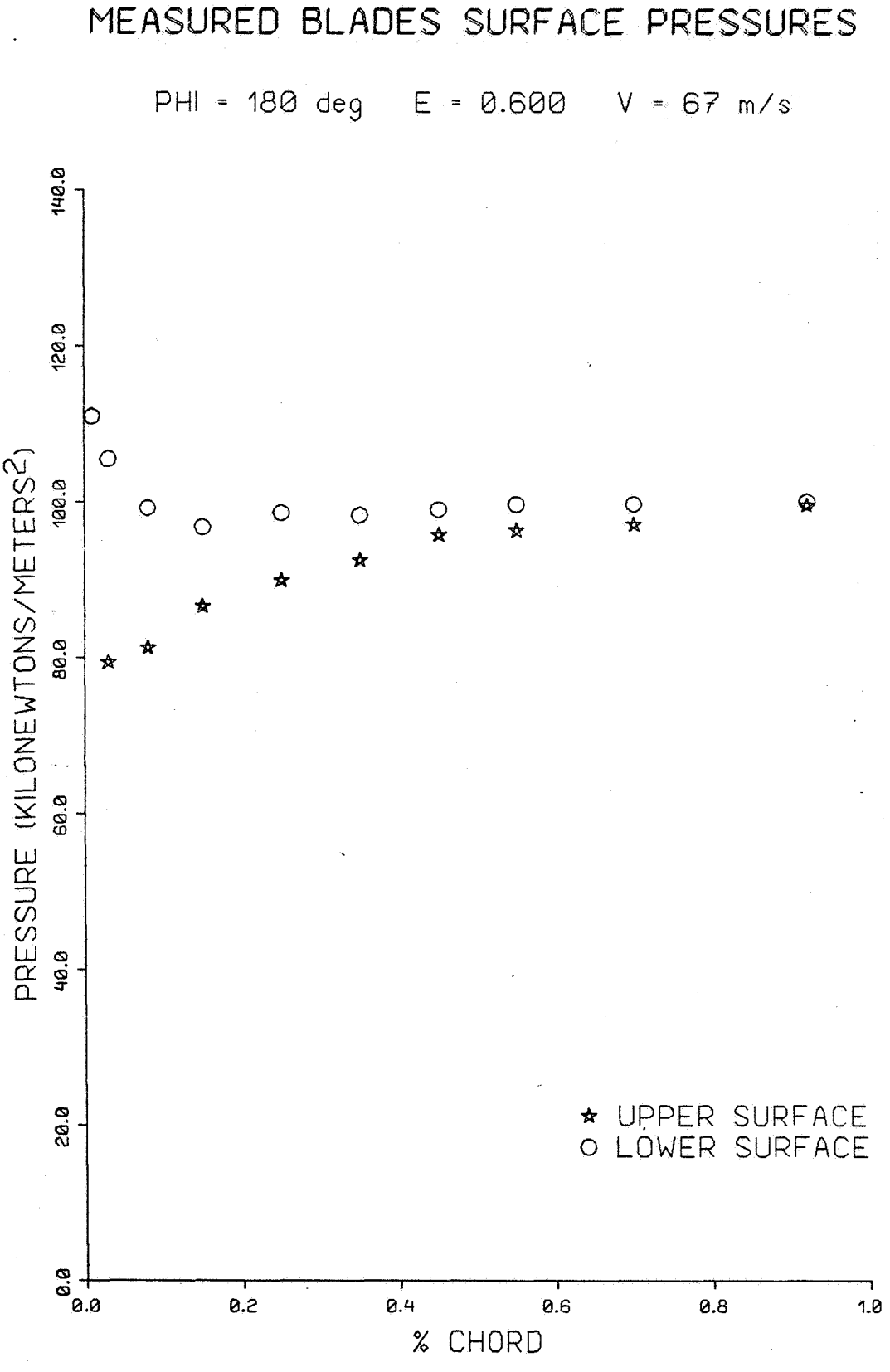

FIG. A-46.

SUCCI-BBN

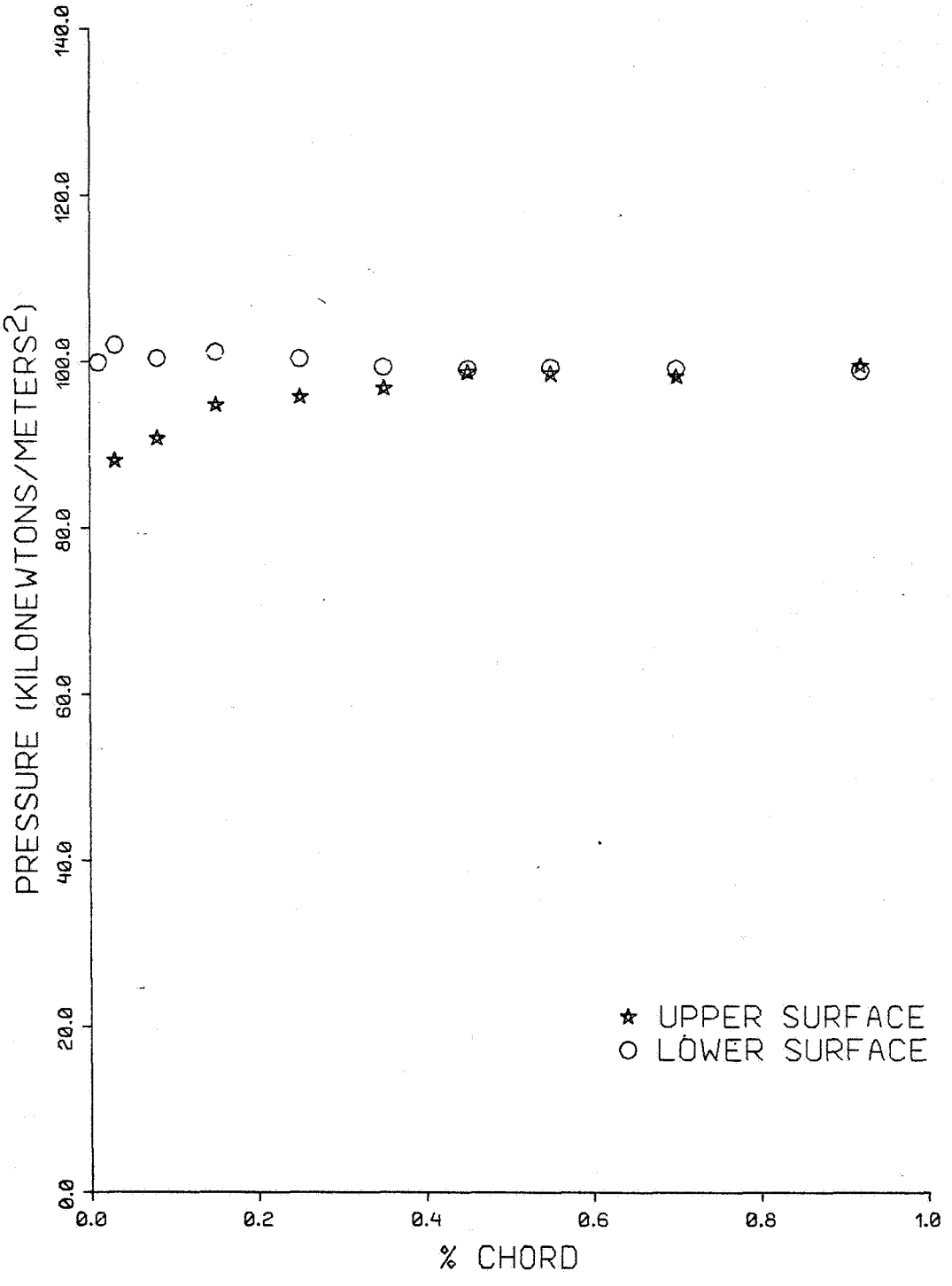

FIG. A-47.

SUCCI-BBN

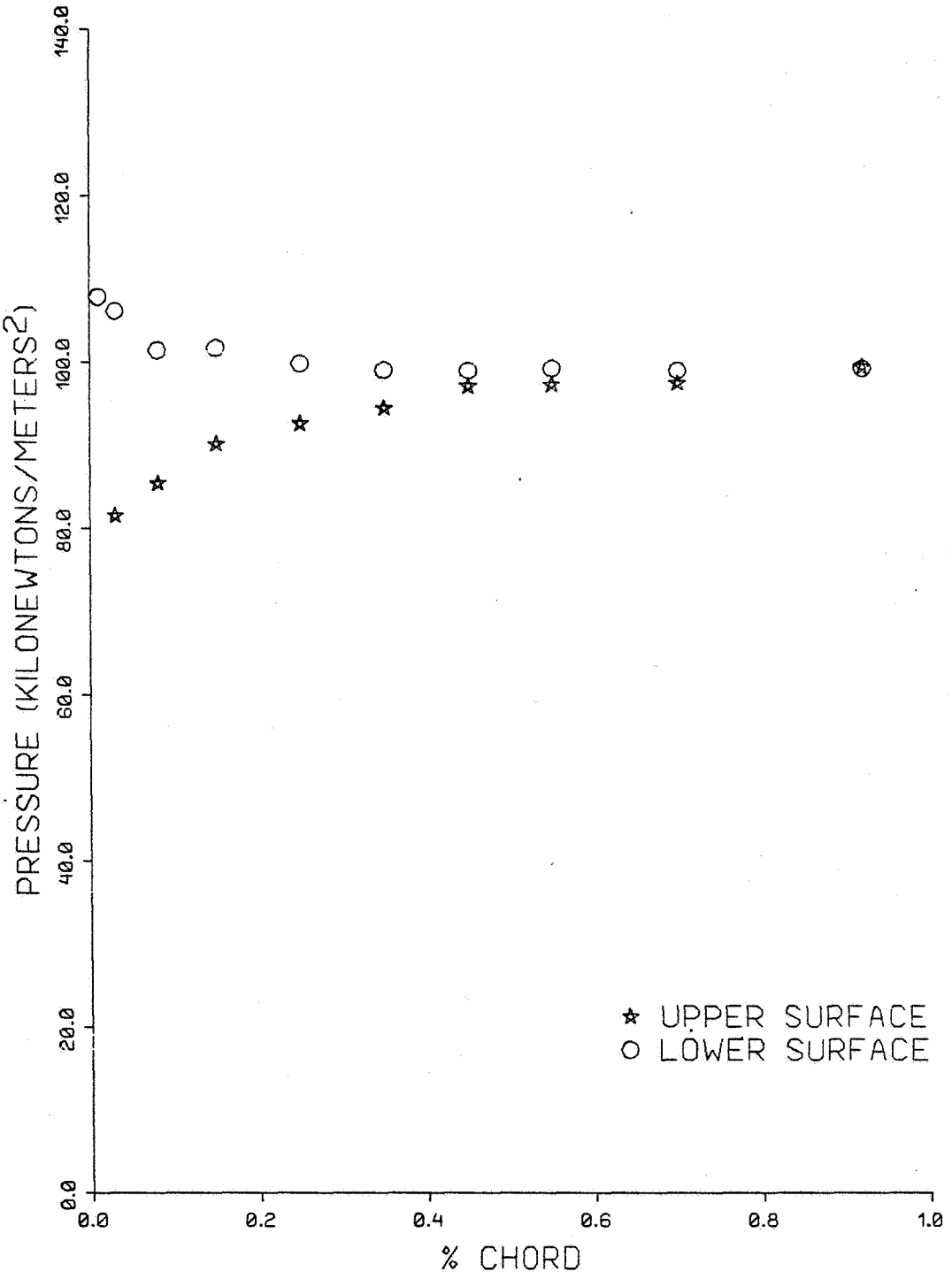

FIG. A-48.

SUCCI-BBN

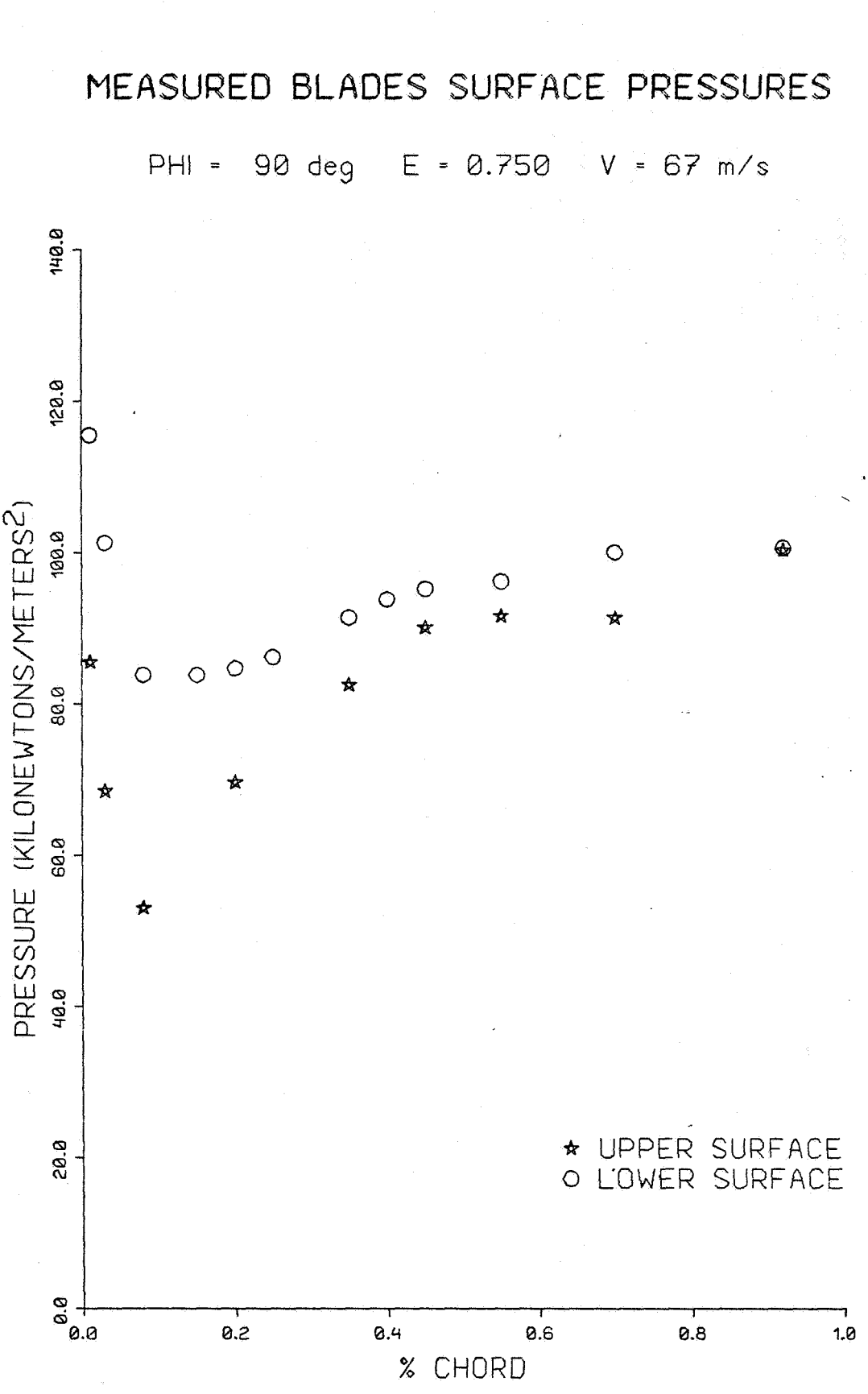

FIG. A-49. SUCCI-BBN

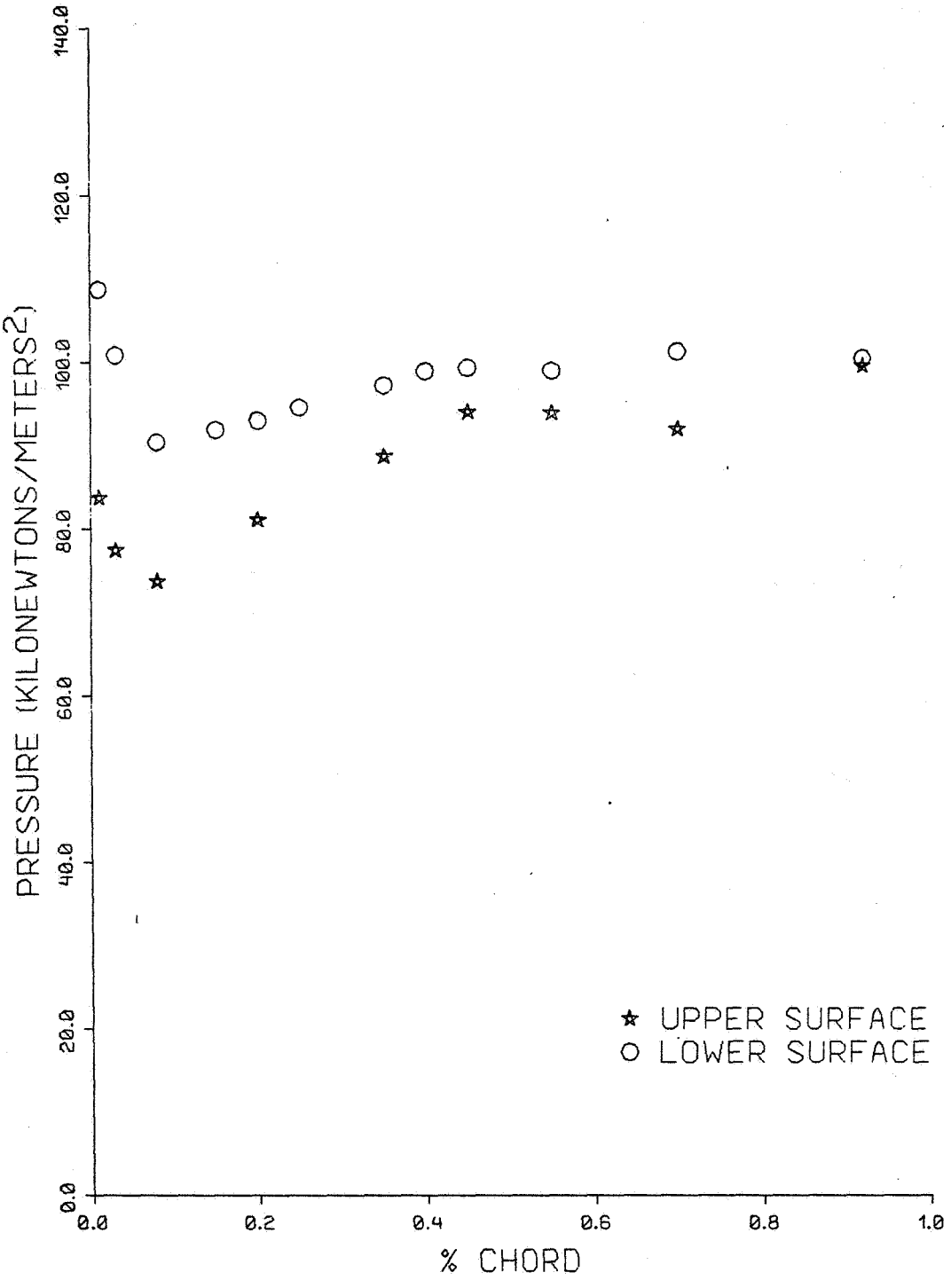

FIG. A-50.

SUCCI-BBN

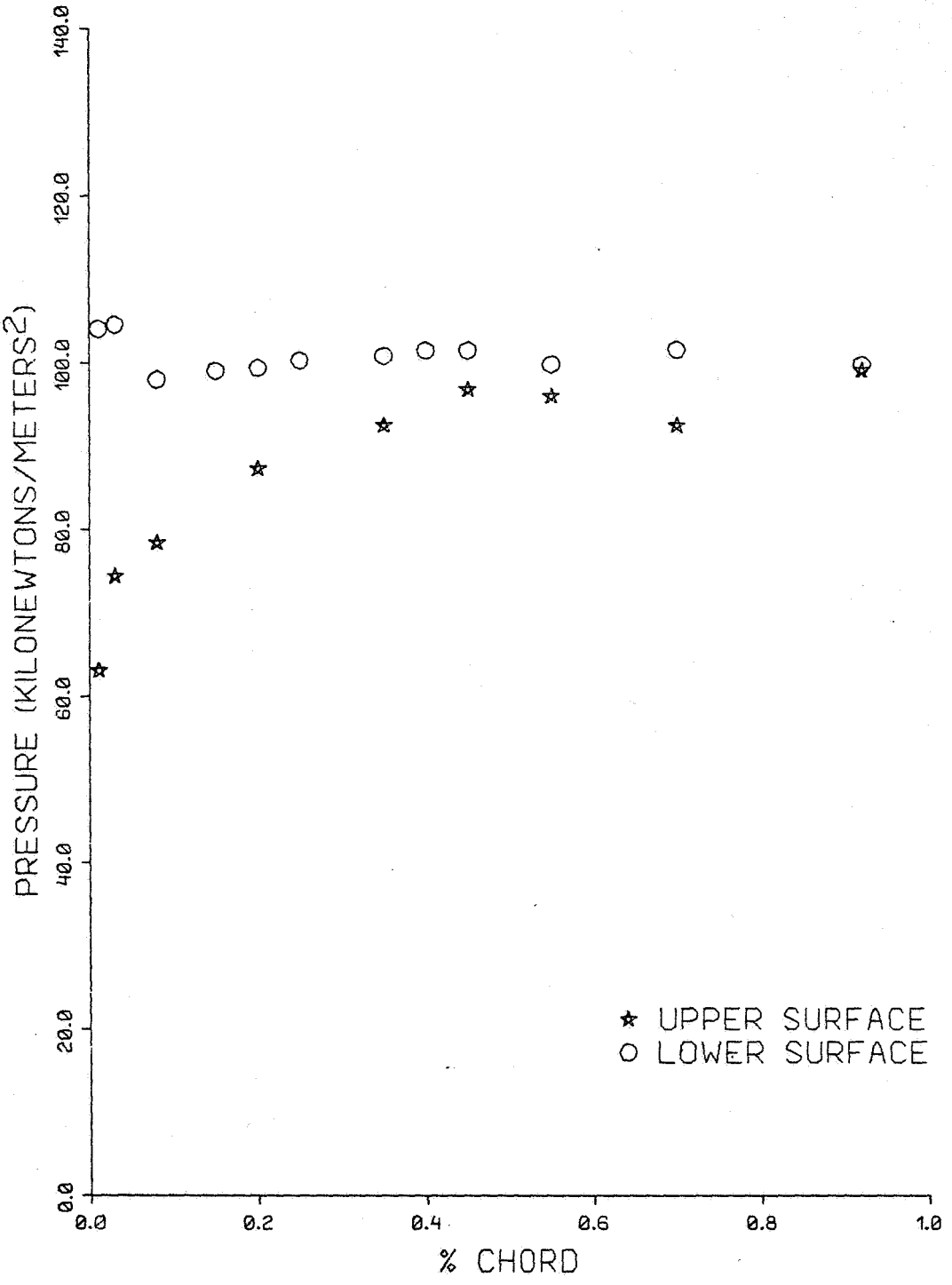

FIG. A-51.

SUCCI-BBN

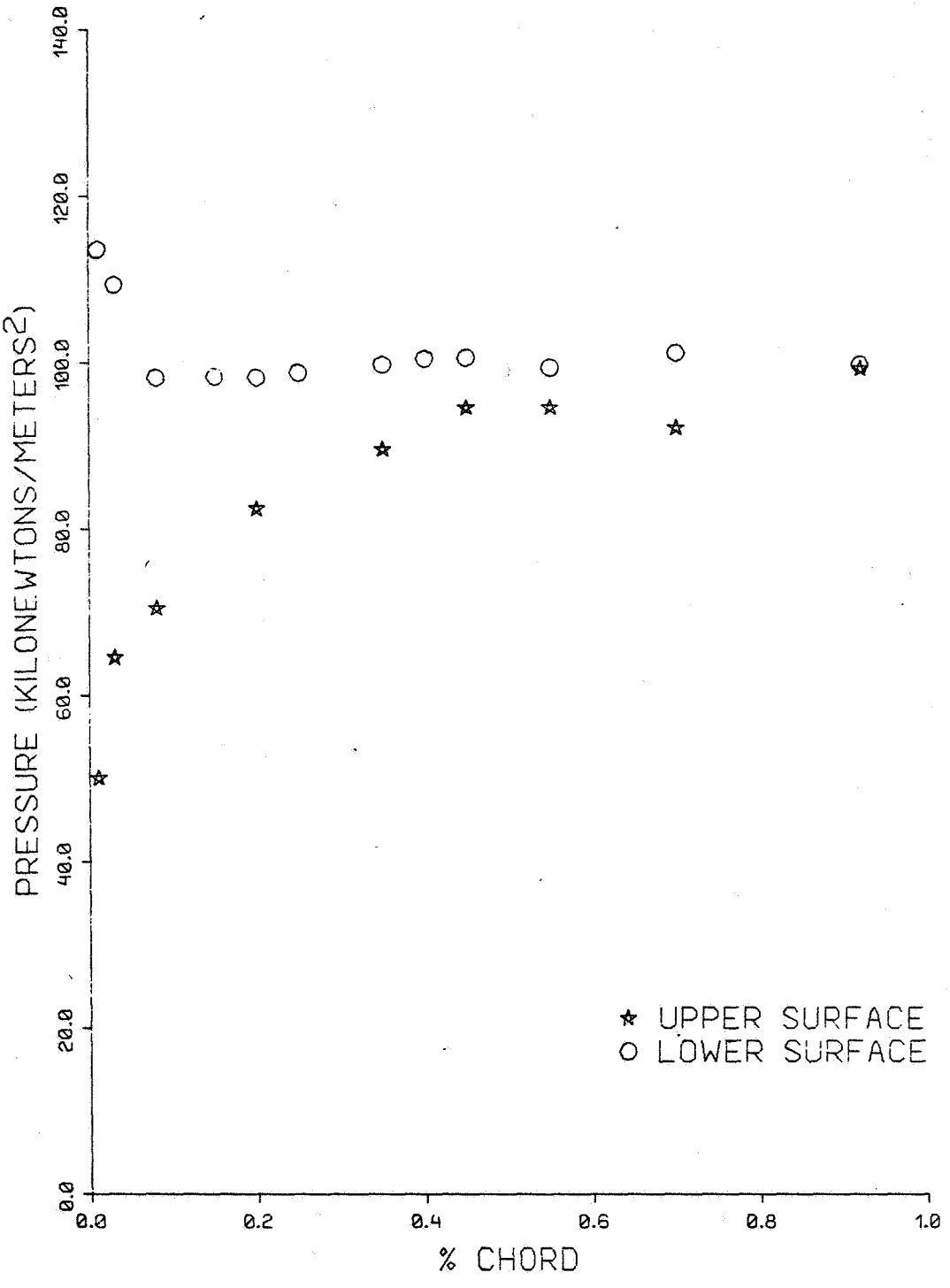

FIG. A-52. SUCCI-BBN

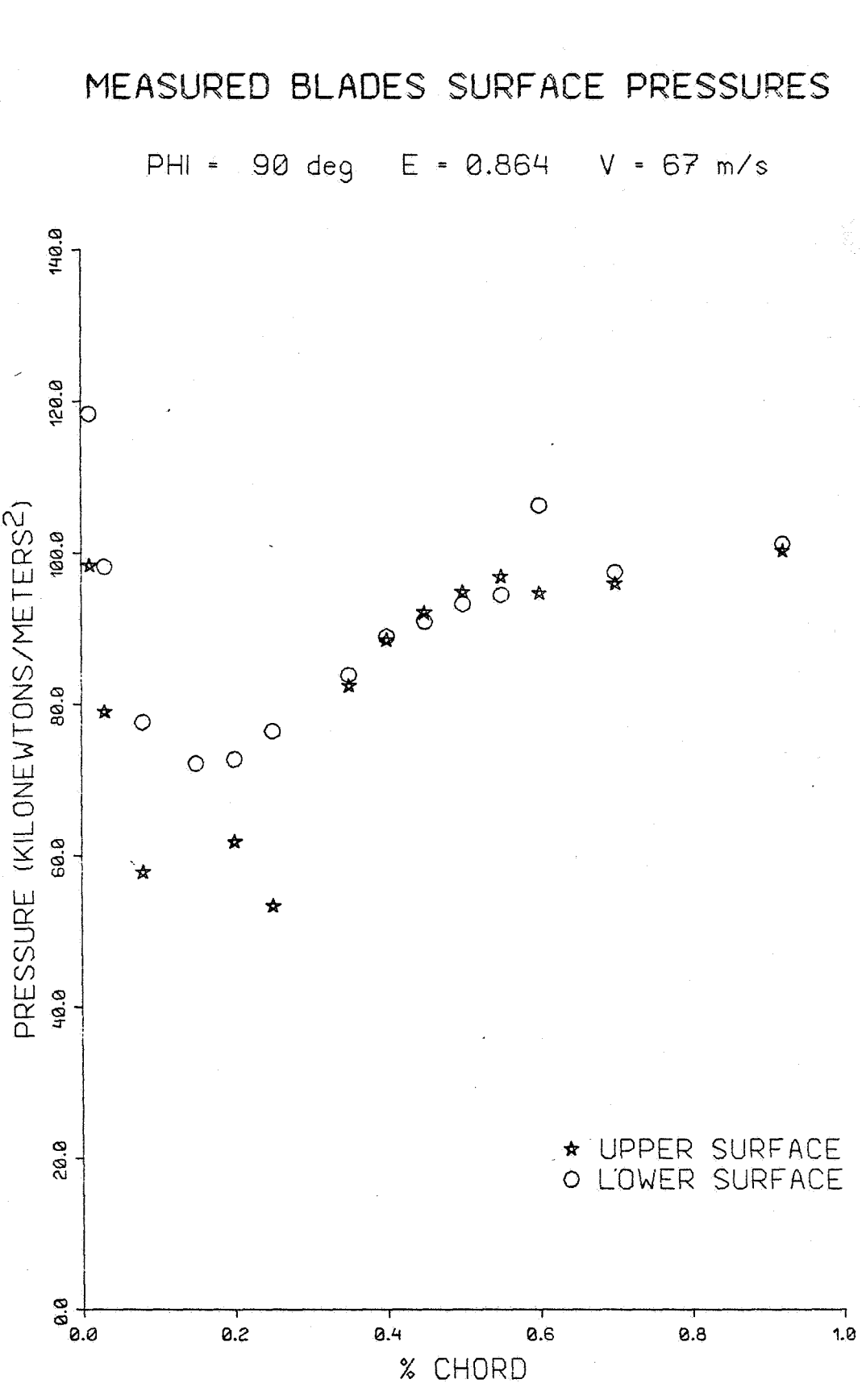

FIG. A-53. SUCCI-BBN

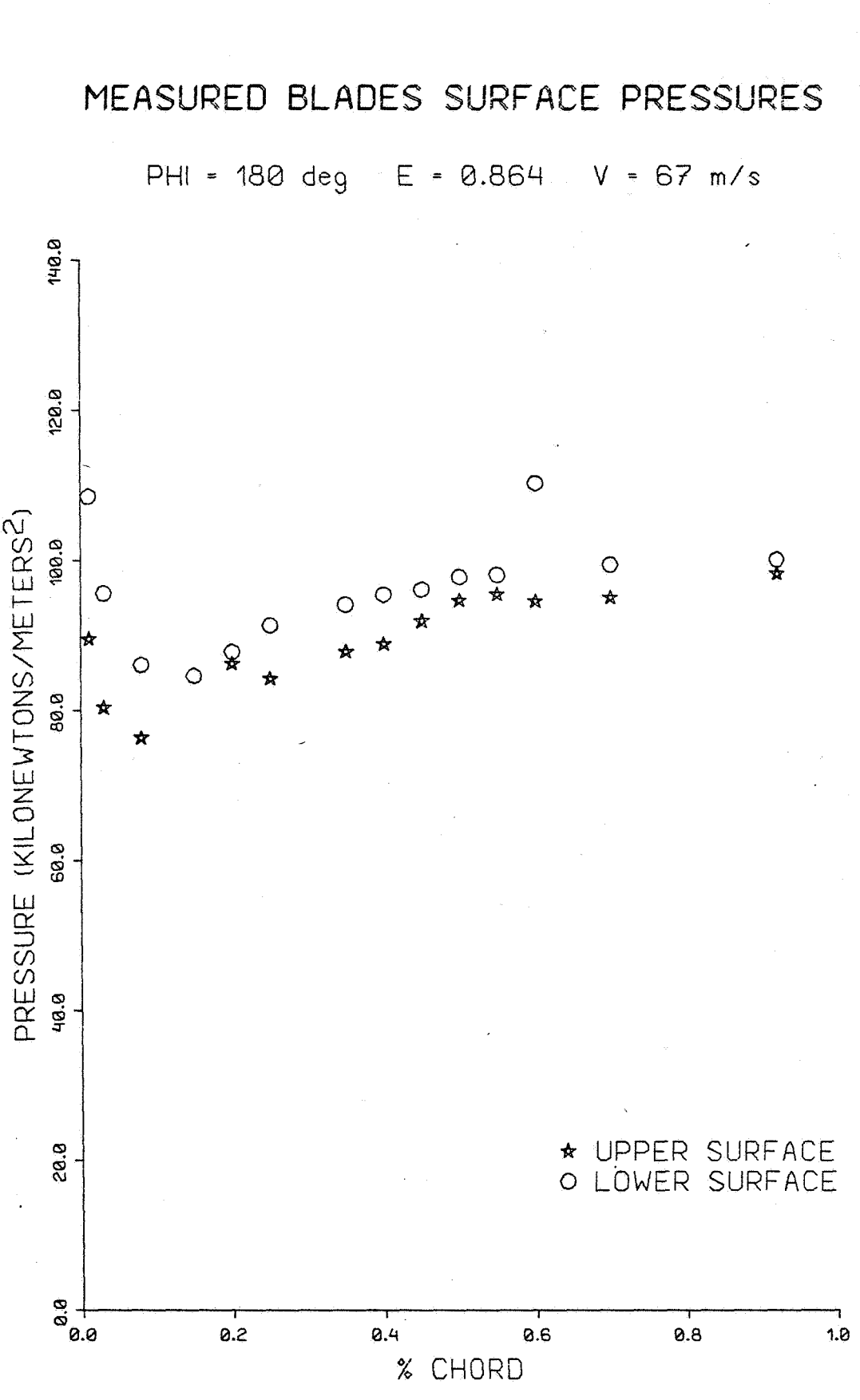

FIG. A-54.

SUCCI-BBN

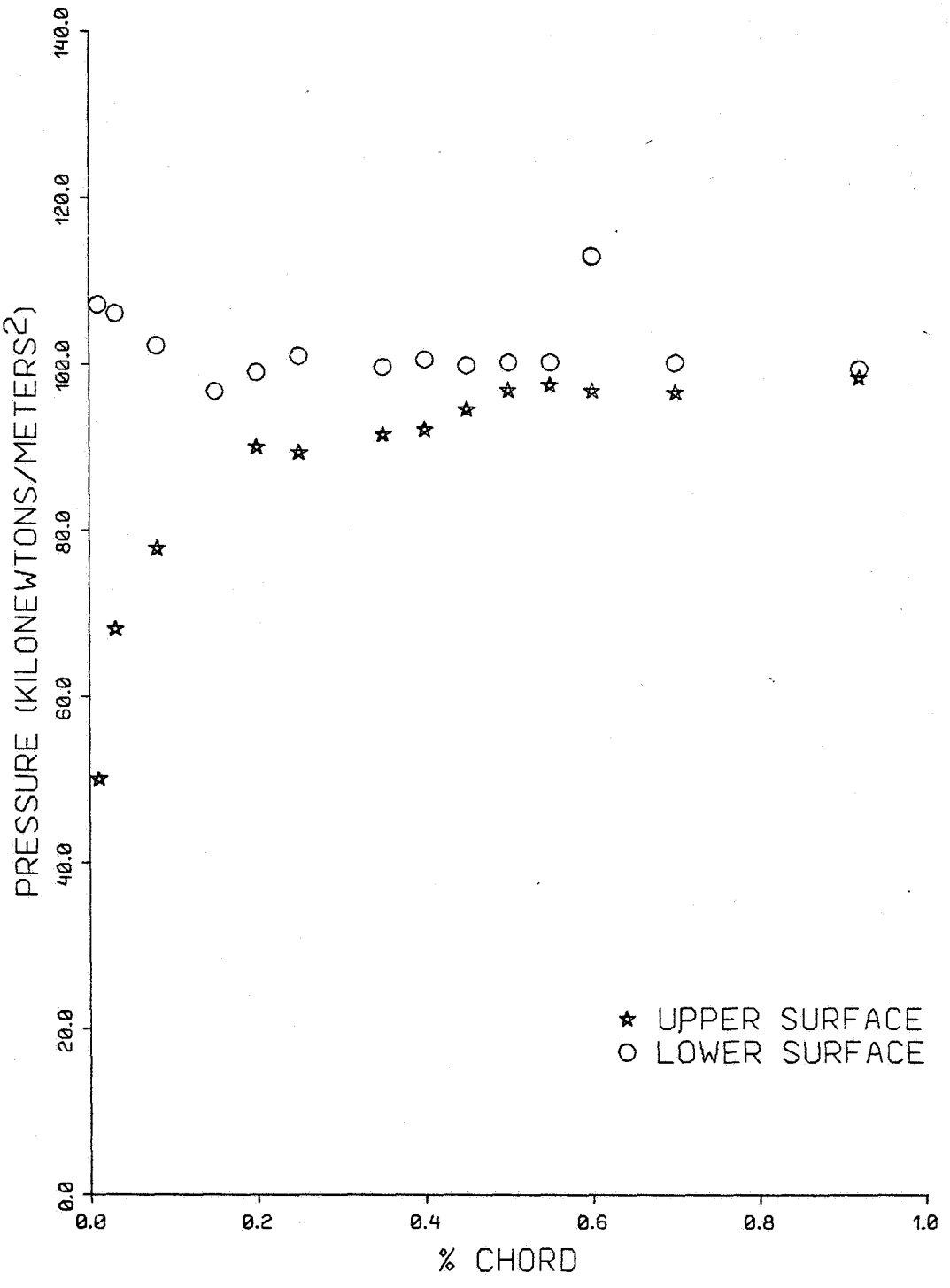

FIG. A-55.

SUCCI-BBN

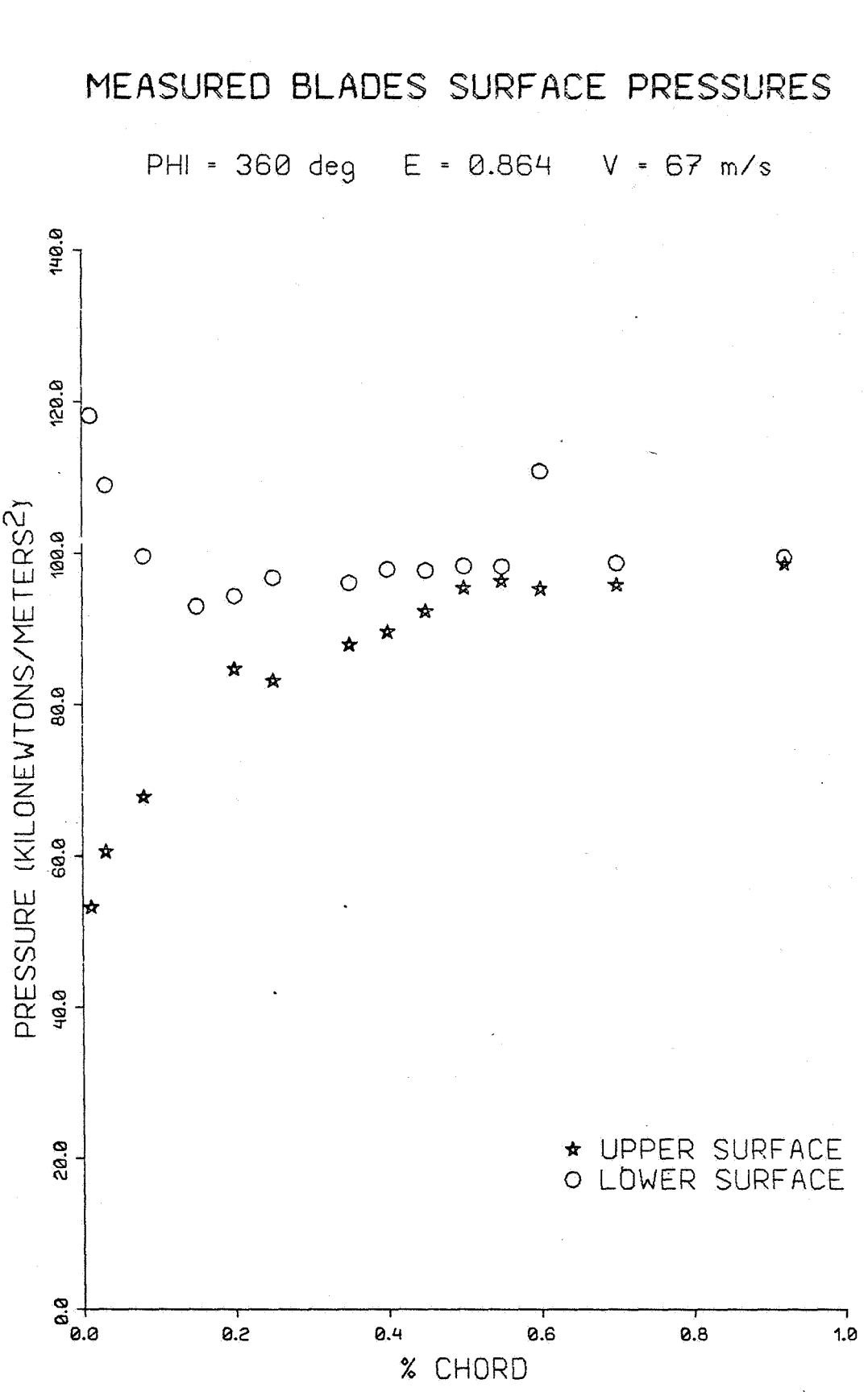

FIG. A-56.

SUCCI-BBN

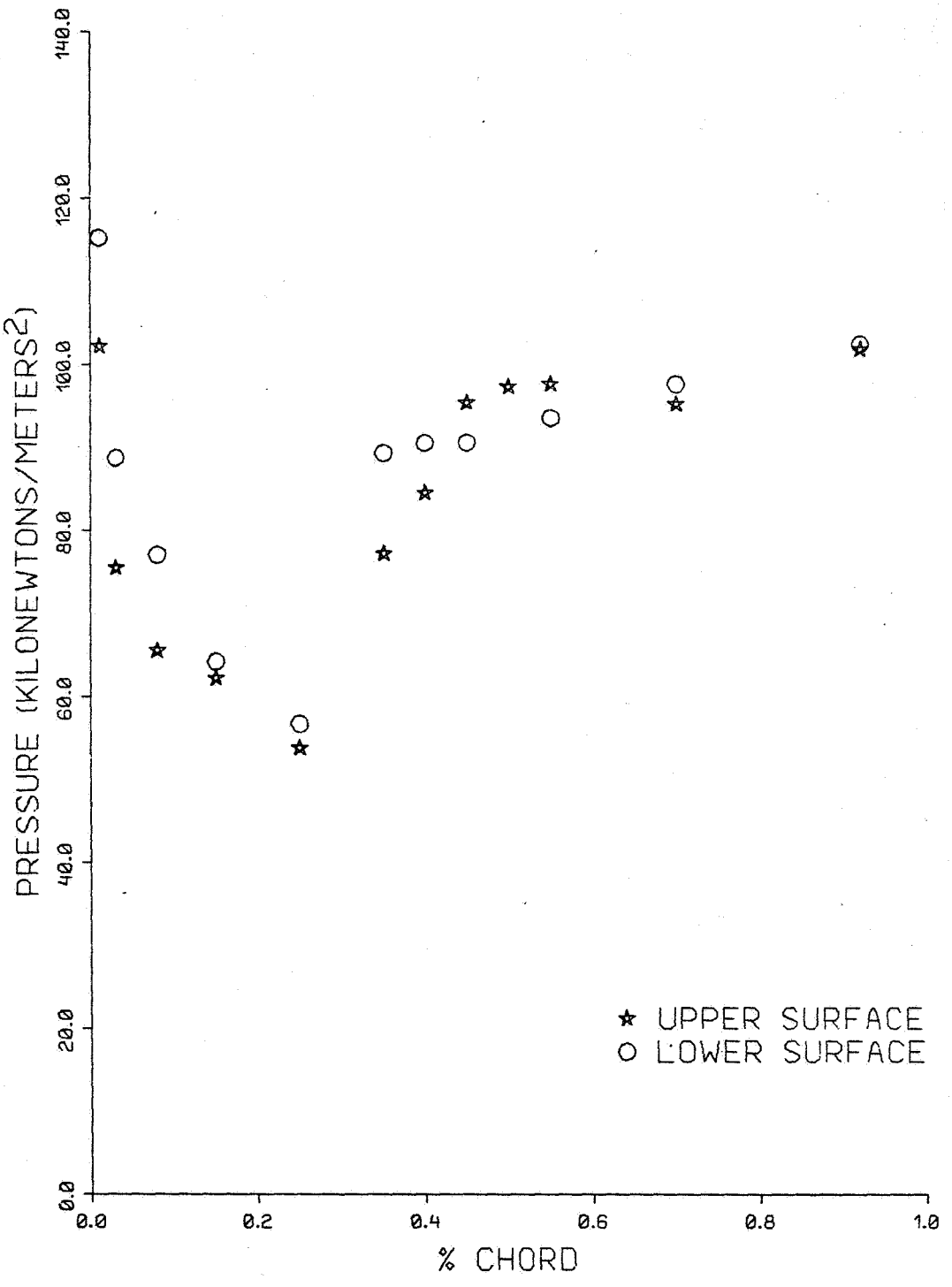

FIG. A-57.

SUCCI-BBN

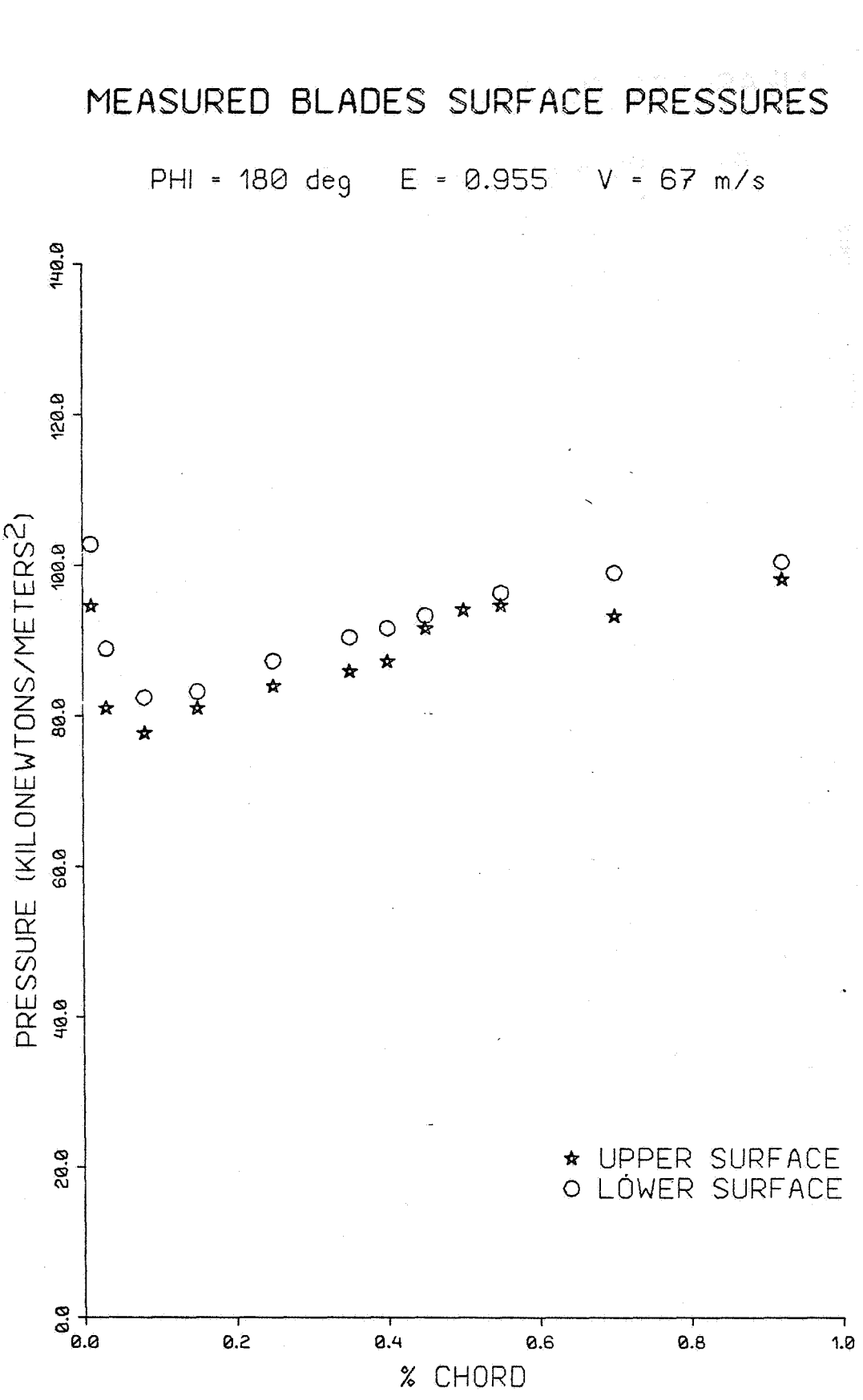

FIG. A-58.

SUCCI-BBN

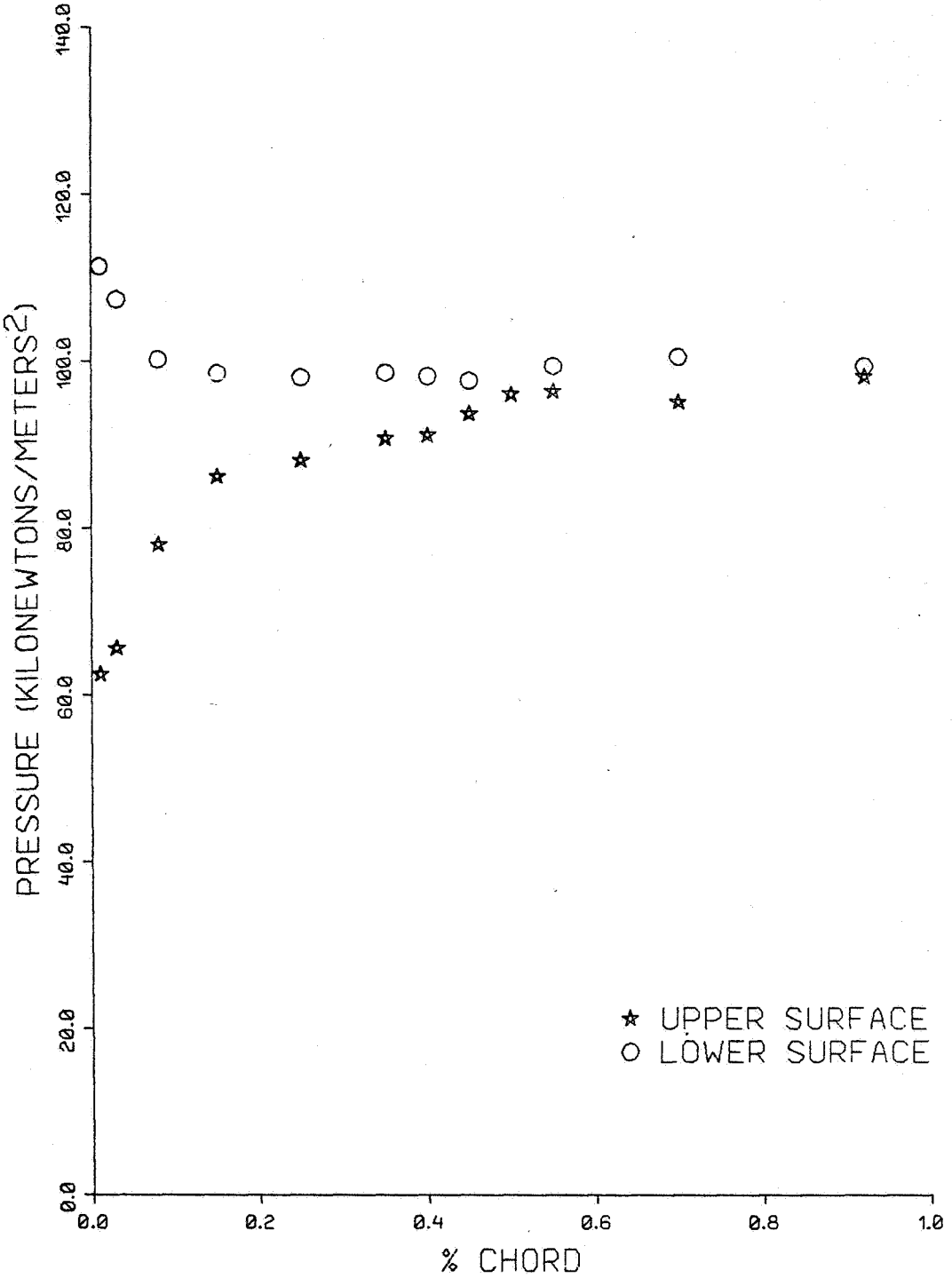

FIG. A-59. SUCCI-BBN

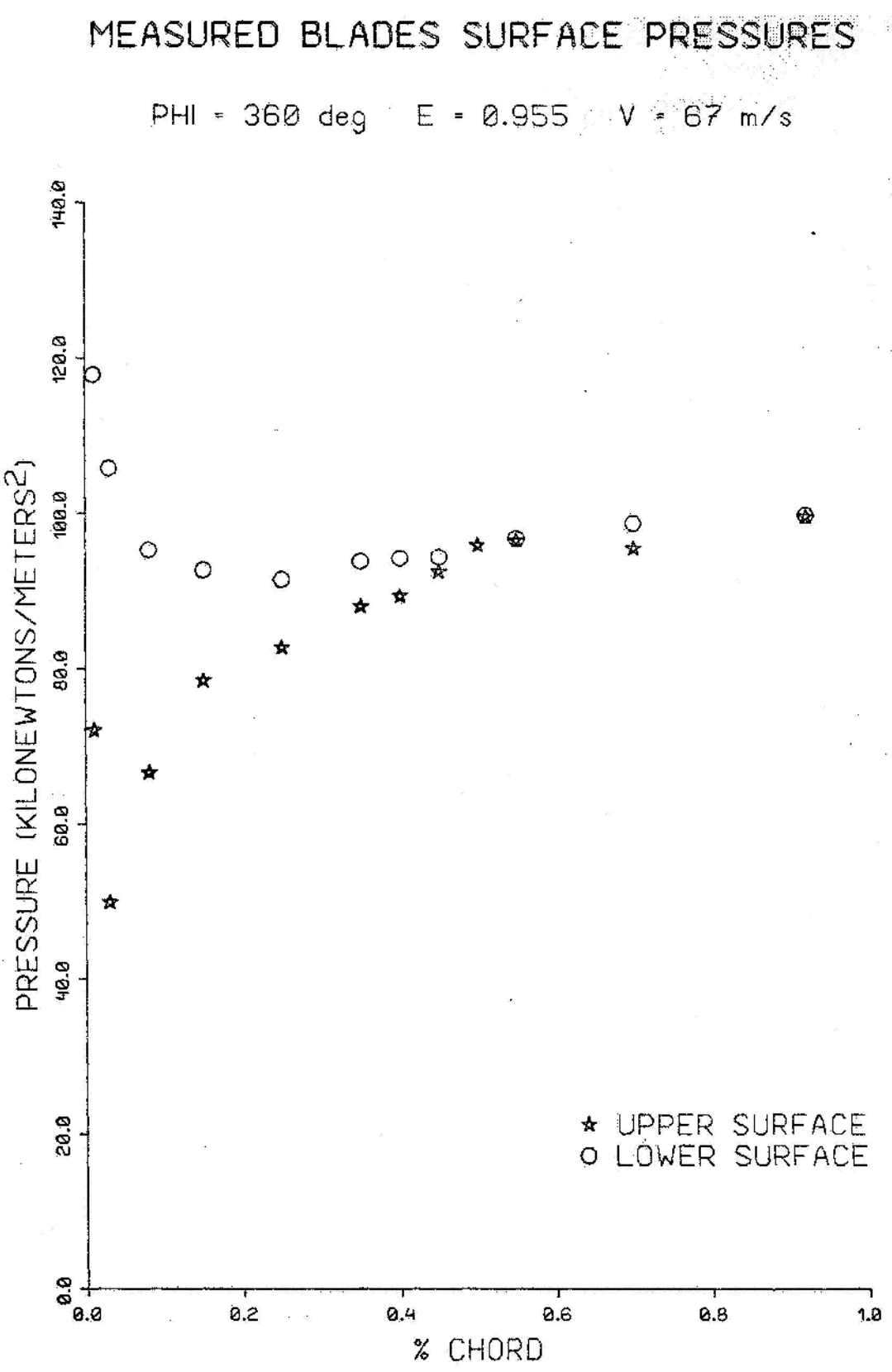

FIG. A-60.

SUCCI-BBN